C–H···O participation in the dimer of aromatic N-sulfinylhydrazines

Stephen Boateng

A Thesis

in

The Department

of

Chemistry and Biochemistry

Presented in Partial Fulfillment of the Requirements for the Degree of Master of Science

at Concordia University

Montreal, Quebec, Canada

December 2013

CONCORDIA UNIVERSITY

School of Graduate Studies

This is to certify that the thesis prepared

By: Stephen Boateng

Entitled: C–H···O participation in the dimer of aromatic N-sulfinylhydrazines

and submitted in partial fulfillment of the requirements for the degree of

Master of Science (Chemistry)

complies with the regulations of this University and meets the accepted standards with respect to originality and quality.

_____Chair

Dr. C.E. DeWolf

_____Examiner

Dr. P. Forgione

_____Examiner

Dr. C. Wilds

_____Supervisor

Dr. H.M. Muchall

Approved by: _____

Chair of Department or Graduate Program Director

December 16, 2013 _____

Dean of Faculty

Abstract

To assess the substituent effect on the stability of hydrogen-bonded dimers from N-phenyl-N'-sulfinylhydrazines (Ph–NH–NSO), and to confirm the suggested participation of C_o–H···O interactions in the dimer from protons in ortho position, ^{1}H NMR (proton nuclear magnetic resonance) dilution studies were carried out on the unsubstituted and the meta- and para-methyl substituted compounds. The ^{1}H NMR spectra of the solutions in $CDCl_3$, recorded from the limit of detectability in dilute solution to the solubility limit, at room and low temperature, show characteristic chemical shift changes to lower field, in the resonances of the N–H as well as of the C_o–H protons. Upon dilution, a dissociation equilibrium exists, and both the monomer and dimer chemical shifts, for N–H and C_o–H, can be obtained from the concentration-dependence regression curves, which allows to establish a measure of the strength of the hydrogen bonding network in the dimer through the equilibrium (dimerization or association) constant. For dimer formation using the ^{1}H NMR data, a small substituent effect is observed in meta- and para-methyl substituted Ph–NH–NSO, whose dimers are both destabilized to approximately the same degree compared to the stability of the unsubstituted dimer. From the studies, and as had been suggested earlier from computational work, it is clear that the C_o–H···O interaction is indeed involved in the hydrogen-bonding network in the dimers of unsubstituted and methyl-substituted Ph–NH–NSO's, based on the characteristic deshielding of the protons that are specifically involved in the hydrogen bond formation. Finally, the experimental ^{1}H NMR results obtained show a remarkable agreement with those obtained from computational work at the density-functional theory level.

Acknowledgments

My first and utmost thanks goes to the Almighty God, whose abundant grace has brought me this far. Without altruistic people around me, this work will not have been complete. I would like to thank all those who have supported me to finish my dissertation. For some of you, it is my heartfelt gratitude to mention your names here.

Above all, I will like to acknowledge my supervisor, Dr. Heidi M. Muchall for all her excellent assistance, support and patience. Without her, this thesis would not have been completed. She has really introduced me to real scientific research.

I am most grateful to Dr. Sébastien Robidoux for all his training and assistance in NMR. I would also like to thank my committee members, Dr. Chris Wilds and Dr. Pat Forgione for their suggestions and valuable comments.

Very special thanks go to my wife, Bernis Zo kone for her kind support, encouragement, and her endless love. I would like to thank my mum, siblings, nephews and nieces for their caring love and support throughout my life. My parent-in laws also deserve my wholehearted thanks. As well, I would like to thank Gifty Gyasi, our acquaintance, for not just taking care of our two kids when our schedules are tight, but also for being there for the family when the need arises. I am extremely grateful to Patrick Appiah, Franco Alo and Michael Antobreh for their advice and encouragements.

I would like to thank Rev. Ellie Hummel, a Chaplain and Coordinator at Multi-faith Chaplaincy and Helen Downie, Loyola Chapel Administrator for not just offering me a position as the Loyola Chapel Student Administrative Assistance but most importantly

for their unwavering love, friendship and kind support. To all the entire Multi-faith Team at Concordia University, I say, thank you for your good interpersonal relationship.

Finally, I would like to thank all past and current group members of Dr. Muchall's group, especially Sima, Martha, François, Irena and the new graduate student, Philippe, and members in CERMM; Soran, Xijun, Chun and more.

Dedicated to my wife, Bernis Zo kone and daughter, Stephanie Bilson Akosua Boateng and my son Stephanos-Kwabena Mighangel Boateng

Table of Contents

List of Figures

List of Schemes

List of Tables

List of Abbreviations and Symbols

2-AEPip	1-(2-aminoethylpiperidine)
AIM	Atoms in Molecules
Anti-H bond	Anti-hydrogen bond
3-APMo	N-(3-amino-1-propyl)morpholine
B3LYP	Becke's three-parameter hybrid exchange/Lee-Yang-Parr-correlation functional
BCP	Bond critical point
δ	Chemical shift
c	Concentration
CP	Critical point
DFT	Density-functional theory
DMPA	3-dimethylamino-l-propylamine
DMSO	Dimethyl sulfoxide
$CDCl_3$	Deuterated chloroform
$\rho(r)$	Electron density
EDA	Ethylenediamine
EDG	Electron-donating group
EWG	Electron-withdrawing group
K	Equilibrium constant
FTIR	Fourier-Transform Infrared
2-GB	2-guanidinobenzimidazole
H-bond	Hydrogen bond

C_o–H	Hydrogen at the ortho position on the aromatic ring
IR	Infrared
$\nabla^2\rho(r)$	Laplacian of the electron density
m.p.	Melting point
m	meta
M	Molar
NIR	Near infrared
NMR	Nuclear magnetic resonance
o2	Doublet signal at the ortho position
o1	Singlet signal at the ortho position
p	para
ppb	Parts per billion
ppm	Parts per million
^{1}H NMR	Proton nuclear magnetic resonance
ν	Stretching vibration
UV/Vis	Ultraviolet/visible

Chapter 1. Introduction

1.1 Background to N-sulfinyl species

The first example of N-sulfinyl species (R–N=S=O) was reported by Böttinger in 1878.[1] However, there was no statement regarding the structure of the compound at that time. Twelve years later, in 1890s, Michaelis and Herz reported the synthesis of N-sulfinyl aniline ("thionyl-aniline", PhNSO) as a product involving the reaction of a primary amine (aniline, $PhNH_2$) with thionyl chloride ($SOCl_2$, Scheme 1.1)[2]. With this, approximately 75 N-sulfinylamines of the type R–NSO with their reactions were further described by Michaelis.[3-6] Thus, Michaelis has provided tremendous contributions to the field, such as structure, properties, reactivity with water, acids and bases, with particular attention to aromatic species, as well as a wide variety of applications of N-sulfinyl species.[3-6]

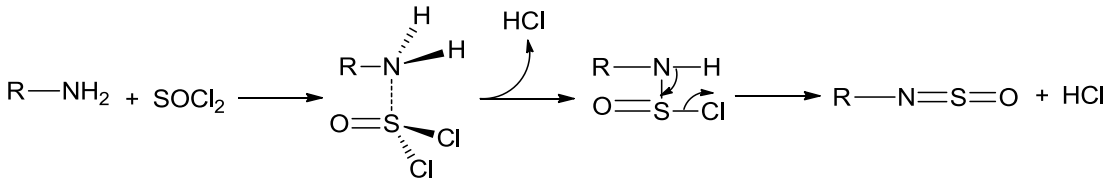

Scheme 1.1 Formation of N-sulfinyl species by reaction of thionyl chloride with amines.[2]

A second efficient route designed to generate N-sulfinyl species is the reaction of N-thionyl aniline (PhNSO) with phenyl hydrazine as shown in Scheme 1.2.[7] In analogy to the formation of N-sulfinylamines, there is a nucleophilic attack of a hydrazine nitrogen atom on the electrophilic sulphur of the N-sulfinylamine[8] as shown in Scheme 1.3.

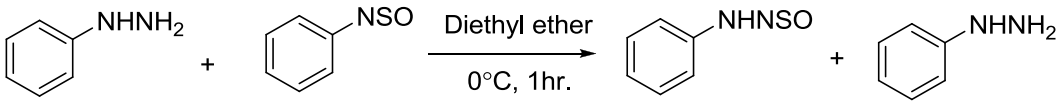

Scheme 1.2 Synthesis of Ph–NH–NSO by reaction of phenyl hydrazine with N-thionyl aniline.[7]

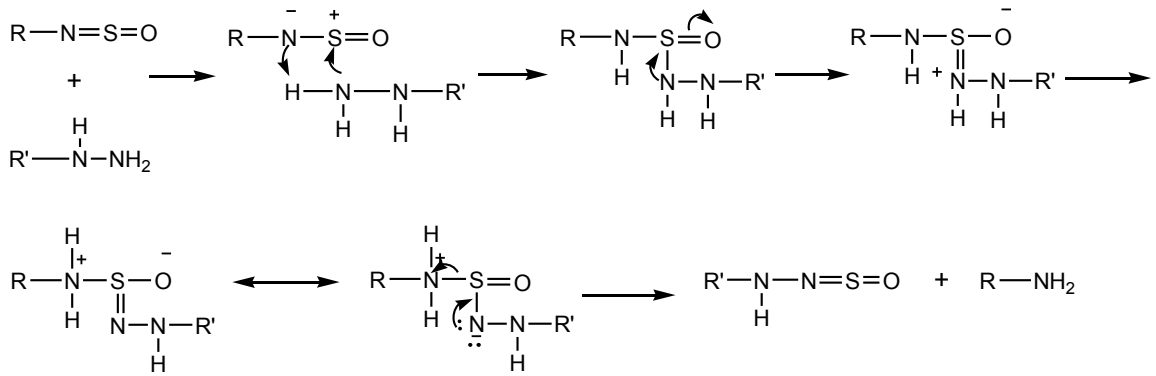

Scheme 1.3 Mechanism of the formation of N-sulfinyl hydrazines.[8]

In spite of the earlier investigation by Michaelis and his associates, less attention has been paid to the class of compounds known as N-thionyl hydrazines. Klamann and his associates reported an approximate 82 % yield from the reaction of phenyl hydrazine with thionyl chloride.[9]

The electronic structure of the N-sulfinyl species is of great interest as multiple resonance structures are possible (Scheme 1.4). The N=S bond is best described as a four electron bond (**I** and **III**).[10] While the SO bond has substantial S^{+}–O^{-} character,[11-16] both Cerioni et al. and Muchall have confirmed its double bond nature through ^{17}O NMR spectroscopic studies.[17,18] The aforementioned findings enable most of the known reactions of N-sulfinyl species to occur across the N=S bond, where the π-bond or both

bonds can break.[10,19] In 1973, Kroner et al. described the N=S=O unit as a cumulated π-system, enabling it to enter into conjugation with an available π-system on the substituent.[20] The bright colours of N-sulfinyl species (PhNSO and PhNHNSO are yellow) are a results of this conjugation.[7,10] Several UV-Vis studies have suggested the excitation of the N=S=O group.[21-24]

With its cumulated double bonds, the N=S=O unit in N-sulfinyl species is similar to sulphur dioxide. The angle on the sulfur atom for both species has been determined to be almost 120°.[25-34]

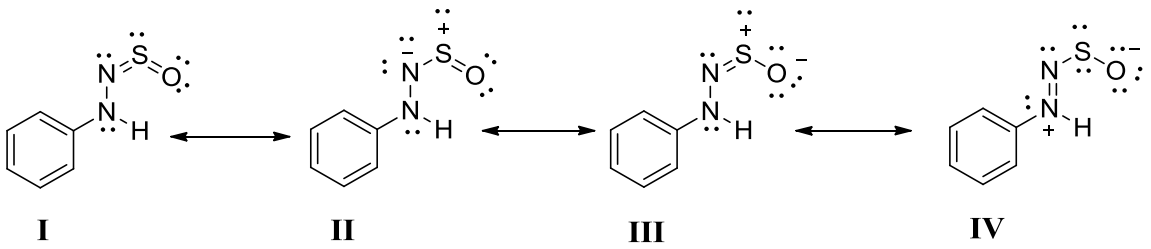

I **II** **III** **IV**

Scheme 1.4 Resonance representations of PhNHNSO, with **I** as the leading structure.

Another area of interest in N-sulfinyl species is their reaction with water, even though there are only a few studies on the hydrolysis of N-sulfinyl species.[10,19,35,36] Depending on the substituent R attached to the N=S=O group (Scheme 1.5), the reactivity of N-sulfinyl species with water varies widely.[10,19,35,36] For example, whereas aliphatic amines (R = Cl) (**I**) reacts explosively with water[35], aromatic amines (**II**) and hydrazides (**III)** hydrolyze more slowly.[10] N-sulfinylhydrazines **IV** and **V** are stable against water.[19,36] Due to their inertness, derivatives of Ph–NH–NSO are considered as a major target for pesticides and crop control agents,[37,38] and some derivatives are also used as prophylaxis against cancer.[24]

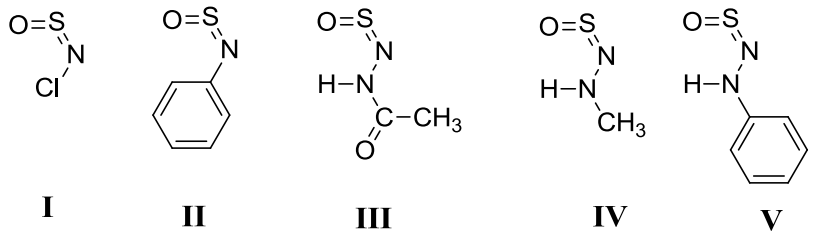

I **II** **III** **IV** **V**

Scheme 1.5 N-sulfinyl species: aliphatic amines (**I**), aromatic amines (**II**), hydrazides (**III**), aliphatic hydrazine (**IV**), aromatic hydrazine (**V**).

In our group, aromatic N-sulfinyl hydrazines have been of long standing interest. The non-linearity of the heterocumulene unit (N=S=O group) leads to *syn*, *sickle* and *anti* configurations and conformations (Scheme 1.6).[39,40]

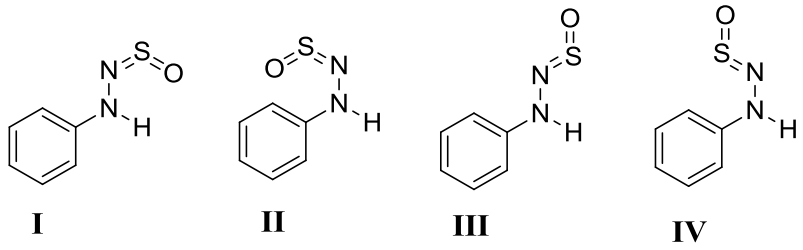

I **II** **III** **IV**

Scheme 1.6 Configurations and conformations of the PhNHNSO monomer: *syn* (**I**), *sickle* (**II**), *anti* (**III** and **IV**).[39,40]

From both experimental[41,42] and computational[39,40] studies, the *syn* form has shown to be the most stable and is responsible for the formation of a hydrogen-bonding network in the dimer of Ph–NH–NSO (Scheme 1.7). In 1977, the first X-ray structure analysis of this compound was performed by Gieren and Dederer.[41] The compound was crystallized from anhydrous ethanol and possesses a monoclinic space group with eight molecules in the unit cell. It was found that the individual *syn*-Ph–NH–NSO molecule is roughly planar

and forms a dimer (Scheme 1.7, **I**) in which the two monomer molecules are linked by two N–H···O=S intermolecular hydrogen bonds with an H···O distance of 213 pm. Furthermore, similar intramolecular interactions of 243 pm were inferred. Thus, it was suggested that both a hydrogen and an oxygen atom operate as a two-fold donor and acceptor, respectively, which results in bifurcated H-bonds as shown in Scheme 1.7 **I**. The same conclusions were drawn in 1984 from neutron diffraction studies.[42]

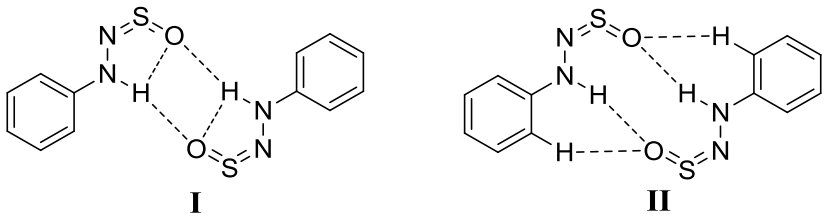

Scheme 1.7 The hydrogen-bonding network in the PhNHNSO dimer, suggested from X-ray and neutron diffraction (**I**)[41,42]and infrared and computational (**II**) studies.[39,40]

The hydrogen-bonding network in Ph–NH–NSO was further analyzed through FTIR (Fourier Transform Infrared) spectroscopy[39,40] and computational studies.[39,40] The FTIR spectra of the neat Ph–NH–NSO showed only one broad absorption band at 3208 cm^{-1} due to an N–H stretch, ν(N–H), from a hydrogen-bonded N–H in the dimer. The dilution spectra showed ν(N–H) bands from both the dimer and the monomer, with the monomer band blue-shifted by about 65 cm^{-1}, pointing to the existence of an association equilibrium. From the invariant position and eventual disappearance of the dimer band, it was concluded that only one dimeric species was present, in solution as in the solid, which ruled out the previously suggested[41,42] intramolecular linkage (Scheme 1.7, **I**).With the use of computed electron densities, it was however found that the oxygen of the

N=S=O group of one monomer can form a blue-shifting hydrogen bond with the ortho hydrogen atom of the aromatic ring of the second monomer, C_o–H···O. In view of this, the alternative hydrogen-bonding network **II** (Scheme 1.7) was suggested.[39,40]

1.2 General introduction to hydrogen bonding

Although weak in comparison to a covalent bond, the hydrogen bond has been known to make a vast difference to the properties of a material, such as in the high boiling point of water, the folding process of proteins, the double-helix structure of DNA and RNA, and also in crystal engineering.[43-46] In organic chemistry, hydrogen bonding is an effect that is seen in the chemistry of alcohols, phenols, acids, amines and other nitrogen compounds and polymers. The involvement of an H-bond in the transition state of a reaction can lead to conformational changes in the transition state and therefore to alternate pathways.[46]

In general, a hydrogen bond is formed when there is an interaction between the hydrogen atom of a group X–H (where X is an electronegative atom with a lone pair of electrons, often called an acceptor, (A)) with a Y atom of another group that has a lone pair of electrons, also called donor (D). The hydrogen bond formed can be represented as X–H···Y.[44] Conventionally, both X and Y can be regarded as F, O, N etc. Due to the polarized nature of the covalent bond X–H, a highly electropositive hydrogen results and the hydrogen atom gets attracted towards a bond formation with the electron rich acceptor (Y). As the bond dipole of X–H and the availability of the electron lone pair on Y increase, the strength of the hydrogen-bonding interaction also increases. Therefore, the strongest hydrogen-bonding interaction can be seen for atoms such as, N, O and F.

The most frequently adopted geometry for hydrogen bonds is a linear or almost close to linear arrangement, which is favoured over bent ones,[47] and linear hydrogen bonds are found to be stronger than those with smaller angles.[44] However, by nature, this linear conformation is not fully achieved due to the constraints of the molecular system, which can lead to distortions.

1.2.2 Conventional hydrogen bonds

The conventional, or proper, hydrogen bond has been thoroughly studied since its introduction into the literature and is well understood.[44,48-50] Formation of such a hydrogen bond is characterized by electron density transfer from an electron lone pair, n_Y, to the antibonding orbital of the proton donor bond, σ^*_{X-H}.[48] The consequence of this is a reduced bond order of X–H with a concomitant lengthening of the bond. In the IR, the band that corresponds to the X–H stretch thus shifts to a lower frequency (red shift), increases in intensity and broadens. The value of the red shift and the strength of the hydrogen bond are usually correlated.[48] Electrostatic forces are mainly responsible for the stability of the conventional hydrogen bond.[51] For most traditional (conventional or proper) hydrogen bonds, nuclei such as ^{13}C, ^{15}N, ^{17}O, ^{19}F and ^{1}H may be observed by NMR spectroscopy.[52,53 54-64] The proton (^{1}H) becomes deshielded in a H-bond, and the downfield shift is often correlated with the length of the interaction.[64] Details of the ^{1}H NMR are addressed in Section 1.3.3.

1.2.3 "Improper" hydrogen bonds

The C–H···O interaction is now well-recognised and has been one of the main topics in weak interaction research, both experimentally[65-72] and computationally.[49,73-77] Its existence was first predicted by Suttor in the 1960s,[78] to much controversy. C–H···O has numerous roles in a wide range of chemical processes, from crystal packing and molecular conformations to supramolecular design.[44,45] For examples, it contributes to the structural stability of proteins.

There are several[79-86] publications regarding the blue shift of the C–H stretching vibration upon interaction and the origin of the shortening of the C–H bond.[80,81] It is known that the consequence of C–H···O formation is a shift to larger frequency (a blue shift) of the C–H stretch due to the shortening of the bond.[39,49,86] Because of this, the interaction was initially called an "anti" and later a "blue-shifting" hydrogen bond.[82,84,86] In addition to the blue shift, which is fairly small in magnitude, the corresponding band loses rather than gains intensity. Dispersion is the main driving force for the stability of the improper hydrogen bond.[51]

The most interesting aspect of this interaction is the C–H donor group. Vibrational spectroscopic data show that the strength of the interaction is dependent on the hybridization of the carbon atom, with an sp-hybridized carbon leading to the strongest C–H···O.[79]

The story of the improper hydrogen bond began in 1989, when the IR spectrum of triformylmethane (TFM) in chloroform showed a noticeable, sharp band (3028 cm^{-1}) near the C–H stretch of chloroform (3021 cm^{-1}); the blue-shifted band was interpreted to arise from the hydrogen-bonded dimer (Scheme 1.8).[80] Other evidence for the formation of a

blue-shifting H-bond has been reported from IR spectra of chloroform, deuterochloroform and bromoform in a mixture of carboxyl, nitro and sulfur compounds.[81] Upon formation of the intermolecular complexes, about 3 – 8 cm^{-1} shifts of the haloform C–H stretching vibration were observed.

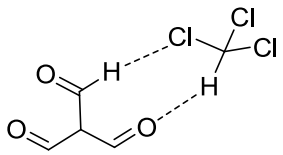

Scheme 1.8 The dimer of triformylmethane and chloroform.

These studies were followed by a first theoretical investigation of the C–H proton donor stretching vibration in the benzene dimer and other C–H donor complexes.[82] In accord with the prior experimental interpretations,[80,81] the benzene dimer showed a shortening of the C–H bond of the proton donor with a blue shift of its corresponding stretching vibration. In addition, Hobza et al.,[84,85] through theoretical studies proposed C–H···O interactions in fluoroform-oxirane complexes, which showed a blue shift of 30 cm^{-1}. The blue shift in the C–H stretching vibration predicted by theory has been confirmed experimentally in the interaction of chloroform with fluorobenzene.[84,85]

As mentioned in Section 1.2.2, the ^{1}H NMR shift of the interacting proton is another useful diagnostic tool for characterizing C–H···O interactions. The resonance of an olefinic proton in α,β-enaminoketones containing a fluoro-substituted alkyl group experiences a downfield shift of about 0.16 ppm upon formation of a hydrogen-bonded dimer (Scheme 1.9).[87] More examples of ^{1}H NMR studies are found in Section 1.4.

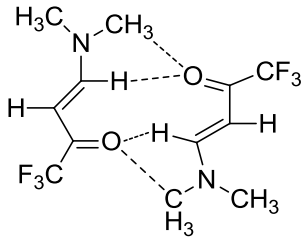

Scheme 1.9 The dimer network in a fluoroenaminoketone.[87]

The electron density, often obtained from electronic structure calculations, is also very important in characterizing hydrogen bonds. Koch and Poplier have proposed eight criteria that can be used for identifying hydrogen bonds, including C–H···O interactions.[88] The first four criteria are based on the H-bonding interaction itself: (1) The presence of a bond critical point (BCP) and a bond path between the donor hydrogen and the acceptor atom. (2) The value of the electron density, $\rho(r)$, at the BCP (0.01 – 0.23 e/Å^3).[44,88] (3) A positive value of the Laplacian of the electron density, $\nabla^2\rho(r)$, at the BCP (0.58 – 3.35 e/Å^5).[89] (4) The mutual penetration of the hydrogen and the acceptor atom. Here the penetration is defined as the difference between the non-bonded and bonded atomic radii. The next four criteria are based on the change in parameters of the hydrogen upon interaction: (5) Loss of electronic charge of the hydrogen atom (0.003 – 0.075 au).[49] (6) Energetic destabilization of the hydrogen atom (0.003 – 0.039 au).[88] (7) Decrease of dipolar polarization of the hydrogen atom (0.008 – 0.038 au).[90] (8) Decrease of the hydrogen atom's volume (2.45 – 13.03 au).[88,90]

In comparison, the use of geometrical parameters in the identification of a C–H···O interaction, (1) covalent bond distance (C–H << H···O), (2) hydrogen bond distance (H···O 2.2 – 3.2 Å), (3) distance between heavy atoms (C···O 3.2 – 4.0 Å) and (4) angle between the three atoms (C–H···O 90 – 150º),[44] seems arbitrary and unreliable.

In conclusion, the C–H···O interaction varies from the regular H-bond in its IR signature but also shares characteristics with the H-bond, such as NMR chemical shifts, (downfield shift of the proton for OH, NH or CH),[91,92] electron density parameters and certain geometric preferences.

1.2.4 Summary of properties of hydrogen bonds

Not surprisingly, there is a continuum between proper and improper H-bonds, in the strength of the interaction and other properties. Very strong H-bonds can resemble covalent bonds, while very weak H-bonds are close to van der Waal's forces. Table 1.1 shows the properties of H-bonds.[44]

Table 1.1 Properties of H-bonds.[44]

	Proper H-bond	Improper H-bond
Example	N–H···O	C–H···O
Bond energy (kcal mol^{-1})	4 – 15	< 4
IR ν shift (%)[a]	10 – 25	< 10
^{1}H downfield shift, Δδ (ppm)	5 – 10[b]	1 – 2[c]
d(H···A) (pm)[d]	150 – 220	200 – 300

[a] Percentage change in the stretching vibration of the covalent bond. [b] Observed by Karger et al.[69] [c] 1.8 ppm observed by Sigalov.[93] [d] "A" is O, N or C.

1.3 Methods for detection of hydrogen bonds

In general, the formation of a hydrogen bond is characterized by a small shift of electron density from the proton acceptor to the donor bond, an $n_Y \rightarrow \sigma^*_{X-H}$ interaction. The methods used to study hydrogen bonds can be grouped as follows: (1) spectroscopy, which comprises of IR and Raman, microwave and NMR; (2) diffraction, which includes X-ray and neutron studies; (3) thermochemistry, which consist of direct calorimetry, and the determination of equilibrium constants and enthalpies; and (4) theory/computation, which includes *ab initio*, density-functional and semi-empirical methods. All of these methods play a critical role by measuring the property that changes upon formation of the hydrogen bond.

In this section, only brief introductions on IR spectroscopy and computational methods (as they are not the focus of this thesis) and some details on NMR spectroscopy will be discussed.

1.3.1 Infrared spectroscopy

Almost all kinds of hydrogen bonds were first discovered through IR spectroscopy. The recognition of hydrogen bond properties, such as strength, geometry and shape of the proton transfer pathway began in the 1930s through the identification of infrared shifts.[94-96] The vibrational frequencies of the system that is involved in the hydrogen bond is affected in various ways; refer to Section 1.2.2 for identification of hydrogen bonds through the use of IR. Near infrared (NIR) spectroscopy also constitutes a beneficial approach in probing the existence of hydrogen bonds. Bands in the NIR are solely due to

overtones or combinations and are therefore isolated and unobstructed, for example, N-H and amide II combination bands of thioacetamides.[97]

1.3.2 Computational chemistry

Theoretical calculations provide a rich source of information concerning hydrogen bonding.[48] For most experimental data, determination of the hydrogen bonds is carried out in solution whereas calculations are often performed on the system of interest in isolation from its surroundings, which allows to probe for intrinsic effects. Concerning the geometry, strength, chemical shifts, the energies of the hydrogen bonds etc., the use of calculations can be very informative and can be addressed directly as compared to spectroscopic studies as such IR and NMR. Quantum chemical investigations on hydrogen bonds are employed using different methods and basis sets. Within density-functional theory, one of the most commonly used methods is the Becke hybrid functional for exchange combined with the correlation functional of Lee, Young and Parr, B3LYP,[98,99] and popular basis sets are based on Pople's 6-31G.[100] In general, a geometry optimization is followed by an analysis of the observable of interest, such as a computed vibrational frequency for comparison with IR data, and a computed chemical shielding for comparison with NMR data. These analyses often require the use of more specialized methods and larger basis sets.

For the detection of hydrogen bonds in controversial cases, and in particular for the detection of C–H···O interactions, the topology of the electron density can be analyzed within the quantum theory of Atoms in Molecules (QTAIM).[101]

1.3.3 Nuclear magnetic resonance spectroscopy

It is probably safe to say that NMR (nuclear magnetic resonance) spectroscopy is one of the most broadly utilized spectroscopic techniques currently available for obtaining detailed information on chemical systems at the molecular level and for studying hydrogen bonding. As mentioned in Section 1.2.2, the ^{1}H chemical shift is a fundamental and informative NMR parameter and so ^{1}H NMR spectroscopy has become the most versatile method used for the direct observation of effects on hydrogen and oxygen atoms for X–H···O systems. Upon formation of a hydrogen bond, the electron density at the proton involved in the hydrogen bond is decreased, and as a result its NMR signal is shifted to a lower magnetic field (downfield).[44,102] The degree of this shift is an indication of the strength of the hydrogen bond. Most hydrogen bonding studies have been performed by monitoring the ^{1}H NMR chemical shift as a function of concentration.

1.4 Examples of ^{1}H NMR studies on hydrogen bonds

Several studies have focused on the investigation of hydrogen bonds through the use of ^{1}H NMR spectra for samples in solution and have revealed the expected downfield shift that is evidenced for hydrogen bond formation. Beyond the mere detection of a hydrogen-bonding interaction, the data can be used for additional insight as given in the following examples.

A series of 1,3-amino, α- and β-naphthols allowed to probe the existence of possible O–H···N or N–H···O inter- and intramolecular hydrogen bonds.[50] Both the OH and NH_2 groups in the system were involved in hydrogen bonding as judged from chemical shift changes of the proton signals. The observed signals for its temperature dependence

showed appreciable changes in the proton chemical shifts. For the OH protons, a strong downfield shift was observed that gave a temperature quotient $\Delta\delta/\Delta T$ of 6.8 ppb, within the range for both intra- and intermolecular H-bonds ($\Delta\delta/\Delta T < 4$ ppb for an intra- and < 7 to 8 ppb for an intermolecular interaction with the OH donor). But as both the OH and the NH_2 protons failed to demonstrate concentration dependent chemical shifts in CD_2Cl_2 solution, intermolecular H-bond formation was ruled out. Based on the experimental and computational data, the presence of intramolecular O–H···N interactions was concluded.

For a series of bi- and poly-functionalized amines, at variable amine concentration in $CDCl_3$ and in DMSO-d_6, it was possible to determine different association behaviour.[103] Thus, while 2-AEPip (**I**), DMPA (**II**) and EDA (**III**) formed hydrogen bonded dimers, histamine (**IV**), 2-GB (**V**) and 3-APMo (**VI**) formed intramolecular, six-membered rings (Scheme 1.10). The authors were able to distinguish between the two different kinds of aggregates based on the fact that there was practically no change in δ(N-H) for histamine, 2-GB and 3-APMo over the range of concentrations, whereas δ(N-H) for 2-AEPip, DMPA and EDA showed substantial concentration dependence with a broad signal.

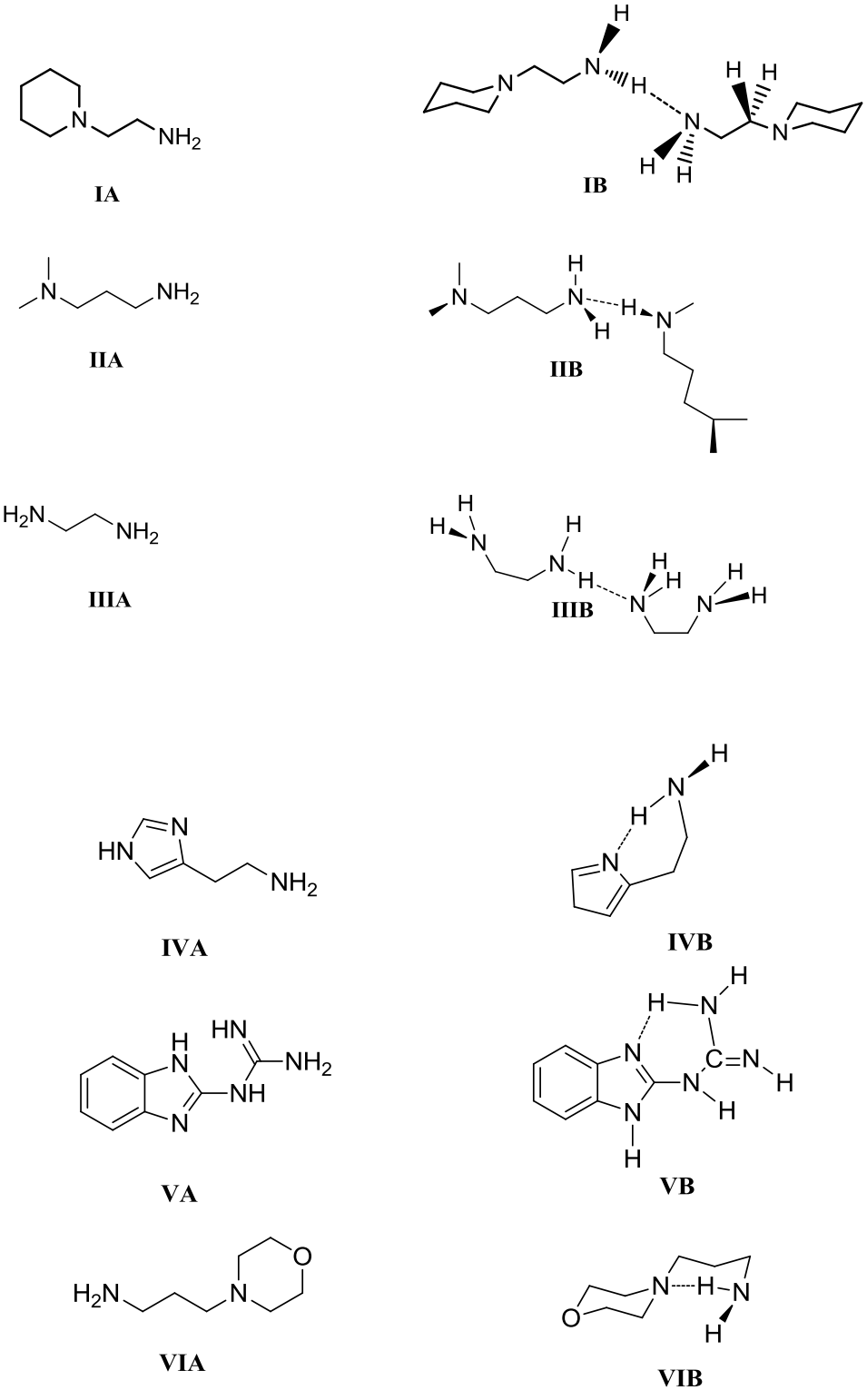

Scheme 1.10 Polyamines; monomer A with its corresponding dimer B.[103]

For the intermolecularly hydrogen-bonded 2-pyridone acid dimer (Scheme 1.11 **I**) in $CDCl_3$ solution, a very strong deshielding for both the carboxylic and the amide hydrogen was observed in their ^1H NMR spectra.[104] Through the information gathered from the ^1H NMR studies, the authors determined the dimerization constant of the system, which exceeded 10^4 M^{-1}. This value was suggested to be very large in comparison with similar studies conducted on dipyrrinones (Scheme 1.11 **II**), with K estimated between 11,600 – 28,700 M^{-1}.[105]

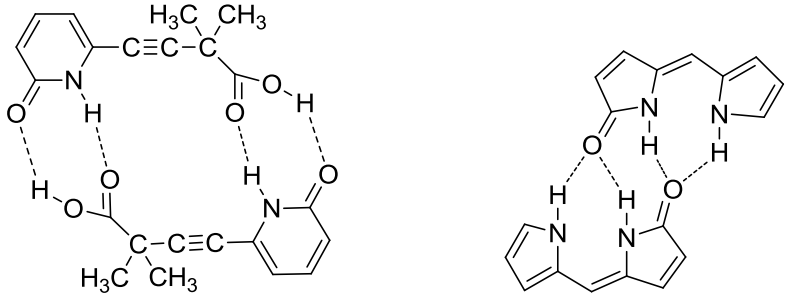

I **II**

Scheme 1.11 Intermolecularly H-bonded dimers. Pyridone acid (**I**),[104] dipyrrinone (**II**) dimer.[105]

Karger et al. investigated C–H···O interactions in 4-methoxybenzaldehyde. The concentration dependence of the proton chemical shift was on the order of tenths of ppm, which was far below that found for conventional hydrogen bonds, 5 – 10 ppm.[69] While the authors argued that a valid conclusion could not be drawn from the ^1H data because the observed changes were in the magnitude of the benzene ring anisotropy effect, additional ^{17}O NMR data and theoretical calculations confirmed the C–H···O interaction.

The presence of C–H···O interactions from aromatic rings in bindone and its analogues has been inferred from experimental and calculated NMR chemical shifts.[93] Upon formation of a hydrogen bond, a downfield shift of 1.8 ppm was observed for the proton that is believed to be involved in the hydrogen bonding. The observed downfield shift also corroborated results obtained through quantum mechanical calculation.

Closely related to the matter of the present study on intermolecular hydrogen bonds is the work on a fumaramide in DMSO-d_6.[106] The fumaramide ester exhibits both N–H···O and C–H···O interactions (Scheme 1.12) in solution and in the solid state, as demonstrated through the qualitatively similar deshielding curves (Fig. 1.1). Again, the magnitude of the H_a deshielding from the C–H···O interaction is only a fraction of that of H_{anti} within its stronger N–H···O interaction.

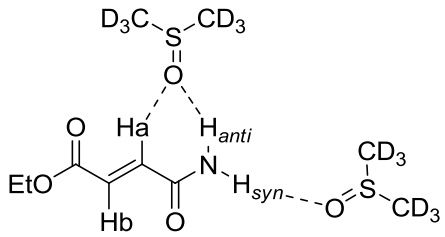

Scheme 1.12 N–H···O Hydrogen bonding between a fumaramide and DMSO-d_6 with a concurrent C–H···O interaction to H_a.[106]

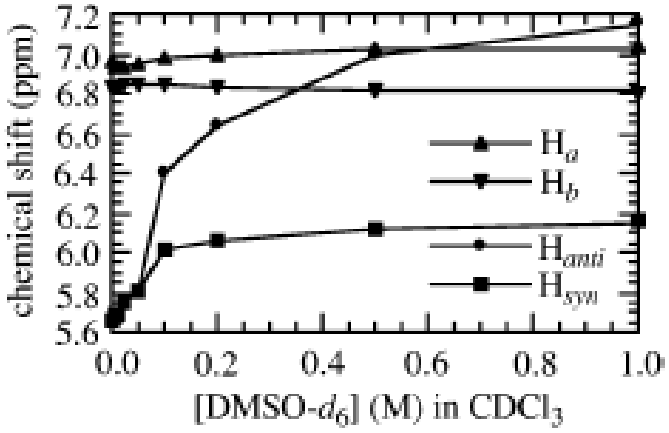

Fig. 1.1 ^{1}H NMR chemical shift data for alkene (tentative assignments) and amide hydrogen of $Et_2OC\text{-}CH_b{=}CH_a\text{-}CONH_2$ in $CDCl_3$ solution containing varying concentrations of DMSO-d_6.[106]

The temperature dependence of a proton chemical shift can be used in the investigation of hydrogen bonds.[107] In particular, the (N)H chemical shifts of amides as a function of temperature has drawn much scrutiny.[108-113] In general, the observed absorption peak shifts upfield (to higher field) as the temperature is increased, because the hydrogen bond is weakened.

The extent of exposure of the hydrogen bond atoms to solvent is captured by the temperature coefficient, $\Delta\delta/\Delta T$. Less negative temperature coefficients are characteristic of strong hydrogen bonds when different types of hydrogen bonds are considered. Temperature coefficients are not addressed in this thesis.

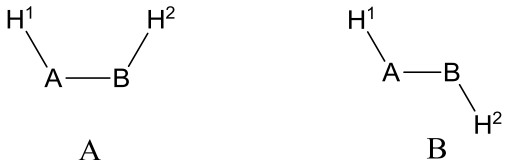

Scheme 1.13 Hypothetical representation of two rotamers, A and B.

Finally, the temperature dependence of torsional equilibria should be addressed. Dynamic NMR spectroscopy provides information about changes in the nuclear environment from the observation of spectra at variable temperature.[113] For the two hypothetical rotamers A and B (Scheme 1.13), the torsional barrier dictates the temperature dependence of the spectra. If there is no rotation about the A–B bond, the two molecules and their ^{1}H NMR spectra are distinct. In contrast, if there is free (fast) rotation about the A–B bond, only an averaged ^{1}H NMR spectrum is observed. In general, the two rotamers are not of equal energy, and the chemical shift and the coupling constant are the result of the population-weighted averages that depend on the fractional populations of species A and B. For an intermediate situation in the size of the torsional barrier, the individual spectra can often be frozen out through a lowering of the temperature. Figure 1.2 illustrates the changes in spectra that can be expected for changes in the ratio of chemical shift difference, $\Delta\nu$, to coupling constant, J.[114] For a sufficiently large ratio, the chemical shift of each proton is observed at the centre of each doublet. For small ratios, the chemical shifts are nearer to the inner lines.

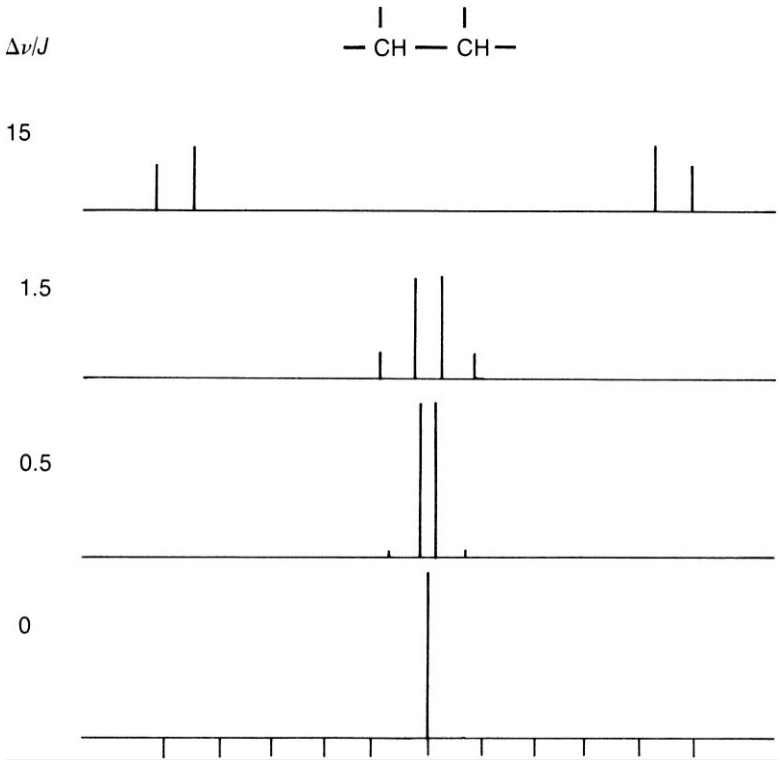

Fig. 1.2 Splitting pattern of a two-proton system HA–BH for various ratios of chemical shift difference (Hz) to coupling constant (Hz), Δν/J. Modified from ref. 114.

1.5 Dimerization constant

Molecules with functional groups such as NH or OH (and maybe CH) in the appropriate configuration can self-associate in cyclic, hydrogen-bonded dimers. Whereas acyclic amides would show hydrogen-bonded polymers, Scheme 1.14 illustrates such dimerization for a cyclic amide in dilute solution.[115-117]

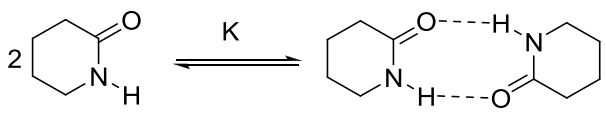

Scheme 1.14 Dimerization equilibrium for 2-piperidone (δ-valerolactam).[117]

The dimerization constant K in Scheme 1.14 can be obtained from the chemical shift difference between the monomer M and the hydrogen-bonded dimer D, and the slope of the concentration dependence at $c_M = 0$ and can be written as in Eq. 1.[118,119]

$$(d\delta/dc_M)_0 = 2\ K\ (\delta_D - \delta_M) \qquad \text{Eq. 1}$$

Here $(d\delta/dc_M)_0$ is the initial slope from the concentration-dependent chemical shift graph, and δ_M and δ_D are the chemical shifts of the monomer and the dimer, respectively. The derivation of Eq. 1 is shown in Appendix A.

Through near-IR spectroscopy, the dimerization constant for δ-valerolactam (Scheme 1.14) was found to be 2.3 M^{-1},[120] while that for the smaller, 5-membered ring γ-butyrolactam in $CDCl_3$ was 5.2 M^{-1} from NMR studies.[121] In general agreement with these values, lactams in $CHCl_3$ are summarized to possess dimerization constants of 1 – 3 M^{-1}.[120]

1.6 Substituent effects

The effect of substituents on covalently bonded systems has been well known for decades and has found wide application in organic chemistry.[122,123] The introduction of substituents can result in structural and reactivity changes in organic molecules and these can contribute to the understanding of chemical mechanisms as well as the establishment of many chemical theories such as the strength of hydrogen bonds, changes in chemical shifts, energies, geometries and more. These changes depend on the position and the

nature of the substituent. In contrast, very little is known about the effect of substituents on hydrogen bonding interactions or dimerization.

For aromatic systems, Hammett parameters show how meta and para substituents on the aromatic ring affect the reactivity of a side chain functional group.[122,124] However, the use of Hammett constants is not necessarily straightforward as inductive and resonance effects need to be considered, evaluated and separated. Alkyl groups as substituents, for example, are inductively electron-donating, whereas substituents such as NO_2 and OCH_3 are inductively electron-withdrawing but have contrasting resonance effects. As only the methyl group, located close to the hydrogen atom as Hammett substituent, was used in this thesis research, these substituent effects are not presented in more detail.

Kim and associates have investigated the effect of alkyl substituents on the hydrogen bond formation between a proton donor thioacetamide and a tertiary amide as a proton acceptor in CCl_4 through the use IR, NIR and ^1H NMR spectroscopies, and theoretical methods.[97] Studies in the IR and NIR revealed an increased stability of the hydrogen bonding upon introduction of a bulky substituent, which was confirmed through the temperature dependence in the NMR. Through computational studies, Chen et al. showed how both inductive and resonance effects affect the hydrogen bonding between substituted X−C≡C−H and NH_3, H_2O and HF systems.[125]

The effect of substitution on hydrogen bonding has also be investigated on Watson-Crick base pair.[126] The authors computed the interaction energy as the energy difference between the complex and the total of the isolated monomers and determined that the stability of the AU base pair is enhanced through the introduction of electron-

withdrawing groups into uracil. More examples of substituent effects on hydrogen bonds are presented in Chapter 4.

Chapter 2. Objectives and organization of Chapters 3 and 4

During the course of our experimental (FT-IR) as well as computational vibrational studies on aromatic Ph–NH–NSO, which, mainly through N–H···O interactions, can form hydrogen-bonded dimers, it became necessary to gather information to confirm the involvement of the ortho protons (C_o–H···O) in the H–bonding network. As the C–H···O interaction is weak and FT-IR studies are thus not practical, experimental ^{1}H NMR spectroscopy, which can reveal the C_o–H···O interaction due to deshielding of the proton that occurs upon H-bond formation, is employed as the main method in these studies. Three main selected compounds, namely unsubstituted Ph–NH–NSO, m-CH_3-C_6H_4–NH–NSO and p-CH_3-C_6H_4–NH–NSO (Scheme 2.1) are investigated.

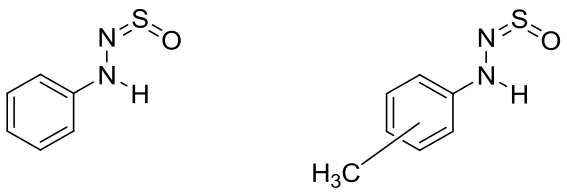

Scheme 2.1 The N-phenyl-N'-sulfinylhydrazines studied (CH_3 in meta- and para-position)

The overall objectives of this research work are to demonstrate the participation of both N–H···O and C_o–H···O interactions in dimers of aromatic N-sulfinylhydrazines (Ph–NH–NSO's) and to determine any methyl-substituent effect on these weak interactions. All three compounds are first to be synthesized from commercially available starting materials, and purified, according to literature procedures.

Experimental ^{1}H NMR analysis is to be conducted on the unsubstituted Ph–NH–NSO to confirm the existence of N–H···O and C_o–H···O interactions. For this, ^{1}H NMR spectra are to be determined at various concentrations, from the detection limit to the solubility limit. From the observed change in chemical shift of the N–H and ortho-C–H protons, the dimerization constant for formation of the hydrogen bonded dimer will be determined. The other protons on the aromatic ring will be monitored for comparison. The experimentally obtained chemical shifts for the protons in the Ph–NH–NSO monomer and dimer will be compared to those obtained from a computational study.

To determine a possible substituent effect on the strength of the H-bonding network, the two methyl-substituted N-sulfinylhydrazines are to be subjected to ^{1}H NMR spectroscopic analysis and interpretation as outlined above for the unsubstituted compound. As all dimerization events in solution to be studied are equilibria, ^{1}H NMR temperature studies will be carried out where necessary for interpretation.

This thesis is based on two main manuscripts, whose abstracts are given below. The first manuscript is based on the study of the unsubstituted N-phenyl-N'-sulfinylhydrazine, the second on those on the substituted species. The manuscripts are presented in Chapters 3 and 4.

2.1 Proof of principle: Evidence of C_o–H···O interactions in N-phenyl-N'-sulfinyl-hydrazine (Ph–NH–NSO) dimers through proton magnetic resonance spectroscopy

To be submitted: Journal of Physical Chemistry A

Authors: Stephen Boateng, Martha N. Kariuki and Heidi M. Muchall

Contribution by S.B.: Carried out all experimental work and analyses of all computational data

Contribution by M.K.: Carried out computational studies

Abstract

Proton magnetic resonance spectroscopy has been used to verify the presence of C_o–H H···O interactions in the hydrogen-bonded dimer of N-phenyl-N'-sulfinylhydrazine (Ph–NH–NSO). A plot of chemical shift of the ortho-protons versus the concentration, from the limit of solubility to the limit of detectability, illustrates a similar dependence than that for the N–H proton, which is involved in a regular N–H···O interaction. In contrast, and as an internal standard, protons in meta- and para-positions exhibit an entirely different and smaller change in chemical shift, consistent with a change in magnetic susceptibility of the solution, and are not involved in interactions between two Ph–NH–NSO. Chemical shifts derived from chemical shielding computed at the density-functional theory level (OPBE/6-311++G(2df,pd)//B3LYP/6-31+G(2d,2p)), for the Ph–NH–NSO monomer and dimer are in good agreement with the experimental results. Thus, N–H···O (a hydrogen bond) and C_o–H···O (a blue-shifting hydrogen bond) interactions both contribute to the stabilization of the Ph–NH–NSO dimer. In contrast to

their opposing behaviour in the infrared, i.e., red versus blue shift, respectively, of the X–H stretching vibration upon hydrogen bonding, their behaviour as probed through proton magnetic resonance spectroscopy, i.e. a deshielding of the X–H proton upon hydrogen bonding, is identical.

2.2 Meta- and para-methyl substituted N-phenyl-N'-sulfinylhydrazines (Ph–NH–NSO): Proton magnetic resonance spectroscopic studies into the network of their hydrogen-bonded dimers

To be submitted: Journal of Physical Chemistry A

Authors: Stephen Boateng, Martha N. Kariuki and Heidi M. Muchall

Contribution by S.B.: Carried out all experimental work and analyses of all computational data

Contribution by M.K.: Carried out computational studies

Abstract

Dilution studies at room and low temperature, using proton nuclear magnetic chemical shifts, were carried out on meta- and para-methyl substituted Ph–NH–NSO, to determine the nature of the hydrogen-bonding network in the dimer and any substituent effects arising from methyl substitution. The concentration dependence for the proton resonances confirm that both N–H···O and C_o–H···O interactions contribute to the stabilization in the dimers, as suggested previously from computational studies and in accord with the hydrogen-bonding network in the unsubstituted dimer. A slight substituent effect on the dimerization constant was detected as compared to the unsubstituted Ph–NH–NSO, suggesting that the remote methyl groups destabilize the dimers. Protons other than N–H and C_o–H do not participate in the dimer formation.

Chapter 3. **Proof of principle: Evidence of C_o–H···O interactions in N-phenyl-N'-sulfinyl-hydrazine (Ph–NH–NSO) dimers through proton magnetic resonance spectroscopy**

3.1 Introduction

It has been demonstrated that N-phenyl-N'-sulfinylhydrazines (Ph–NH–NSO) can form hydrogen-bonded dimers when unsubstituted in ortho–position (Scheme 1.7, Chapter 1).[39-42] Network **I**, which was proposed initially from diffraction data,[41,42] exhibits four N–H···O interactions, which comprises of two inter- and two intramolecular H-bonds. This network was conceived from the general idea that the N–H donor group can readily form hydrogen bonds with the nearby oxygen atom. However, computational studies have suggested network **II** with the participation of N–H···O and C_o–H···O interactions, from an ortho-H atom on each aromatic ring.[39,40]

In a recent experimental FTIR study, it has been shown that only one broad absorption band at 3208 cm^{-1} due to ν(N–H) of the dimer was observed in the spectrum of the neat Ph–NH–NSO.[39] In contrast, bands from both dimer and monomer were present in dilute solution spectra due to the existence of a dissociation equilibrium. The ν(N–H) band of the dimer was red-shifted from that of the monomer by about 65 cm^{-1} and disappeared gradually (with constant position) and completely for high dilutions. In this respect and with regard to the H-bonding network in the unsubstituted Ph–NH–NSO, it was concluded that only one dimeric species (with four intermolecular interactions) exists in solution.[39] This of course was in agreement with the diffraction studies,[41,42]

however, evidence for a weak intramolecular linkage as suggested in **I** was not found, which lent support for network **II**.

To further support network **II**, it remains to find experimental evidence for the C_o–H···O interaction. IR spectroscopy, however, is not an ideal technique to demonstrate C–H involvement in the hydrogen bonding network, because of the comparatively small size of the blue shift (38 cm^{-1} calculated from B3LYP/6-31+G(d))[39] and the complexity of the aromatic C–H stretching region in the absorption spectra. ^{1}H NMR dilution studies, on the other hand, are expected to reveal the C–H···O interaction because of the deshielding of the proton that occurs upon hydrogen bond formation.[44,50,69,93,102,104,106]

In particular relevance to the proposed interactions within network **II**, an NMR titration study of a fumaramide with DMSO-d_6 suggested bifurcated H-bonds on the DMSO oxygen (Scheme 1.12).[106] An about 1.5 ppm downfield shift for the amide proton involved in the bifurcated H-bond was accompanied by an about 0.1 ppm downfield shift for the olefinic C–H involved with the same DMSO oxygen (Fig. 1.1).

Herein we present the dilution behaviour of Ph–NH–NSO using ^{1}H NMR. The purpose of this present study is to investigate the presence of a C_o–H···O interaction in the dimer of the unsubstituted Ph–NH–NSO. The experimental data are interpreted with the help of chemical shifts obtained from computational studies.

3.2 Experimental and computational details

The procedure for the preparation of Ph–NH–NSO is derived from the transsulfinylation previously described and as shown in Scheme 1.2.[7] N-thionylaniline and phenyl hydrazine were procured from Sigma Aldrich and Alfa Aesar, respectively, and were

used without further purification. Solvents and reagents used were of analytical grade. The pure, bright yellow crystals were obtained by recrystallization from anhydrous ethanol. Details on the synthesis and characterization can be found in Chapter 6.

Ph–NH–NSO was studied in deuterated chloroform ($CDCl_3$) solution from the limit of detectability in dilute solution to the solubility limit. The chemical shifts were recorded in the concentration range of 0.005 – 1.2 M. All ^{1}H NMR spectra were recorded at room temperature (25 ºC) using a Varian 500 NMR spectrometer. A 5-mm probe was used and the spectra were referenced to tetramethylsilane (TMS). Data were determined from three independent experiments. All chemical shifts, δ in ppm downfield from TMS, are the average of at least 32 scans.

All calculations were performed using the Gaussian 09 package.[127] The geometries of the *syn* monomer and the hydrogen-bonded dimer were optimized without symmetry constraints, using the Becke three-parameter exchange functional[98,99] with the Lee-Yang-Parr correlation functional (B3LYP)[128] and the 6-31+G(2d,2p) basis set. B3LYP has been shown to perform well in similar H-bonding studies,[129-132] and has been employed in our previous work on the Ph–NH–NSO dimer.[39] We chose the polarized basis set for its flexibility with respect to the description of the hydrogen atoms. Monomer and dimer geometries were confirmed as minima from vibrational frequency analyses at the same model chemistry. The proton isotropic shieldings (σ_{iso}) were obtained from the B3LYP optimized geometries using the OPBE functional (Handy's OPTX[54] combined with the Perdew-Burke-Ernzerhof PBE[133] functional) and the larger 6-311++G(2df,pd) basis set, as OPBE has been shown to give a superior performance for magnetic shieldings and chemical shifts compared to other popular density-functional methods.[134] The OPBE/6-

311++G(2df,pd)//B3LYP/6-31+G(2d,2p) combination has been shown to perform well in the calculation of ^{17}O isotropic shieldings, including that of Ph–NSO with its intramolecular C–H···O interaction.[18] We employed the gauge including atomic orbitals (GIAO)[135-137] method and report the chemical shifts, δ in ppm downfield from tetramethylsilane (σ_{iso} for the proton is 31.51 ppm from OPBE/6-311++G(2df,pd)// B3LYP/6-31+G(2d,2p)).

3.3 Results and discussion

3.3.1 The N–H···O interaction

The room-temperature (25 °C) ^1H NMR spectra for the most concentrated (1.2 M) and diluted (0.005 M) solutions in the N–H region are shown in Fig. 3.1. As expected, the spectra for each of the serial dilutions display one signal for the N–H proton only, and the position of the signal is concentration dependent due to the shift in the monomer-dimer equilibrium. The average of three N–H chemical shifts, δ(N–H), measured at different concentrations in $CDCl_3$, are reported in Table 3.1, and the table data are plotted in Fig. 3.2.

The change in chemical shift as shown in Table 3.1 is a clear indication of the shift of the monomer-dimer equilibrium and the extent of hydrogen bonding. As can be inferred from the data and the plot (Fig. 3.2), δ(N–H) at high concentration corresponds (mostly) to the hydrogen-bonded, dimeric species, whereas the value at the lowest concentration reflects mostly the non-hydrogen-bonded, free Ph–NH–NSO monomer.

Qualitatively, Fig. 3.2 is similar to that for an amide hydrogen undergoing an N–H···O interaction, for example in fumaramides as shown in Fig. 1.1. The correlation coefficient of the fitted curve in Fig. 3.3 shows an excellent fit.

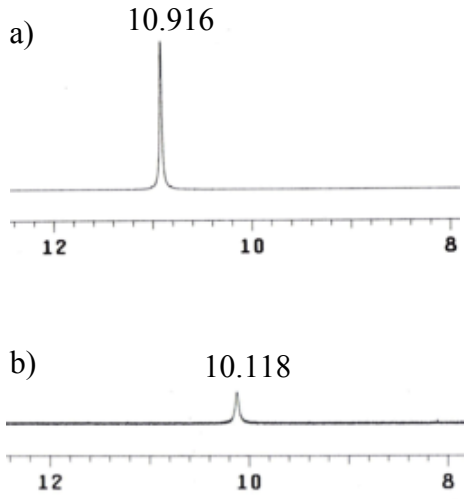

Fig. 3.1 ^{1}H NMR spectra of Ph–NH–NSO in the N–H region for a) 1.2 and b) 0.005 M in $CDCl_3$.

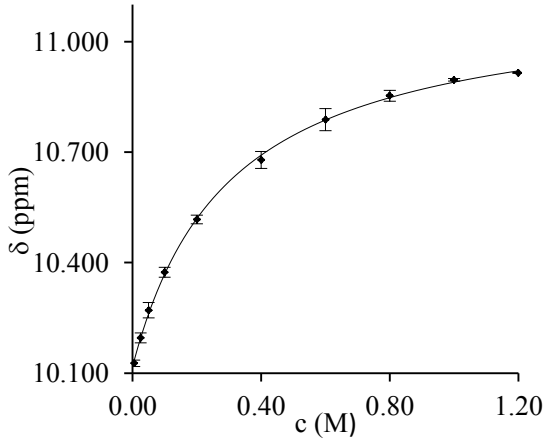

Fig. 3.2 Concentration dependence of the N–H proton resonance of Ph–NH–NSO in $CDCl_3$ (average from three experiments). R^2 for the fitted curve is 0.999.

Table 3.1 N–H and C–H chemical shifts (ppm) for varying concentrations (M) of Ph–NH–NSO in $CDCl_3$.

c	δ(N–H)	δ(ortho C–H)	δ(meta C–H)	δ(para C–H)
1.200	10.915	7.287	7.328	7.073
1.000	10.896	7.285	7.328	7.073
0.800	10.853	7.284	7.339	7.074
0.600	10.788	7.285	7.349	7.087
0.400	10.679	7.282	7.362	7.102
0.200	10.517	7.273	7.373	7.117
0.100	10.374	7.261	7.381	7.122
0.050	10.271	7.251	7.382	7.125
0.025	10.196	7.244	7.384	7.128
0.005	10.127	7.236	7.387	7.130

Nuclear magnetic resonance has been extensively applied for the study of hydrogen-bonding equilibria, and the chemical shifts can be used to estimate the equilibrium constant. As dimer formation for Ph–NH–NSO is driven by the N–H···O interactions (Scheme 1.7, Chapter 1), Fig. 3.2, with its dependence of the N–H chemical shift on the concentration, allows to establish a measure of the strength of the hydrogen bond network in the dimer through the determination of the equilibrium (dimerization or association) constant, K, for dimer formation using the ^{1}H NMR data, specifically the chemical shift for the monomer and dimer, and the limiting slope. The dimerization constant is calculated, as proposed by Schoolery,[118] as

$$(d\delta/dc_M)_0 = 2K\,(\delta_D - \delta_M),$$

where $(d\delta/dc_M)_0$ is the limiting slope and $(\delta_D - \delta_M)$ is the change in chemical shift, $\Delta\delta$, between dimer (δ_D) and monomer (δ_M). The chemical shifts are the proton chemical shifts obtained from the equation for the fitted curve in Fig. 3.2.

To determine δ_D and δ_M, the equation $y = y_0 + a \cdot x/(b+x)$ was employed. Here (Fig. 3.2), $y_0 = 10.1181$, $a = 1.0024$ and $b = 0.2990$. From this, the data points for infinite dilution and concentration can be obtained. For $x \approx 0$, the monomer shift, δ_M, approaches 10.118 ppm, and for $x \approx \infty$, the dimer shift, δ_D, approaches 11.121 ppm. The chemical shifts for monomer and dimer are summarized in Table 3.2.

The equilibrium constant thus calculated is 1.7 M^{-1} (Table 3.2). Figure 3.2 suggests that the chemical shift at the infinite limit might be overestimated. If this chemical shift rather is assumed to be 11 ppm, the calculated K changes to be 1.9 M^{-1}. In either case, the two values of K fall in line with the earlier determined self-association constants for dimer formation of cyclic amides (lactams).[120] From near-IR spectra, the dimerization constants for lactams were determined to be between 1 and 3 M^{-1} in $CHCl_3$.[120] Since lactams with their *cis* arrangement of N–H and C=O functionalities form hydrogen-bonded dimers quite related to those studied here, this agreement is not entirely unexpected but welcome.

Table 3.2 Selected experimental ^{1}H chemical shifts δ (ppm) for the Ph–NH–NSO monomer and dimer in $CDCl_3$, obtained as described in the text, initial slope and derived equilibrium constant, K.

nucleus	M	D	Δδ	$(d\delta/dc_M)_0$	K
N–H	10.118	11.120	1.002	3.346	1.67[a]
ortho C_o–H	7.233	7.292	0.059	0.562	4.76.[b]

[a] The regression from Fig. 3.2 is $y = y_0 + a \cdot x/(b+x)$, with y_0 10.110, a 1.025 and b 0.406.

[b] The regression from Fig. 4.4a is $y = y_0 + a \cdot x/(b+x)$, with y_0 7.128, a 0.060 and b 0.118.

3.3.2 The C_o–H···O interaction

In analogy to the identification of a regular hydrogen bond, a favourable C–H donor within a molecule can be identified by ^{1}H NMR spectroscopy through the well-defined change in chemical shift of the proton when it becomes involved in a C–H···O interaction. The ^{1}H NMR spectra of Ph–NH–NSO in the aromatic region at the solubility limit (1.2 M) and the limit of detectability in dilute solution (0.005 M) are given in Fig. 3.3. Table 3.1 lists the chemical shifts of the aromatic protons for the serial dilution in $CDCl_3$. The data indicate that signals for protons in both meta- (C_m–H) and para- (C_p–H) positions shift upfield as the concentration increases. This concentration dependence is plotted in Fig. 3.4 (a and b). The changes presumably reflect a change in the susceptibility of the solution upon dilution (but see Section 3.3.3 for further discussion).

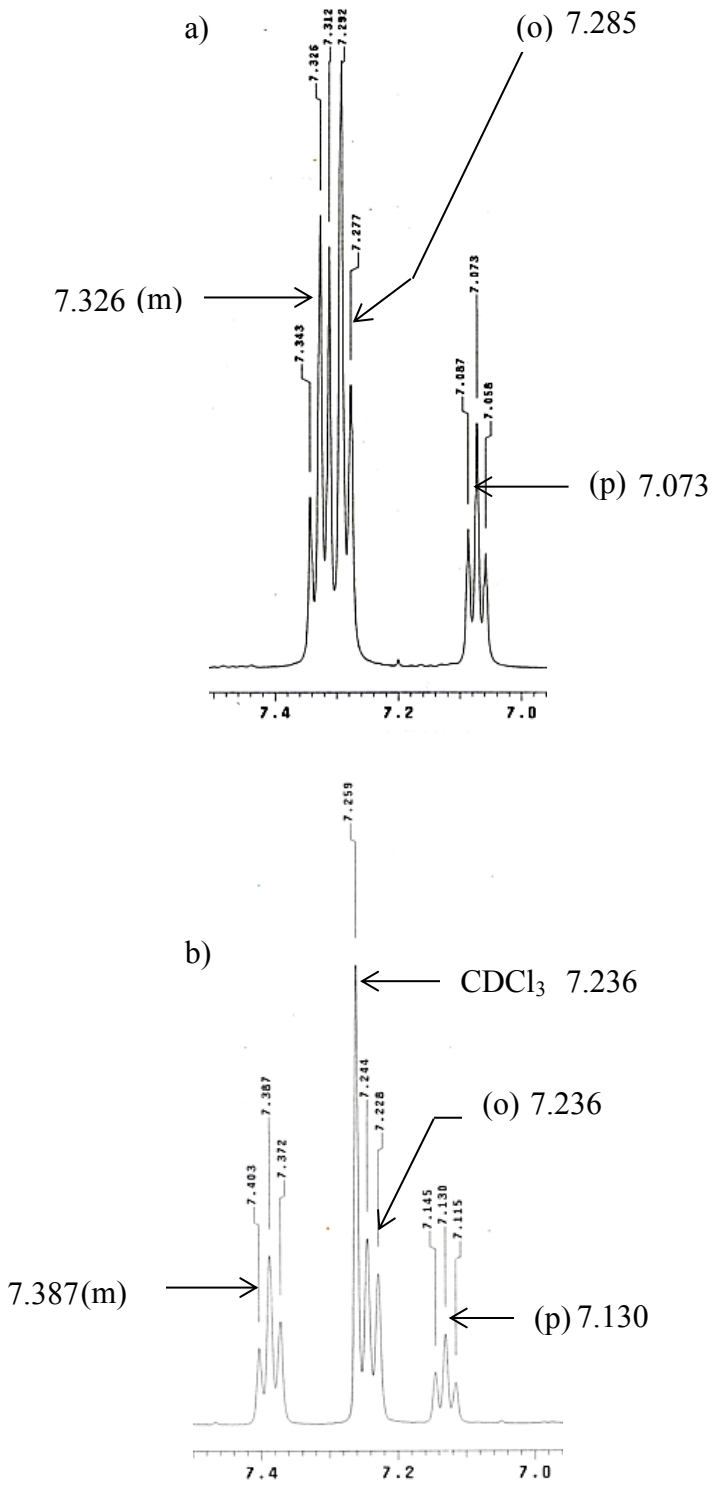

Fig. 3.3 ^{1}H NMR spectra of Ph–NH–NSO in the aromatic region for a) 1.2 and b) 0.005 M in $CDCl_3$. The centers of the signals are given in large labels for clarity.

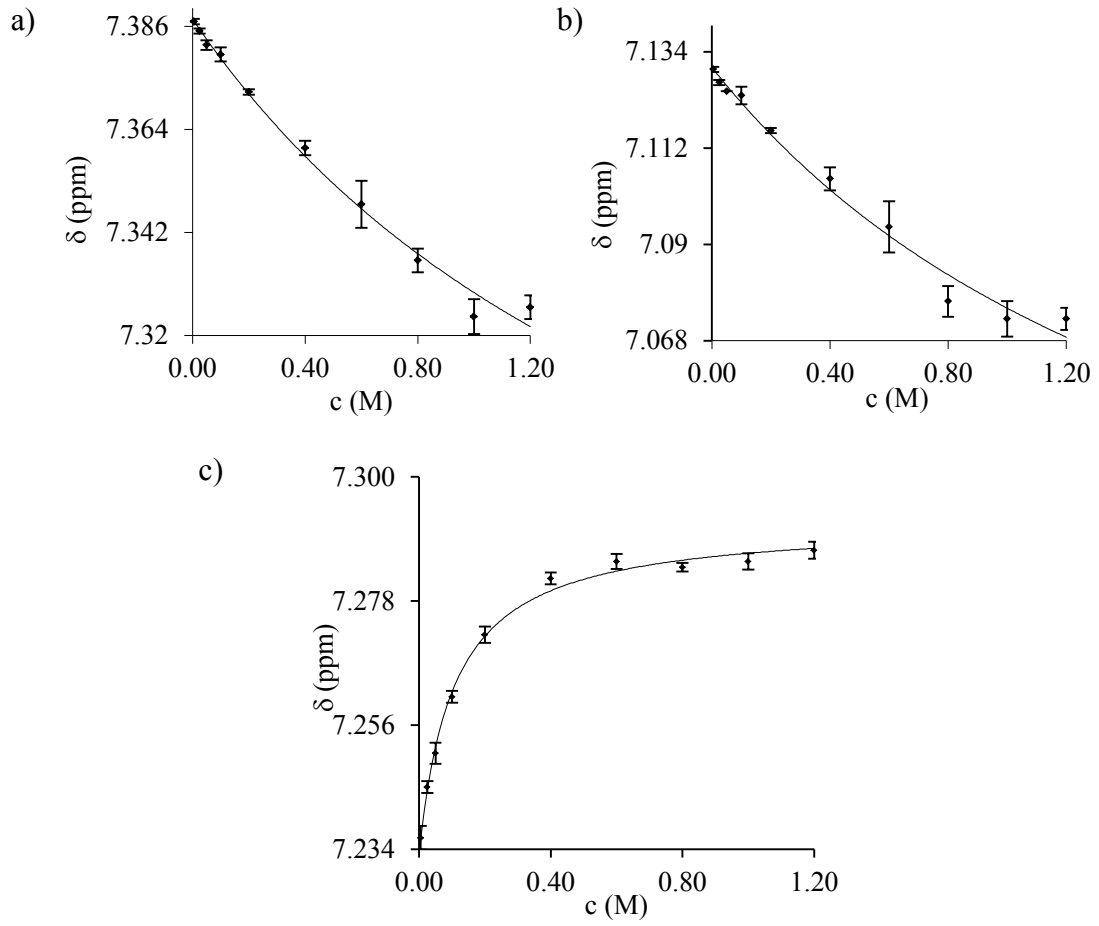

Fig. 3.4 Concentration dependence of the a) meta b) para and c) ortho C–H signal of Ph–NH–NSO in $CDCl_3$ (average from three experiments). R^2 for the fitted curve in c) is 0.995.

In contrast, the ortho-proton signal exhibits a downfield shift upon an increase in concentration (Fig. 3.4c), in analogy to the chemical shift change for the proton on nitrogen (see Section 3.3.1) that was already shown to be involved in hydrogen bonding through IR spectroscopy.[39] Therefore, this characteristic downfield shift is believed to corroborate the involvement of the C_o–H bond in the hydrogen bonding network of the Ph–NH–NSO dimer, as has been predicted from an analysis of the electron density using

the quantum theory of atoms in molecules,[39] with the O=S unit as H-bond acceptor for both N–H and C–H bonds, and as given in network **II** (Scheme 1.7).

Compared to the change in N–H chemical shift, the change for C_o–H is much smaller (Fig. 3.3c and Table 3.2), in accord with the computed values (see Section 3.3.3). While the observed changes from Figs. 3.2 and 3.3c are conceptually similar, they are qualitatively different. Notably, the initial slope in Fig. 3.3c (0.562 ppm/M) is much less steep than that in Fig. 3.2 (3.346 ppm/M). Whereas the change in local environment of the N–H proton giving rise to Fig. 3.2 is simple in that it only consists of the dimer formation, that of the ortho C–H proton involves a pre-dimerization equilibrium. In the Ph–NH–NSO monomer, torsion about the C–N bond leads to the interconversion of the two ortho C–H bonds. And although the equilibrium involves two indistinguishable rotamers, the two ortho protons find themselves in two distinct chemical environments, with one expected to be more deshielded due to the proximity of the N=S=O π-system. Because at low concentration the solution consists to a large degree of unbound monomers, this equilibrium will affect the initial slope for C_o–H but not for N–H and hence lead to a much increased and unrealistic value for K (Table 3.2). A realistic value for K would have to be adjusted for the pre-dimerization equilibrium.

3.3.3 Comparison with computed chemical shifts

To lend further support to the analyses in Sections 3.3.1 (N–H···O interaction) and particularly 3.3.2 (proposed C–H···O interaction), we employed calculated chemical shifts for comparison. The assignments of the computed ^{1}H chemical shifts in the monomer and dimer are displayed in Schemes 3.1 and 3.2, respectively.

In analogy to the experimentally observed downfield shifts with increasing concentration, there is a 2.04 ppm deshielding upon H-bonding for the N–H proton, and the computed chemical shift for the ortho-proton involved in the C–H···O interaction is affected similarly. As can be seen from Scheme 3.1, and in accord with simple considerations of N=S=O anisotropy criteria, the two ortho protons exhibit two distinct intrinsic chemical shifts, even in the monomer, while experimentally only one signal is observed. The computed ortho average of 7.43 ppm in the monomer shifts to a computed average of 7.93 ppm in the dimer, representing a deshielding of 0.50 ppm. In contrast to these changes, it is notable that the computed values for C_m–H (Δ 0.03 ppm) and C_p–H (Δ 0.04 ppm) upon dimerization remain almost unaffected.

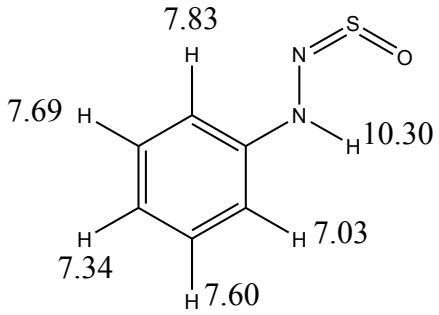

Scheme 3.1 Calculated chemical shifts (ppm) of the protons in the *syn* Ph–NH–NSO monomer from OPBE/6-311++G(2df,pd)//B3LYP/6-31+G(2d,2p).

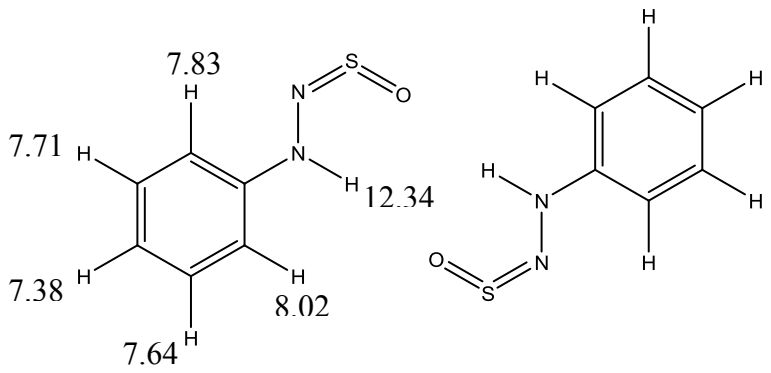

Scheme 3.2 Calculated chemical shifts (ppm) of the protons in the Ph–NH–NSO dimer from OPBE/6-311++G(2df,pd)//B3LYP/6-31+G(2d,2p).

Thus, overall, the deshielding of N–H and C_o–H protons upon dimerization is confirmed computationally, even if the computed chemical shift differences are too large. For C_m–H and C_p–H, expectedly, there is no intrinsic change in chemical shift upon dimerization, yet experimentally a distinct shielding on the order of 0.06 ppm is seen (Fig. 3.4a and b). These deviations between the computed and the experimental data do not come as a surprise, because here the calculations were performed a) without accounting for a possible basis set superposition error, b) in the absence of solvent and c) on the isolated monomer and dimer.

A basis set superposition error, in which basis functions on the H-bonding atoms in one monomer of the dimer help with the mathematical description of the H-bonding atoms in the other monomer, can lead to an underestimation of the distance at which the two monomers are found in the dimer. This would lead to an overestimation of the computed deshielding experienced by the N–H and C_o–H protons in the dimer. Previously, though, the basis set superposition error was shown to be small at the related B3LYP/6-31+G(d) level.[39] With respect to solvent, its accessibility to N–H and C_o–H

protons in particular is restricted in the dimer. These chemical shifts are therefore probably influenced differently in monomer and dimer, which is not accounted for in the data in Schemes 3.1 and 3.2. Finally, and with respect to the isolation of the molecules in the calculations, in dilute solution the monomer will only experience, on average, solvent interactions, while the dimer, especially in concentrated solution, will also experience interactions with other dimers. The magnetic anisotropy provided from the π-systems of other dimers would be experienced in π-stacking interactions and could thus lead to smaller (face-face interaction) or larger (edge-face interaction) chemical shifts in the dimer protons. A shielding from face-face interactions in the concentrated solution would, in fact, account for all observed discrepancies, because the computed values would not capture the attenuation and would thus predict larger deshieldings than experimentally observed.

3.4 Conclusions

From changes in the position of the N–H proton signal in Ph–NH–NSO for different concentrations in $CDCl_3$, an equilibrium constant for association (monomer to cyclic, hydrogen-bonded dimer) of 1.67 M^{-1} was determined by ^1H NMR spectroscopy. From the observed deshielding curve, the involvement of the N–H proton in an intermolecular N–H···O hydrogen bond, already demonstrated in the infrared, was confirmed. The presence of a C_o–H···O interaction in the hydrogen-bonded dimer, suggested from analyses of the electron density, was confirmed through ^1H NMR studies. The ortho C_o–H signal in the monomer exhibited a 0.06 ppm downfield shift in $CDCl_3$ as the concentration was increased. In contrast, signals for protons in meta- and para-position

exhibited a small shielding effect upon an increase in concentration. Overall, chemical shifts computed from OPBE/6-311++G(2df,pd)//B3LYP/6-31+G(2d,2p) confirmed and helped explain the experimental findings. To summarize, the observed deshieldings are smaller than the calculated intrinsic changes in chemical shift, which can be understood if π-π interactions between dimers in concentrated solution are invoked.

Finally, from vibrational analyses, the N–H···O and the C–H···O interaction in the cyclic dimer of Ph–NH–NSO do not behave alike even qualitatively. Whereas the N–H bond undergoes a lengthening upon interaction with the oxygen atom, the C–H bond undergoes a shortening, with corresponding red and blue, respectively, shift of the vibrational frequency. In contrast, this work shows clearly that both exhibit the same characteristics in the ^{1}H NMR, a deshielding of the proton upon interaction with the oxygen.

Chapter 4. Meta- and para-methyl substituted N-phenyl-N'-sulfinylhydrazines (Ph–NH–NSO): Proton magnetic resonance spectroscopic studies into the network of their hydrogen-bonded dimers

4.1 Introduction

The existence of hydrogen bonds has long been established as they have a vital role in various chemical and biological processes, as well as the development of new materials.[43-46,49,50,138] One fundamental parameter that can have an influence on the strength of the hydrogen bonding interaction is the substituent effect.[97,122-126,139] Due to this, substituent effects on H-bonds are often used to rationalize the molecular properties of a compound. The effect is usually observed when the substituent acts on the reaction site of the interacting molecule, and the nitrogen atom of an N–H···O interaction, for example, constitutes such a reaction site. The size of a substituent effect strongly depends on the nature of the substituent and its position with respect to the reactive site,[123,139] and the electronic properties of a substituent on an aromatic ring are often quantified through the use of one of Hammett's substituent constants σ.[122,124] The para-substituent effect in a series of mono-aryl thioureas on hydrogen bonding to the SO_3^--headgroup of a zwitterion in deutero-chloroform solution was reported to be substantial.[140] For the σ^- dependence, the reaction parameter ρ was determined at 1.77, reflecting the increased downfield shift of the monitored H-bonded proton upon the introduction of increasingly electron-withdrawing substituents and indicating the corresponding stronger N–H···O interactions. Similarly, computational studies of substituent effects on the stability of the Watson-Crick adenine-uracil base pair revealed that the introduction of electron-withdrawing

groups at the uracil C^5 position (the location of the thymine methyl group) enhanced the strength of the interaction.[126] Whereas the study considered a range of substituents from strongly electron-withdrawing (nitro group) to strongly electron-donating (amino group), even the small substituent effect exerted by the methyl group can be captured. Thus, in a related computational study, the stability of the adenine-thymine base pair was found to be increased as compared to that of the adenine-uracil pair in which the methyl group is missing.[123] Such a methyl-group effect was also shown intramolecularly. Picolinic acid N-oxide possesses an intramolecular hydrogen bond,[141] and its strength can be tuned through substituents that alter the proton acceptor and the proton donor properties of the N-oxide and the carboxylic group, respectively.[139] In this case, the introduction of electron-donating substituents led to a downfield shift of the H-bonded proton, and a methyl group para to the nitroxide moiety had a larger effect ($\Delta\delta$ 0.50 ppm) than if para to the carboxyl moiety ($\Delta\delta$ 0.14 ppm).

Our group is involved in studies of this kind as part of our research in the area of N–H···O=S and ortho-C–H···O=S interactions. Results gathered from computational studies that make use of the quantum theory of Atoms in Molecules (electron density analysis) and IR spectroscopy reveal that N-sulfinylhydrazines, Ph–NH–NSO's, form hydrogen bonded dimers.[39] Our recent work (Chapter 3) has focussed on the unsubstituted Ph–NH–NSO dimer using ^{1}H NMR dilution and computational studies.[142] We have confirmed the presence of both N–H···O and C–H···O interactions through the deshielding that was observed only for the protons involved in the hydrogen-bonding network. Dimers are still supposed to form when the Ph–NH–NSO is substituted in meta or para position on the aromatic ring.[40] Yet, neither N–H···O nor C–H···O interaction is suggested to be affected

much by the presence of a methyl group. For example, the dimer's asymmetric N–H stretch was calculated (B3LYP/6-31+G(d)) to red-shift from 3189 (unsubstituted) to 3186 (para-methyl substituted) cm^{-1}, in accord with the experimentally observed red-shift upon substitution of 5 cm^{-1} in $CHCl_3$; a similar but even smaller shift was calculated for the asymmetric C–H stretch, 3097 to 3095 cm^{-1}, respectively.

As such a small difference in the busy C–H stretching region in the IR would be difficult to determine accurately, we decided that ^{1}H NMR spectroscopy should be the method of choice instead. Changes in proton chemical shifts, $\Delta\delta$, upon a change in concentration allow an evaluation of the dimerization (association) constant, K, which for the unsubstituted Ph–NH–NSO was determined at 1.67 M^{-1} in $CDCl_3$ (see Chapter 3). If there is indeed a substituent effect exerted by a methyl group, one can expect to see changes in either $\Delta\delta$ or K, or in both. In the following, we present the ^{1}H NMR spectroscopic dilution studies for para- and meta-methyl substituted Ph–NH–NSO (Scheme 4.1), at room temperature and lowered temperatures.

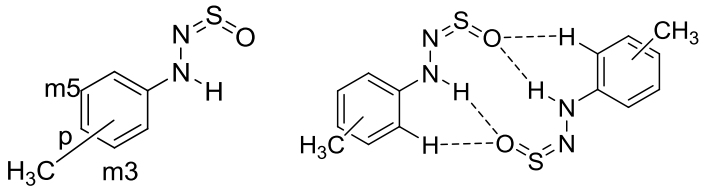

I **II**

Scheme 4.1 Methyl-substituted Ph–NH–NSO, monomer (**I**) and dimer (**II**).

4.2 Experimental and computational details

The syntheses of the methyl-substituted Ph–NH–NSO's were accomplished as derived from the transthionylation previously described by Pearce.[7] As the substituted hydrazines

were purchased in their hydrochloride forms, they were converted into the free base by neutralizing with aqueous NaOH solution. N-thionylaniline was procured from Sigma Aldrich, m- and p-tolylhydrazine hydrochloride from Alfa Aesar, and all were used as received. Solvents and reagents used were of analytical grade. Pure, bright yellow crystals were obtained by recrystallization from anhydrous ethanol. Details on the synthesis and characterization can be found in Chapter 6.

Meta- and para-methyl Ph–NH–NSO were each studied in deuterated chloroform ($CDCl_3$) solution from the limit of detectability in dilute solution to the solubility limit. The chemical shifts were recorded in the concentration range of 0.005 – 1.2 M at room temperature (25 ºC). The concentration range was 0.005 – 0.3 M for both Ph–NH–NSO's at –30 ºC and 0.005 – 0.4 M for the meta-substituted product –15 ºC. All ^{1}H NMR measurements were obtained using a Varian 500 NMR spectrometer. A 5-mm probe was used and the spectra were referenced to tetramethylsilane (TMS). Data were determined from three independent experiments for studies done at room temperature, and from a single determination for the low temperature studies.

All calculations were performed using the Gaussian 09 package.[127] The molecular geometries of the *syn* monomers and the hydrogen-bonded dimers were optimized without symmetry constraints, using the Becke three-parameter exchange functional[98] with the Lee-Yang-Parr correlation functional[99] (B3LYP)[128] and the 6-31+G(2d,2p) basis set. B3LYP has been shown to perform well in similar H-bonding studies,[129-132] and has been employed in our previous work on the Ph–NH–NSO dimer (and Chapter 3).[39] We chose the polarized basis set for its flexibility with respect to the description of the hydrogen atoms. Monomer and dimer geometries were confirmed as minima from

vibrational frequency analyses at the same model chemistry. The proton isotropic shieldings (σ_{iso}) were obtained from the B3LYP optimized geometries using the OPBE functional (Handy's OPTX[54] combined with the Perdew-Burke-Ernzerhof PBE[133] functional) and the larger 6-311++G(2df,pd) basis set, as OPBE has been shown to give a superior performance for magnetic shieldings and chemical shifts compared to other popular density-functional methods.[134] The OPBE/6-311++G(2df,pd)//B3LYP/6-31+G(2d,2p) combination has been shown to perform well in the calculation of ^{17}O isotropic shieldings, including that of Ph–NSO with its intramolecular C–H···O interaction.[18] We employed the gauge including atomic orbitals (GIAO) method[135-137] and report the chemical shifts, δ in ppm downfield from tetramethylsilane (σ_{iso} for the proton is 31.51 ppm from OPBE/6-311++G(2df,pd)//B3LYP/6-31+G(2d,2p)).

4.3 Results and discussion

4.3.1 para-Methyl substitution

4.3.1.1 The N–H···O interaction

The ^1H NMR spectrum in $CDCl_3$ reveals one signal for the N–H proton only, with substantial concentration dependence of the chemical shift. On average from three independent experiments, a concentration of 1.2 M produces a downfield signal at 10.881 ppm, a concentration of 0.005 M an upfield signal at 10.104 ppm. Figure 4.1 shows the partial room temperature (25 °C) ^1H NMR spectra for the most concentrated (1.2 M) and diluted (0.005 M) solutions in the N–H region. The full assignment of the ^1H NMR spectra of the para-methyl substituted Ph–NH–NSO can be found in Appendix B. Listed

in Table 4.1 is the average of three N–H chemical shifts, δ(N–H), observed at different concentrations, and the table data are plotted in Fig. 4.2.

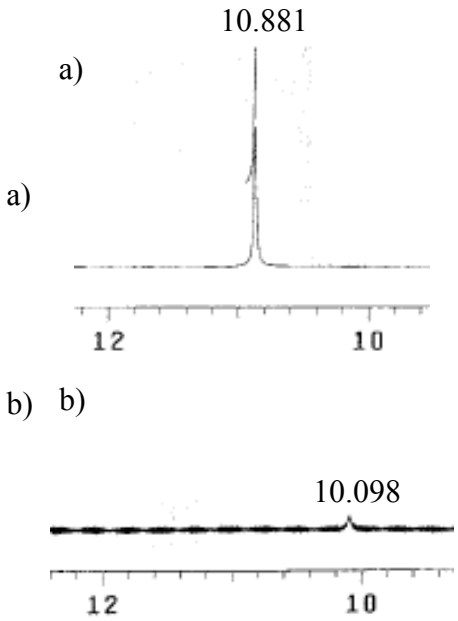

Fig. 4.1 ^{1}H NMR spectra (ppm) of p-methyl Ph–NH–NSO in the N–H region for a) 1.2 and b) 0.005 M in $CDCl_3$ at 25 °C.

Table 4.1 demonstrates the change in the chemical shift for the monomer-dimer equilibrium and the extent of hydrogen bonding for the N–H interaction. From the data and the plot (Fig. 4.2), δ(N–H) at high concentration corresponds (mostly) to the hydrogen-bonded, dimeric species, whereas the value at the lowest concentration indicates mostly the non-hydrogen-bonded, free p-methyl Ph–NH–NSO monomer. As expected, the observed chemical shifts are not dissimilar to those for the unsubstituted Ph–NH–NSO (see Chapter 3; 10.915 – 10.127 ppm for the same range of concentrations), which were explained with the dissociation of the hydrogen-bonded dimer upon dilution. Figure 4.2 therefore also qualitatively resembles the plot obtained for the unsubstituted

compound (Fig. 3.2), and the regression curve shows an excellent fit with the experimental data.

Table 4.1 N–H and C–H chemical shifts (ppm) for varying concentrations (M) of p-methyl Ph–NH–NSO in $CDCl_3$ at 25 °C.

c	δ(N–H)	δ(ortho C–H)	δ(meta C–H)	δ(CH_3)
1.200	10.881	7.180	7.120	2.290
1.000	10.842	7.181	7.131	2.296
0.800	10.783	7.181	7.138	2.303
0.600	10.701	7.179	7.156	2.312
0.400	10.701	7.175	7.162	2.320
0.200	10.619	7.167	7.161	2.324
0.100	10.454	7.156	7.172	2.332
0.050	10.320	7.143	7.179	2.333
0.025	10.155	7.137	7.181	2.335
0.005	10.104	7.132	7.184	2.337

The curve data are provided in Table 4.2 and are employed to evaluate the strength of the hydrogen bond network in the dimer through the determination of the equilibrium (dimerization or association) constant, K (see Chapter 3.3). With the chemical shift for the monomer (δ_D) and dimer (δ_M), obtained at infinite dilution and concentration, respectively, and the initial slope, K is obtained as 1.2 M^{-1} (Table 4.2).

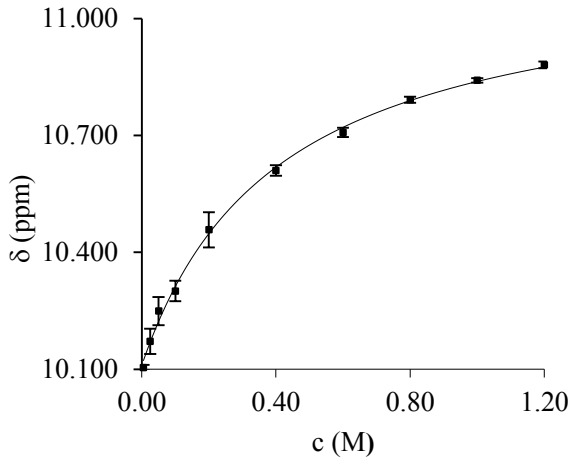

Fig. 4.2 Concentration dependence of the N–H proton resonance of p-methyl Ph–NH–NSO in $CDCl_3$ at 25 °C (average from three experiments). R^2 for the fitted curve is 0.998.

Thus, the K value for the p-methyl Ph–NH–NSO is only slightly smaller than that for dimer formation for the unsubstituted Ph–NH–NSO (1.67 M^{-1}, Chapter 3). The difference is a reflection of the small substituent effect of the methyl group in para position, and its presence destabilizes the hydrogen-bonded dimer. This is in full accord with the calculated (B3LYP/6-31+G(d)) zero-point vibrational energy corrected binding energies of 11.4 (unsubstituted Ph–NH–NSO) and 11.3 kcal mol^{-1} (p-methyl Ph–NH–NSO), and the calculated shifts in N–H stretching frequency upon dimerization of 92 (unsubstituted) and 91 (p-methyl Ph–NH–NSO) cm^{-1}.[39] Even though both the experimental and the computed difference upon introduction of the methyl group are very small, the picture is consistent.

Table 4.2 Selected experimental ^{1}H chemical shifts δ (ppm) for the p-methyl Ph–NH–NSO monomer and dimer in $CDCl_3$, obtained as described in the text, initial slope and derived equilibrium constant, K.

nucleus	monomer	dimer	Δδ	$(\Delta\delta/\Delta c_M)_0$	K
N–H	10.110	11.134	1.024	2.525	1.233[a]
ortho C–H	7.128	7.188	0.060	0.511	4.252[b]

[a] The regression from Fig. 4.2 is $y = y_0 + a \cdot x/(b+x)$, with y_0 10.110, a 1.025 and b 0.406.

[b] The regression from Fig. 4.4a is $y = y_0 + a \cdot x/(b+x)$, with y_0 7.128, a 0.060 and b 0.118.

4.3.1.2 The C_o–H···O interaction

The experimental assessment of the aromatic protons for the para-methyl substituted Ph–NH–NSO was more challenging than that of the unsubstituted compound, because methyl substitution causes both ortho- and meta-proton signals to appear in the same, narrow spectroscopic window. The opposing trends in their shifts upon dilution lead to a cross-over at a concentration of about 0.2 M. The partial ^{1}H NMR spectra of p-methyl Ph–NH–NSO in the aromatic region at the solubility limit (1.2 M), near the cross-over (0.2 M) and at the limit of detectability in dilute solution (0.005 M) are shown in Fig. 4.3; the full set of spectra is given in Appendix C.

The plots of the concentration dependences for the signals from ortho-, meta- and methyl-protons from 1.2 – 0.005 M are shown in Fig. 4.4. The signals from the meta- and methyl-protons, none of which are involved in hydrogen-bonding interactions, show the monotonous shielding that was already observed for meta- and para-protons in the unsubstituted Ph–NH–NSO (Chapter 3).

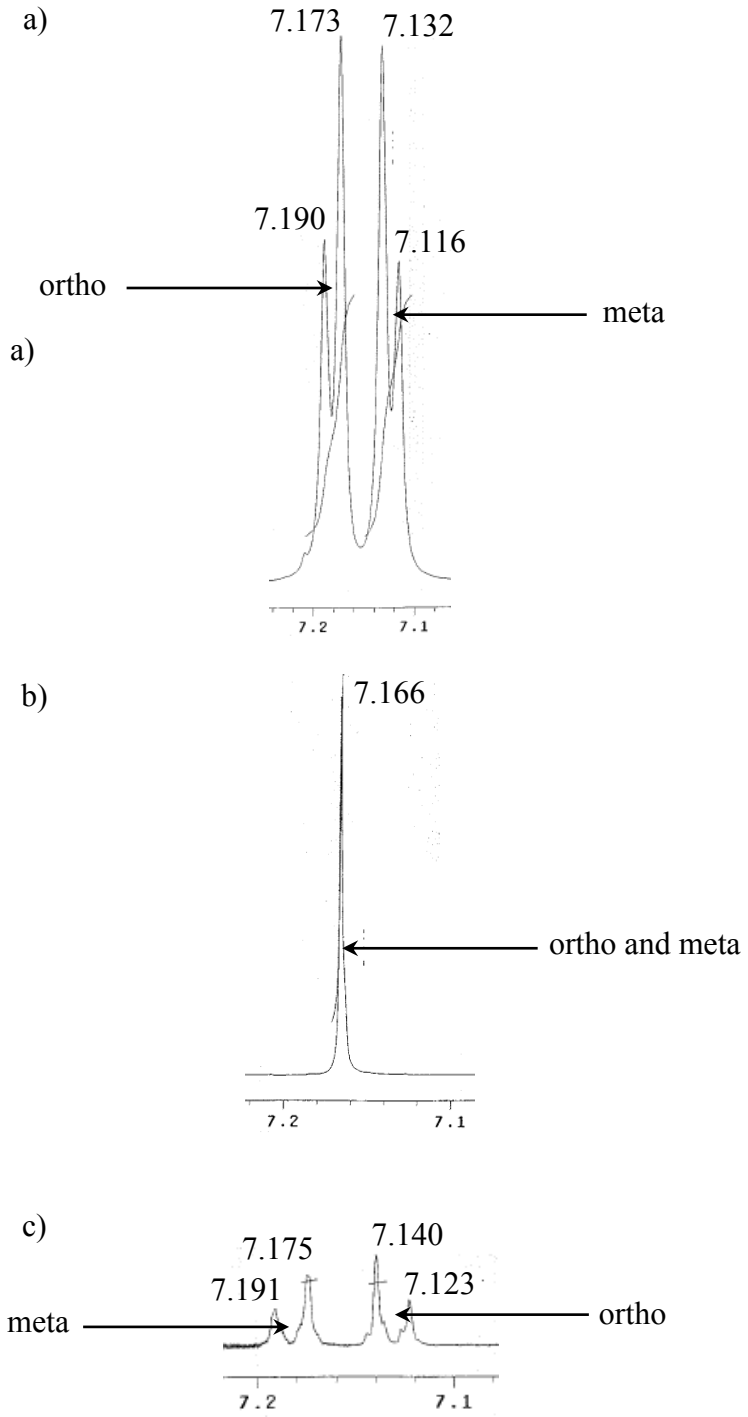

Fig. 4.3 ^{1}H NMR spectra of p-methyl Ph–NH–NSO in the aromatic region for a) 1.2, b) 0.2 and c) 0.005 M in $CDCl_3$ at 25 °C. The lines of the signals are given in large labels for clarity, and signals are identified as to their molecular origin.

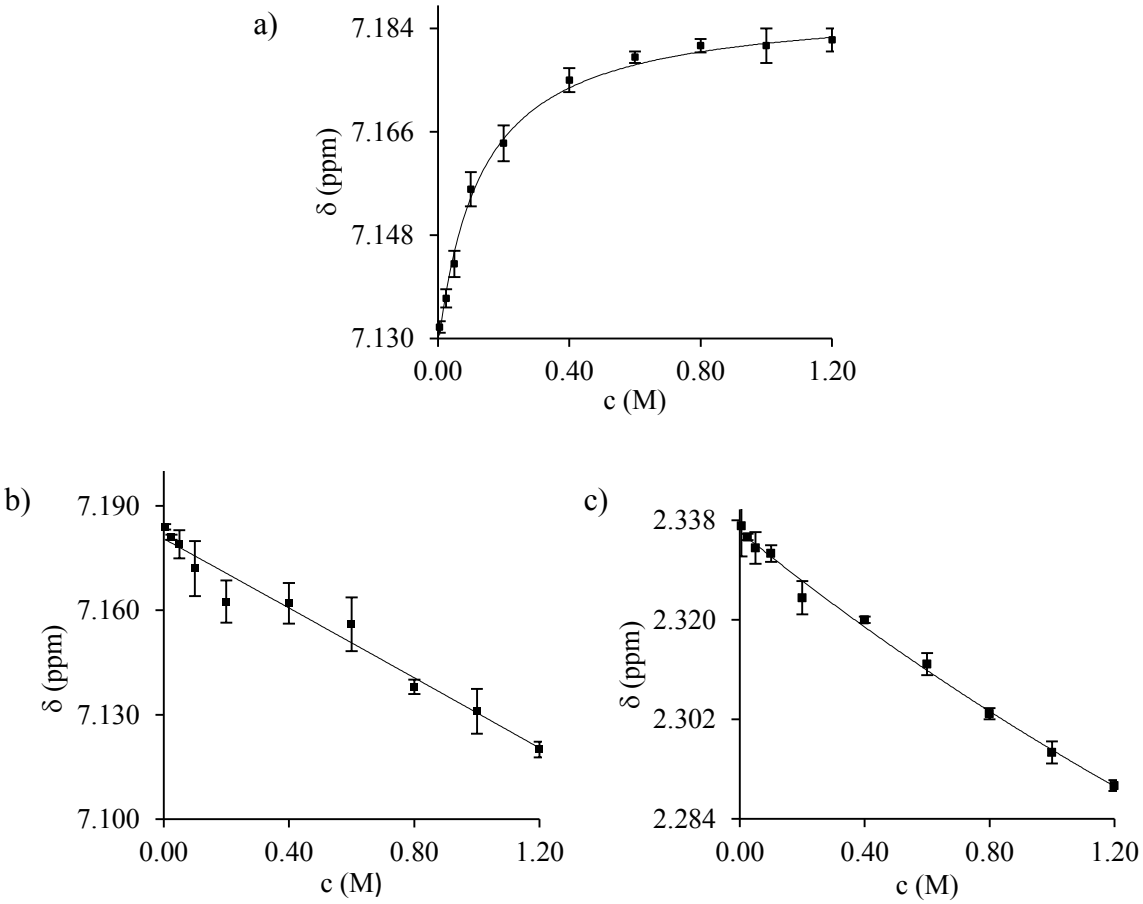

Fig. 4.4 Concentration dependence of the a) ortho, b) meta and c) methyl C–H signal of p-methyl Ph–NH–NSO in $CDCl_3$ at 25 °C (average from three experiments). R^2 for the fitted curve in a) is 0.993.

But, as in the unsubstituted compound, the signal from the ortho-protons shifts downfield with higher concentrations, indicating the formation of C–H···O interactions (Fig. 4.4a). The data from Table 4.2 show that, again as expected from the unsubstituted compound (Chapter 3), the change in chemical shift upon C–H···O formation is much smaller than that upon N–H···O formation. But whereas there was a substituent effect on the N–H···O interaction, the Δδ for C–H···O formation is either unaffected by the

presence of the p-methyl substituent or the influence is so small that it is not detected. The curve data from Table 4.2 leads to an estimated association constant, but the same discussion as in Chapter 3 holds here, and so there is no practical significance to this value.

4.3.1.3 Low-temperature studies

The dilution experiment was repeated at low temperature, –30 °C. At this lower temperature, the solubility limit was already reached at 0.3 M. The ^{1}H NMR spectra for the N–H proton for the two extreme concentrations are shown in Fig. 4.5a and b, those for the aromatic and methyl protons in Fig. 4.5c and d, and Table 4.3 lists the changes in ^{1}H chemical shift for varying concentrations of p-methyl Ph–NH–NSO in $CDCl_3$. Figures 4.6 and 4.7 show the plotted data from Table 4.3.

The most striking difference between the room and low temperature data lies in the fact that the latter do not exhibit a cross-over point for signals from ortho- and meta-protons below a concentration of 0.3 M (Fig. 4.5c and d). The analysis for the ortho-proton signal is therefore much simplified through this lowering in temperature, and the final result, i.e. the involvement of the ortho-proton in a C–H···O interaction, is verified. The origin for the lack of cross-over lies in the altered trend for the meta-proton signal upon an increase in concentration. Whereas at room temperature there is a slight shielding effect (Fig. 4.4b), at low temperature a slight monotonous deshielding is observed instead (Fig. 4.7a). The origin of this change is unknown at this time, but of no great concern.

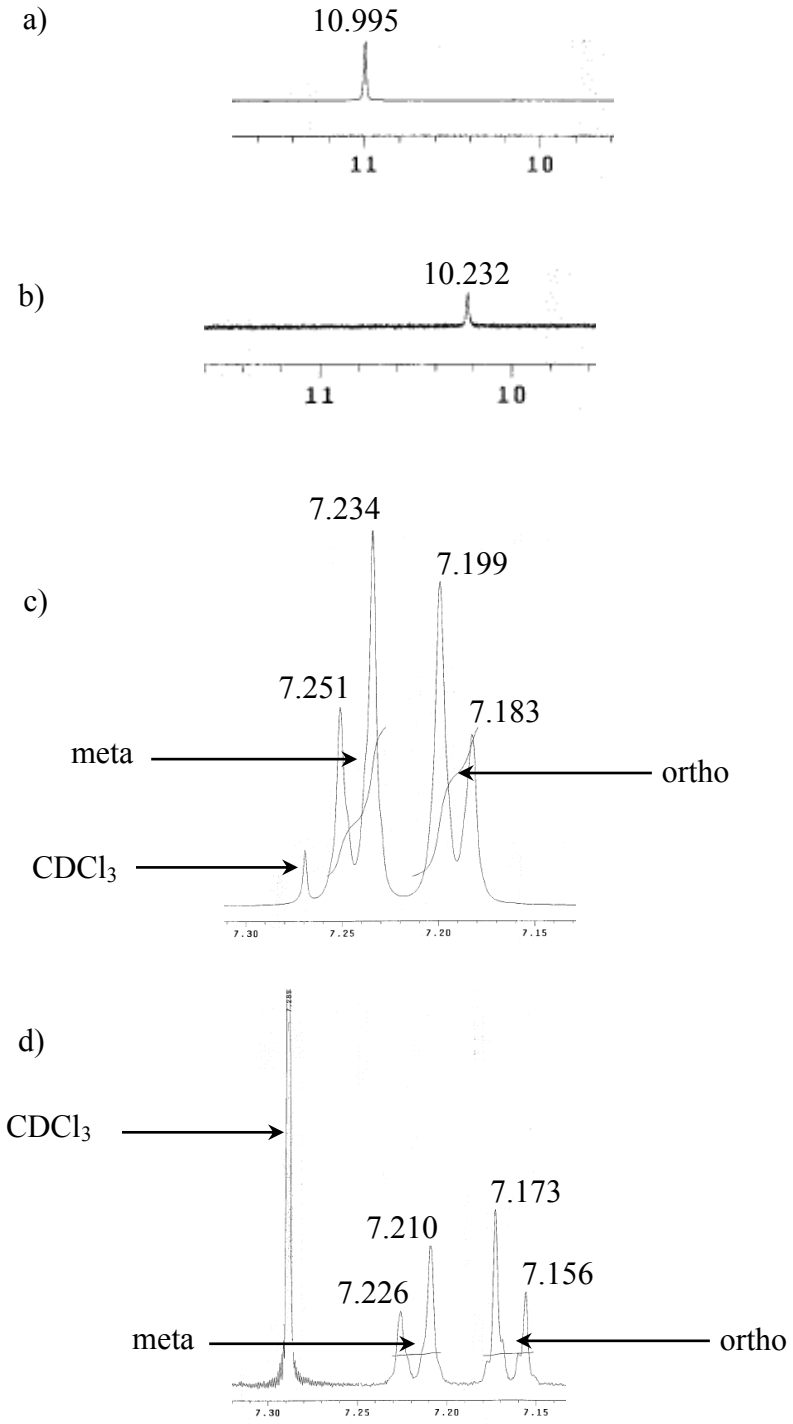

Fig. 4.5 ^{1}H NMR spectra of p-methyl Ph–NH–NSO in the N–H region for a) 1.2 and b) 0.005 M and in the aromatic region for c) 1.2 and d) 0.005 M, in $CDCl_3$ at –30 °C. The lines of the signals are given in large labels for clarity, and signals are identified as to their molecular origin.

Table 4.3 N–H and C–H chemical shifts (ppm) for varying concentrations (M) of p-methyl Ph–NH–NSO in $CDCl_3$ at –30 °C (from one experiment only).

c	δ(N–H)	δ(ortho C–H)	δ(meta C–H)	δ(CH_3)
0.300	10.995	7.191	7.243	2.345
0.200	10.905	7.197	7.237	2.349
0.100	10.700	7.196	7.228	2.354
0.050	10.559	7.191	7.222	2.356
0.025	10.397	7.183	7.216	2.358
0.005	10.232	7.165	7.218	2.360

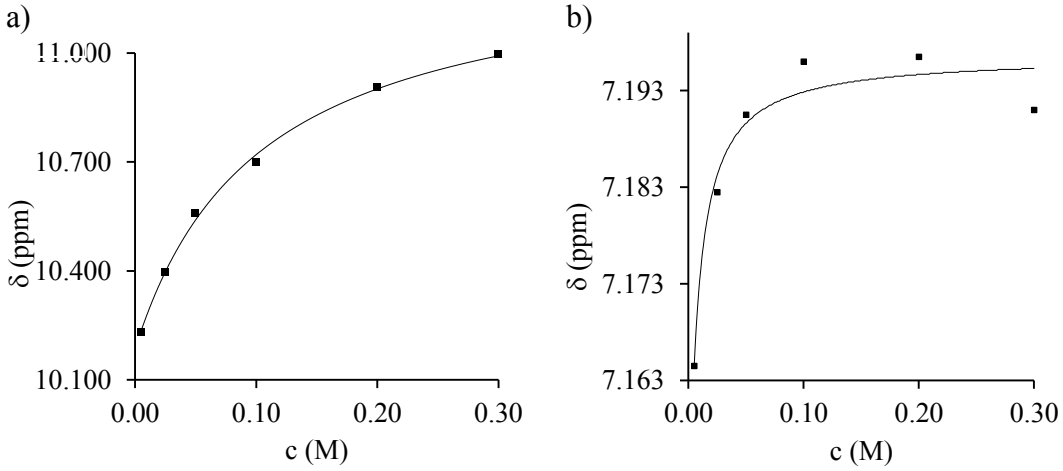

Fig. 4.6 Concentration dependence of the a) N–H and b) ortho C–H signal of p-methyl Ph–NH–NSO in $CDCl_3$ at –30 ° C (from one experiment only). R^2 for the fitted curve is a) 0.998 and b) 0.964.

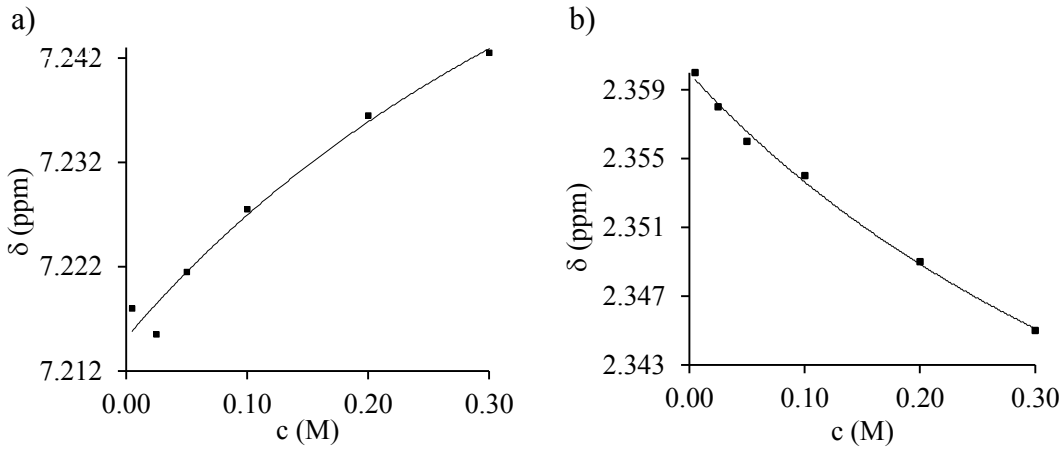

Fig. 4.7 Concentration dependence of the a) meta- and b) methyl-proton resonance in p-methyl Ph–NH–NSO in $CDCl_3$ at –30 °C (from one experiment only).

Table 4.4 lists the important data from the regression curves of Fig. 4.6 and shows the derived association constant, K. It is not surprising to see that the dimerization equilibrium is greatly affected by the temperature, and K is much increased, by nearly a factor of 4, at –30 °C.

Table 4.4 Selected experimental ^1H chemical shifts δ (ppm) for the p-methyl Ph–NH–NSO monomer and dimer in $CDCl_3$ at –30 °C, obtained as described in the text, initial slope and derived equilibrium constant, K.

nucleus	monomer	dimer	Δδ	$(\Delta\delta/\Delta c_M)_0$	K
N–H	10.185	11.268	1.083	10.592	4.892[a]
ortho C–H	7.143	7.197	0.054	0.720	6.759[b]

[a] The regression from Fig. 4.6a is $y = y_0 + a \cdot x/(b+x)$, with y_0 10.185, a 1.083 and b 0.102.

[b] The regression from Fig. 4.6b is $y = y_0 + a \cdot x/(b+x)$, with y_0 7.143, a 0.054 and b 0.074.

4.3.1.4 Comparison with computed chemical shifts

The calculated chemical shifts for the monomer and dimer are shown in Schemes 4.2 and 4.3, respectively. Overall, the computed results ($\Delta\delta$) support the experimental ^{1}H NMR findings.

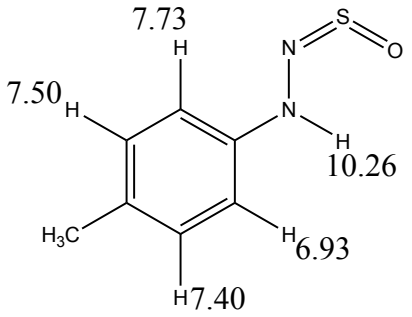

Scheme 4.2 Calculated chemical shifts (ppm) of the protons in the *syn* p-methyl Ph–NH–NSO monomer from OPBE/6-311++G(2df,pd)//B3LYP/6-31+G(2d,2p).

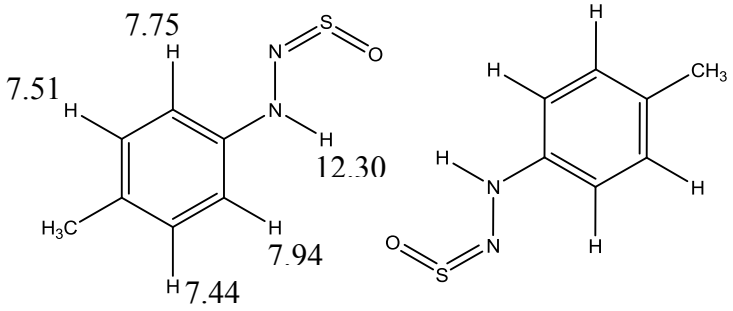

Scheme 4.3 Calculated chemical shifts (ppm) of the protons in the p-methyl Ph–NH–NSO dimer from OPBE/6-311++G(2df,pd)//B3LYP/6-31+G(2d,2p).

The deshielding of 2.04 ppm calculated for the N–H proton upon H-bonding is identical to that observed in the unsubstituted compound (Chapter 3), and even though the calculated chemical shifts between the unsubstituted and the p-methyl substituted Ph–

NH–NSO are slightly different, the methyl group effect on the N–H proton in both monomer and dimer is the same. This picture for the ortho C–H protons is similar, but not identical. The computed ortho average of 7.33 ppm in the monomer shifts to a computed average of 7.94 ppm in the dimer, representing a deshielding of 0.52 ppm, whereas only a 0.50 ppm deshielding is computed for the unsubstituted compound (Chapter 3). Thus, the substituent effect manifests itself in the C–H···O interaction. If the size of the deshielding is indeed a measure of the strength of the interaction, as it is for N–H···O, then the methyl group strengthens C–H···O. This is an interesting finding, even though it is irrelevant for the stability of the dimer, seeing that this small effect vanishes in light of all the other, more energetically important, changes that occur upon dimerization.

In accord with findings on the unsubstituted compound (Chapter 3), the computed values for C_m–H upon dimerization remain almost unchanged. The meta-protons show a change from a 7.45 ppm average in the monomer to a 7.48 ppm average in the dimer. This same 0.03 ppm deshielding was observed for the unsubstituted computed, which showed an experimental small shielding trend (Chapter 3), whereas for the p-methyl substituted compound this shielding is only observed at room temperature, and a similarly small deshielding is observed at –30 °C. These different observations are certainly not trivial in their explanation, and no further attempt at clarification has been made (but see Chapter 3.3.3 for further general discussion).

4.3.2 meta-Methyl substitution

4.3.2.1 The N–H···O interaction

The situtation for the m-methyl Ph–NH–NSO ^{1}H NMR spectra in the N–H region is very similar to both the unsubstituted (Chapter 3) and the p-methyl substituted compound. Once again, only one averaged signal is observed in the N–H region, and its position is concentration dependent. Compared to the unsubstituted and the p-methyl substituted Ph–NH–NSO, meta substitution decreases δ(N–H) at both limits, that is, for the most concentrated and the most diluted solution (Table 4.5). Also, while the unsubstituted and p-methyl substituted compound show approximately the same chemical shift difference over the 1.2 – 0.005 M concentration range, Δδ 0.8 ppm, meta substitution leads to a Δδ of approximately 0.7 ppm. Even though these changes are not very large, they suggest that the N–H···O interaction is affected by methyl-substitution in the meta position.

The complete assignment of the room temperature ^{1}H NMR dilution spectra, which are averaged over three independent determinations, is given in Table 4.5. Figure 4.8 depicts the corresponding N–H resonance concentration dependence, and Table 4.6 gives the relevant data from the regression curve and derived association constant.

As was observed upon para-methyl substitution, dimerization is affected by the methyl substituent at the meta position. While K values of 1.67 and 1.23 M^{-1} were found for the unsubstituted and the p-methyl Ph–NH–NSO, respectively, the even lower value of 1.14 M^{-1} is determined for the m-methyl compound, indicating that this is the least stable dimer in the series.

Table 4.5 N–H and C–H chemical shifts (ppm) for varying concentrations (M) of m-methyl Ph–NH–NSO in $CDCl_3$ at 25 °C.[a]

c	δ(N–H)	δ(ortho1 C–H)	δ(ortho2 C–H)	δ(meta C–H)	δ(para C–H)	δ(CH_3)
1.200	10.760	7.098	7.071	7.214	6.896	2.338
1.000	10.730	7.099	7.071	7.219	6.901	2.343
0.800	10.683	7.101	7.069	7.223	6.907	2.345
0.600	10.625	7.103	7.068	7.233	6.916	2.356
0.400	10.528	7.101	7.063	7.242	6.925	2.366
0.200	10.363	7.094	7.049	7.251	6.933	2.371
0.100	10.244	7.085	7.038	7.253	6.939	2.372
0.050	10.180	7.083	7.031	7.257	6.941	2.375
0.025	10.132	7.079	7.027	7.260	6.943	2.377
0.005	10.082	7.074	7.023	7.259	6.944	2.377

[a] Protons in ortho position are: ortho1 singlet, ortho2 doublet signal.

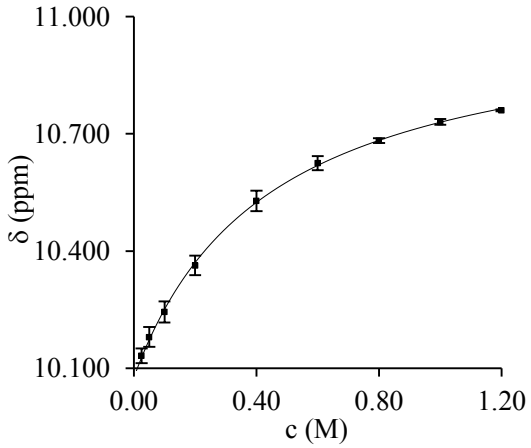

Fig. 4.8.Concentration dependence of the N–H proton resonance of m-methyl Ph–NH–NSO in $CDCl_3$ at 25 °C (average from three experiments). R^2 for the fitted curve is 0.996.

Table 4.6 Selected experimental ^{1}H chemical shifts δ (ppm) for the m-methyl Ph–NH–NSO monomer and dimer in $CDCl_3$, obtained as described in the text, initial slope and derived equilibrium constant, K.

nucleus	monomer	dimer	Δδ	$(\Delta\delta/\Delta c_M)_0$	K
N–H	10.077	11.016	0.939	2.140	1.14[a]
ortho1 C–H	7.072	7.104	0.032	0.314	4.90[b]
ortho2 C–H	7.021	7.083	0.062	0.276	2.23[c]

[a] The regression from Fig. 4.8 is $y = y_0 + a \cdot x/(b+x)$, with y_0 10.077, a 0.940 and b 0.439.

[b] The regression from Fig. 4.10d is $y = y_0 + a \cdot x/(b+x)$, with y_0 7.072, a 0.033 and b 0.104.

[c] The regression from Fig. 4.10d is $y = y_0 + a \cdot x/(b+x)$, with y_0 7.021, a 0.063 and b 0.227.

4.3.2.2 The C_o–H···O interaction

Unlike the unsubstituted and the p-methyl substituted phenyl ring, which are invariant in their two rotamers, substitution in meta position leads to two distinguishable rotamers that are referred to as meta-3 (methyl group and N–H on the same side) and meta-5 (Scheme 4.4).[40] Hence, dimerization leads to three different species, two homo-dimers and one hetero-dimer (Scheme 4.5), in all of which the two ortho positions are also distinct. Thus, the main distinguishing characteristic of the ^{1}H NMR spectra in the aromatic region of m-methyl Ph–NH–NSO is the presence of two ortho proton signals, a singlet (referred to as ortho1) and a doublet (ortho2). Figure 4.9 displays the spectra at the solubility limit (1.2 M) and the limit of detectability in dilute solution (0.005 M) in the aromatic region. The average chemical shifts from three independent experiments are reported for all C–H protons in Table 4.5.

The data from Table 4.5 indicate that resonances from protons in meta- and para-positions as well as the methyl group shift upfield as the concentration increases, in accord with those of the unsubstituted (Chapter 3) and the p-methyl substituted Ph–NH–NSO. This concentration dependence is depicted in Fig. 4.10a to c. In contrast, the resonances of the two distinct ortho protons exhibit a similar pattern, the well-defined deshielding, in their concentration dependence (Fig. 4.10d), indicating that both are involved in C–H···O interactions. Thus, the ortho1 C–H is interacting in the meta-3 rotamer, ortho2 in meta-5 and both are interacting in the hetero-dimer.

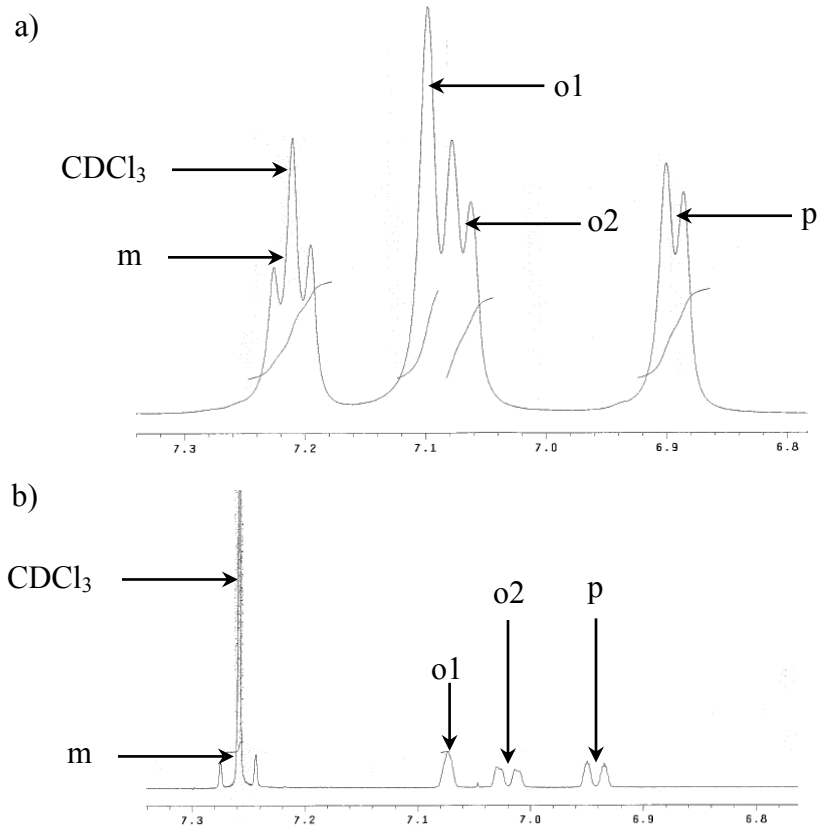

Fig. 4.9 ^{1}H NMR spectra of m-methyl Ph–NH–NSO in the aromatic region for a) 1.2 and b) 0.005 M in $CDCl_3$ at 25 °C (three independent experiments). The signals are identified as to their molecular origin. Refer to Table 4.5 for the average chemical shifts.

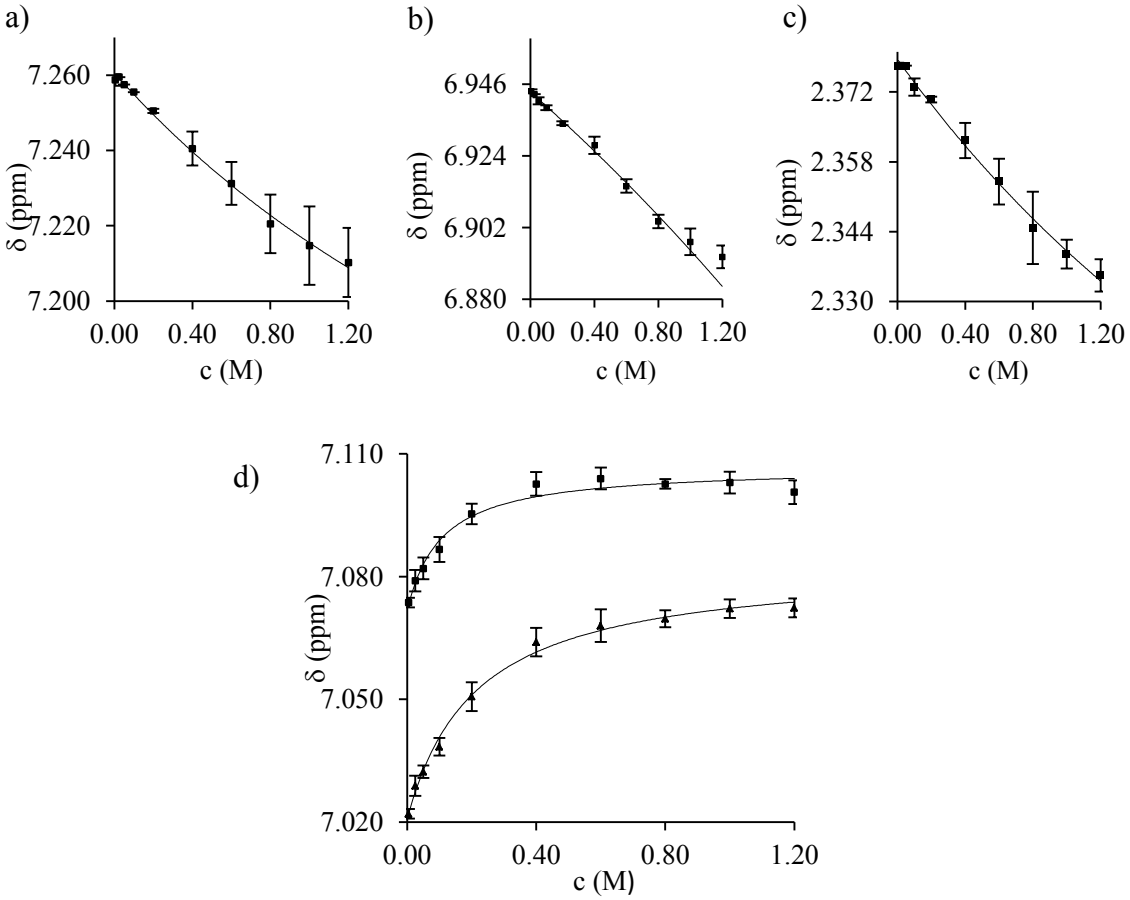

Fig. 4.10 Concentration dependence of the a) meta, b) para, c) methyl and d) ortho C–H resonance in m-methyl Ph–NH–NSO in $CDCl_3$ at 25 °C (average from three experiments). R^2 for the fitted curves is C_{o1} 0.945 (■) and C_{o2} 0.994 (▲).

Compared to the change in N–H chemical shift, the change for both $\delta(C_o–H)$ is again much smaller, but, more importantly, the change for ortho1 is smaller than that for ortho2 (Table 4.6), and two different values for K were determined from the values for the two ortho protons. While the values of K are once again not practically relevant (see discussion in Chapter 3), the significance of the two differently sized ortho-proton deshieldings is discussed together with the computational data in Chapter 4.3.2.4.

4.3.2.3 Low-temperature studies

The temperature dependence of the proton resonances is similar to that observed for para-methyl substitution. Sample spectra are plotted for –15 °C and –30°C in Fig. 4.11. Tables 4.7 and 4.8 list the proton chemical shifts for different concentrations at –15 and –30 °C, and the table data are plotted in Figs. 4.12 to 4.15.

Unlike Fig. 4.7a, which revealed an unexpected near linear increase, rather than the expected decrease, in chemical shift for the meta-protons in the p-methyl Ph–NH–NSO at –30 °C, the corresponding Figs. 4.12 and 4.13 exhibit the general shielding effect observed for hydrogen atoms that are not involved in hydrogen-bonding interactions.

Table 4.9 lists the data obtained from the regression curves for the N–H (Fig. 4.14) and ortho-proton (Fig. 4.15) concentration dependences at the two different low temperatures. Once again, K derived from the N–H dependences is larger than at room temperature, and the lower the temperature is, the larger the K, which is in accord with the expected shift of the dimerization equilibrium. The calculated K for the ortho-protons follow that same trend.

Table 4.7 N–H and C–H chemical shifts (ppm) for varying concentrations (M) of m-methyl Ph–NH–NSO in $CDCl_3$ at –15 °C.

c	N–H	C_{o1}–H	C_{o2}–H	C_m–H	C_p–H	CH_3
0.400	10.914	7.147	7.116	7.250	6.934	2.369
0.200	10.754	7.143	7.104	7.272	6.95	2.382
0.100	10.592	7.134	7.089	7.280	6.959	2.389
0.050	10.411	7.120	7.07	7.286	6.963	2.394
0.025	10.337	7.113	7.061	7.287	6.966	2.394
0.005	10.180	7.098	7.044	7.2897	6.967	2.394

Table 4.8 N–H and C–H chemical shifts (ppm) for varying concentrations (M) of m-methyl Ph–NH–NSO in $CDCl_3$ at –30 °C.

c	N–H	C_{o1}–H	C_{o2}–H	C_m–H	C_p–H	CH_3
0.300	10.843	7.160	7.122	7.287	6.962	2.392
0.200	10.729	7.153	7.111	7.292	6.969	2.396
0.100	10.658	7.148	7.104	7.294	6.969	2.398
0.050	10.564	7.135	7.087	7.297	6.973	2.400
0.025	10.369	7.123	7.071	7.30	6.976	2.400
0.005	10.181	7.106	7.049	7.302	6.978	2.401

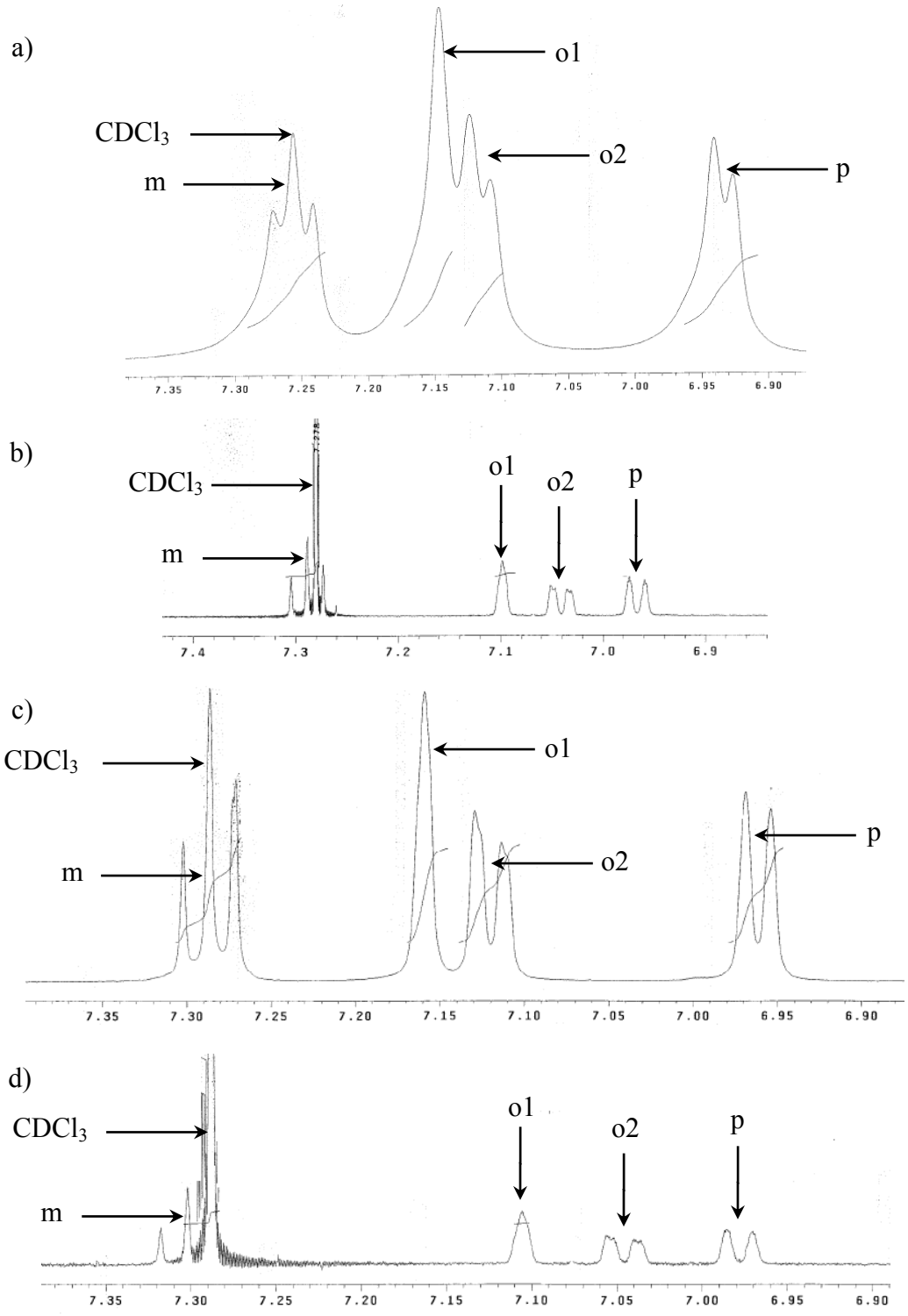

Fig. 4.11 ^{1}H NMR spectra of m-methyl Ph–NH–NSO in the aromatic region at –15 °C for a) 1.2 and b) 0.005 M and at –30 °C for c) 1.2 and d) 0.005 M, in $CDCl_3$. Signals are identified as to their molecular origin.

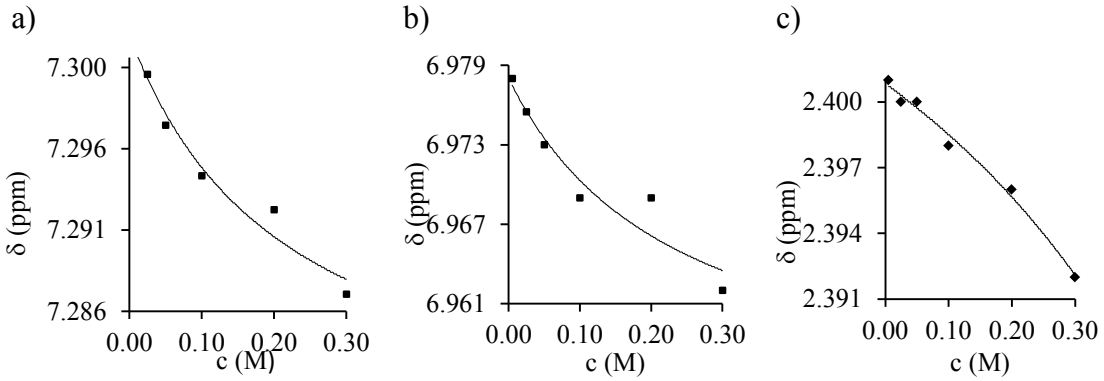

Fig. 4.12 Concentration dependence of the a) meta, b) para and c) methyl C–H signal of m-methyl Ph–NH–NSO in $CDCl_3$ at –15 °C (from one experiment only).

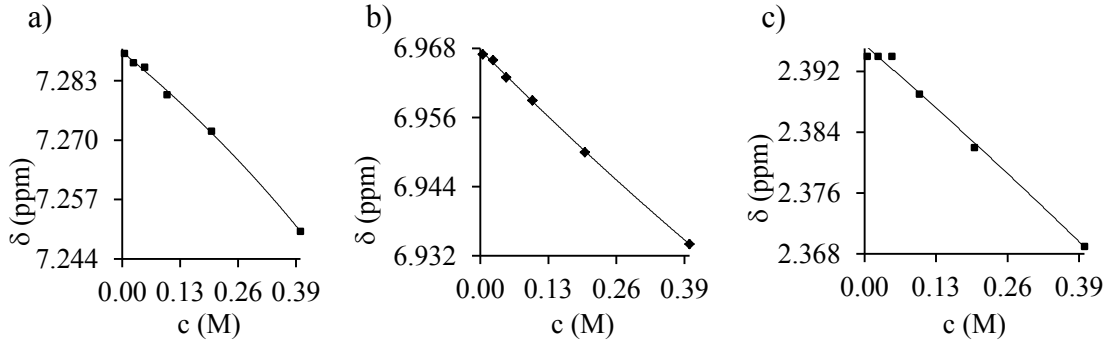

Fig. 4.13 Concentration dependence of the a) meta, b) para and c) methyl C–H signal of m-methyl Ph–NH–NSO in $CDCl_3$ at –30 °C (from one experiment only).

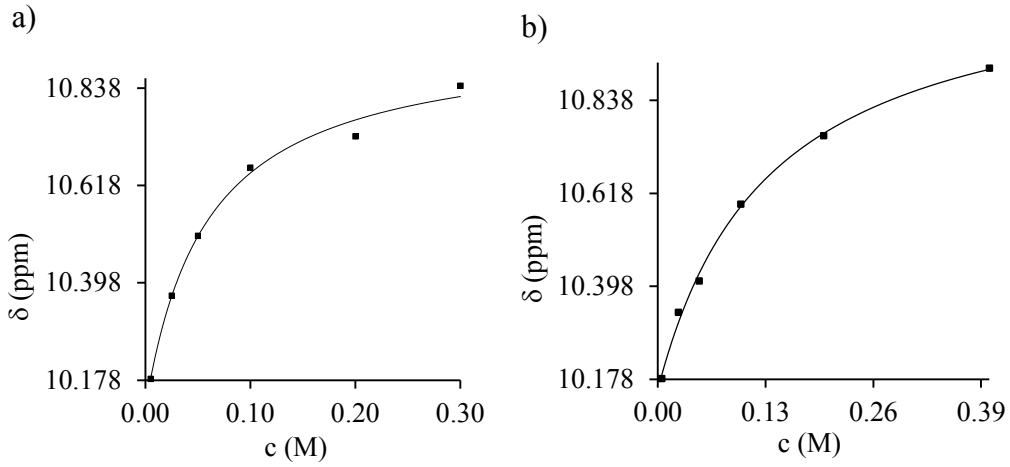

Fig. 4.14 Concentration dependence of the N–H proton resonance in m-methyl Ph–NH–NSO in $CDCl_3$ at a) –15 and b) –30 °C (one experiment each only). R^2 for the fitted curves is a) 0.998 and b) 0.964.

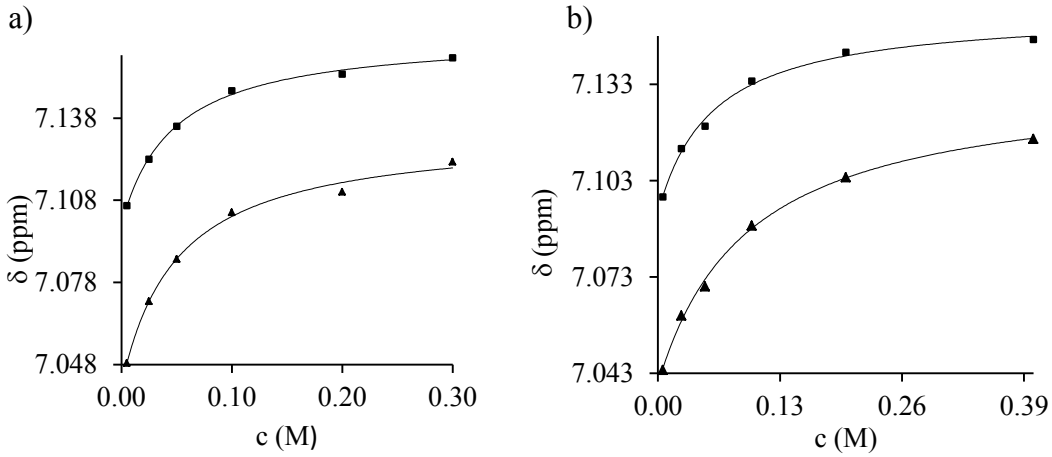

Fig. 4.15 Concentration dependence of the two ortho proton resonances of the m-methyl Ph–NH–NSO in $CDCl_3$ at a) –30 and b) –15 °C (one experiment only). R^2 for the fitted curves is a) 0.993 (■ C_{o1}) and 0.996 (▲ C_{o2}) and b) 0.995 (■ C_{o1}) and 0.998 (▲ C_{o2}).

Table 4.9 Selected experimental ^{1}H chemical shifts δ (ppm) for the meta-methyl Ph–NH–NSO monomer and dimer in $CDCl_3$, at –15 and –30 °C, obtained as described in the text, initial slope and derived equilibrium constant, K.

nucleus	monomer	dimer	Δδ	$(\Delta\delta/\Delta c_M)_0$	K
		–15 °C			
N–H	10.153	11.164	1.011	7.602	3.76[a]
ortho1 C–H	7.093	7.156	0.063	1.090	8.65[b]
ortho2 C–H	7.040	7.135	0.095	0.990	5.21[c]
		–30 °C			
N–H	10.116	10.956	0.840	14.372	8.55[d]
ortho1 C–H	7.099	7.169	0.070	1.503	10.74[e]
ortho2 C–H	7.040	7.133	0.093	1.856	9.98[f]

[a] The regression from Fig. 4.14a is $y = y_0 + a \cdot x/(b+x)$, with y_0 10.153, a 1.011 and b 0.133. [b] The regression from Fig. 4.15a is $y = y_0 + a \cdot x/(b+x)$, with y_0 7.093, a 0.063 and b 0.058. [c] The regression from Fig. 4.15a is $y = y_0 + a \cdot x/(b+x)$, with y_0 7.040, a 0.095 and b 0.096. [d] The regression from Fig. 14b is $y = y_0 + a \cdot x/(b+x)$, with y_0 10.116, a 0.839 and b 0.0.058. [e] The regression from Fig. 4.15b is $y = y_0 + a \cdot x/(b+x)$, with y_0 7.099, a 0.070 and b 0.046. [f] The regression from Fig. 4.15b is $y = y_0 + a \cdot x/(b+x)$, with y_0 7.04, a 0.093 and b 0.050.

4.3.2.4 Comparison with computed chemical shifts

Methyl substitution in meta position results in two different conformers, meta-3 and meta-5 (Scheme 4.4). From B3LYP/6-31+G(2d,2p), the free energy difference at room

temperature (ΔG_{298}) between meta-3 and meta-5 is 0.5 kcal mol^{-1}, with meta-3 being more stable; meta-5 is more stable from the electronic energies (E_{el}) by only 0.04 kcal mol^{-1}. This translates into an equilibrium population of 70:30 (from ΔG_{298}) or 48:52 (from ΔE_{el}). Scheme 4.4 shows the computed proton chemical shifts for the two monomers, and Table 4.10 gives the averages as they would be observed for the torsional equilibrium at low concentration, estimated from ΔG_{298} and ΔE_{el}. As can be seen for the N–H values from either Scheme 4.4 or Table 4.10, the substitution pattern of the aromatic ring does basically not affect these protons, either between the two rotamers or with respect to para-substitution (Scheme 4.2). Even though Scheme 4.4 shows that the individual chemical shifts for each proton do not differ much between the two monomers, Table 4.10 illustrates that the chemical shift difference between the two ortho protons, as shown in Fig. 4.9 and Table 4.6, at low concentration is only reproduced in the ΔE_{el} averaged data, i.e. the doublet signal is found at a smaller δ value. In other words, the monomer equilibrium is close to a K of 1.

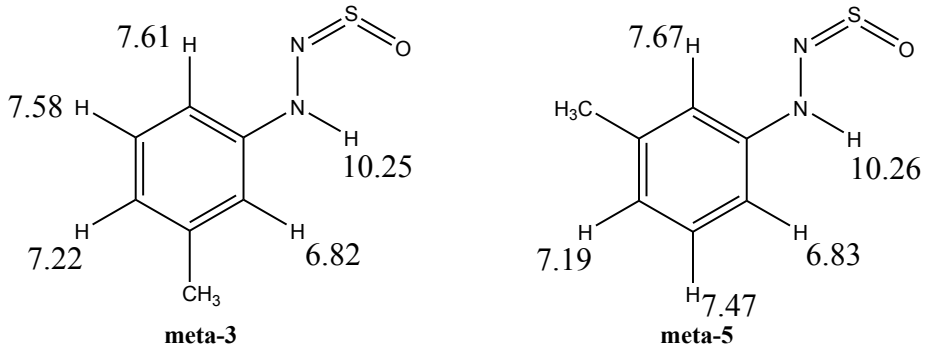

Scheme 4.4 Calculated chemical shifts (ppm) of the protons in the two rotamers of the *syn* m-methyl Ph–NH–NSO monomer from OPBE/6-311++G(2df,pd)//B3LYP/6-31+G(2d,2p)

Table 4.10 Computed average ^{1}H chemical shifts δ (ppm) in the *syn* m-methyl Ph–NH–NSO monomer and dimer.

nucleus	monomer average δ		dimer average δ	
	from ΔG_{298}[a]	from ΔE_{el}[b]	from ΔG_{298}[c]	from ΔE_{el}[d]
N–H	10.25	10.26	12.29	12.29
ortho1 C–H[e]	7.04	7.26	7.75	7.77
ortho2 C–H[f]	7.41	7.20	7.75	7.73
meta C–H	7.55	7.52	7.55	7.56
para C–H	7.21	7.20	7.25	7.25

[a] Equilibrium population is 74 % meta-3, 26 % meta-5. [b] Equilibrium population is 48 % meta-3, 52 % meta-5. [c] Equilibrium population is 22 % 2-meta-3, 45 % 2-meta-5, 33 % meta-3,5. [d] Equilibrium population is 33 % 2-meta-3, 33 % 2-meta-5, 34 % meta-3,5. [e] Singlet signal. [f] Doublet signal.

The two monomers can hydrogen bond into two homo-dimers and one hetero-dimer (Scheme 4.5). From the three possible dimers, the meta-5 homo-dimer is most stable in ΔG_{298}, whereas the hetero-dimer is most stable in ΔE_{el}, yet the equilibrium populations at high concentration do not differ much. For 2-meta-3:2-meta-5:meta-3,5, the composition is 22:45:33 (ΔG_{298}) or 33:33:34 (ΔE_{el}). Scheme 4.5 shows the computed chemical shifts for all three dimers, and their comparison demonstrates, again, only small differences between the two sets of ortho proton values. For the N–H chemical shift difference upon dimerization, the difference in equilibrium composition is again not relevant (Table 4.10), and a deshielding of 2.03 – 2.04 ppm is calculated, in accord with the size of the

deshieldings in the unsubstituted and the para-methyl substituted Ph–NH–NSO upon dimerization. More interesting is the situation for the two ortho protons. From Fig. 4.10d, it is clear that these two proton resonances converge for high concentration, and this is captured by either of the two equilibrium compositions. Yet, once again, it is the composition from ΔE_{el} that maintains a small chemical shift difference, and so the conclusion is the same for the dimers as it is for the monomers. The dimer equilibrium is about 1:1:1.

With the ΔE_{el} data from Table 4.10, the changes in chemical shift for the ortho protons observed upon an increase in concentration (Fig. 4.10) can now be understood. It is the singlet signal (ortho1) that is affected less ($\Delta\delta$ 0.51 ppm) than the doublet signal (ortho2, $\Delta\delta$ 0.53 ppm), but this is only possible if meta-5 is present to at least about 50 %.

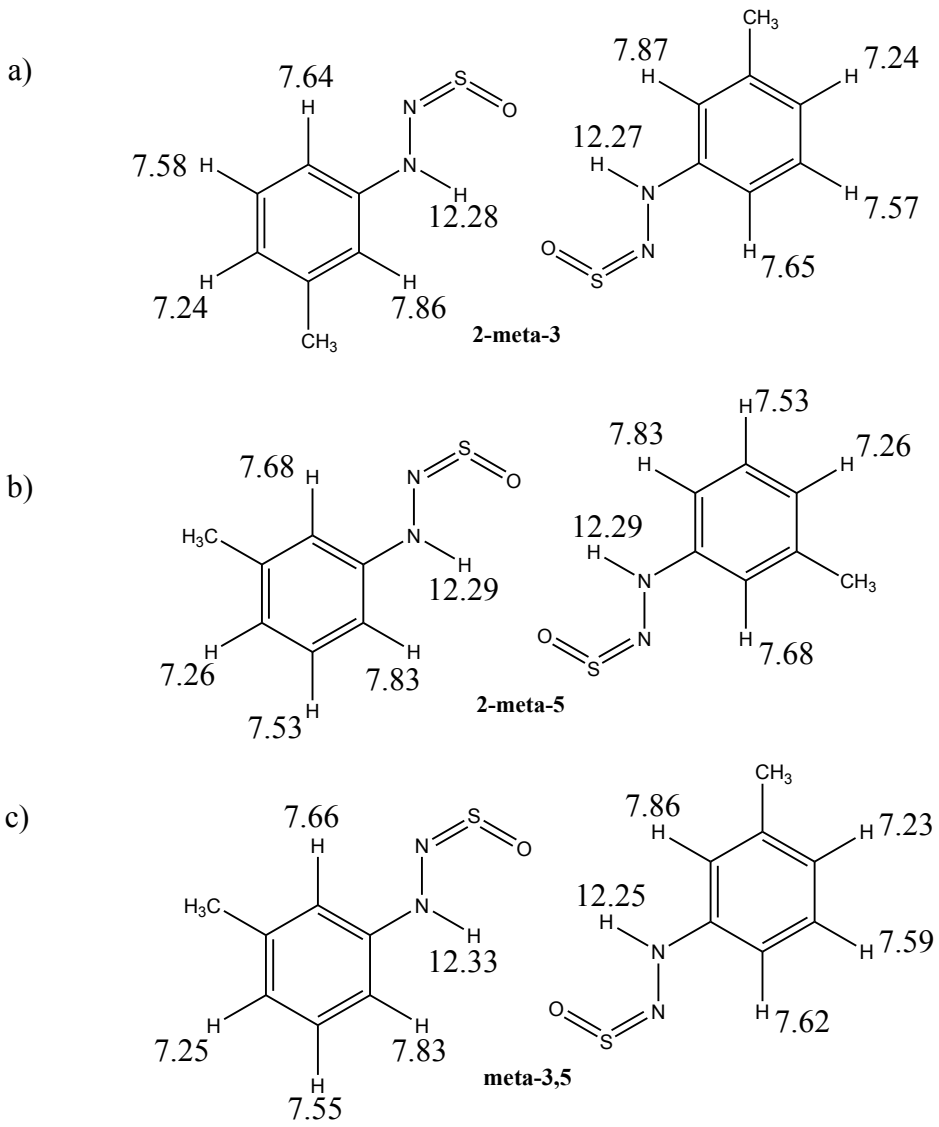

Scheme 4.5 Calculated chemical shifts (ppm) of the protons in the m-methyl Ph–NH–NSO dimers from a) two meta-3, b) two meta-5 and c) meta-3 and -5 monomers, from OPBE/6-311++G(2df,pd)//B3LYP/6-31+G(2d,2p).

4.4 Conclusions

Two methyl substituted Ph–NH–NSO's were studied, through ^{1}H NMR dilution and computationally, with respect to the nature of the hydrogen-bonding network in the dimer as well as to a potential methyl substituent effect. Overall, for meta and para substitution,

the formation of hydrogen-bonded dimers was demonstrated through the characteristic downfield shift of N–H and ortho C–H proton resonances, indicating both N–H···O and C–H···O interactions, similar to what was found in the unsubstituted compound. The dimerization constants obtained from the N–H concentration dependences were somewhat smaller than that previously observed for the unsubstituted compound, indicating a small substituent effect and weaker dimers.

The computed N–H resonances are at smaller chemical shifts for meta and para substitution than for the unsubstituted Ph–NH–NSO, again demonstrating a small methyl substituent effect on the remote N–H proton in the monomers. Overall, the computational results agree well with the experimental findings, even though the absolute size of the deshielding for N–H and ortho C–H protons is overestimated computationally. Protons in meta and para position are not substantially effected upon dimer formation. For meta substitution, the computational results for the two distinct ortho protons enabled a detailed analysis of the experimental results with respect to monomer and dimer equilibrium composition. Thus, the observed differences in chemical shift as well as size of the deshielding upon dimerization were only reproduced for balanced equilibria, that is, a 1:1 population of the two monomer rotamers and a 1:1:1 population of the three possible hydrogen-bonded dimers.

Chapter 5. Conclusions and future work

The incentive for carrying out this ^{1}H NMR study in the dimerization behaviour of N-phenyl-N'-sulfinylhydrazine (Ph–NH–NSO) is the belief that some aspect of the weak interactions that are present upon dimerization may only be probed conveniently through the use of proton resonance. Prior work, using infrared spectroscopy and computed electron densities, in this group had highlighted N–H···O interactions in the hydrogen-bonding network in the cyclic dimer. Computationally, the further participation of C–H···O interactions from ortho-protons was suggested. Therefore, in particular, this present study was performed to understand the participation of C_o–H···O (C_o–H indicating the ortho position) interactions in the dimers of Ph–NH–NSO's. Proton NMR spectra in $CDCl_3$, recorded from the limit of detectability in dilute solution to the solubility limit, were conducted and analyses were carried out with specific emphasis on the N–H and C_o–H protons. Upon dilution, a dissociation equilibrium exists and a measure of the strength of the hydrogen-bonding network in the dimer can be obtained through the equilibrium (dimerization or association) constant derived from the concentration dependence regression curve for the N–H proton. The B3LYP/6-31+G(2d,2p) model chemistry was used to characterize the monomer and dimer through geometry optimization, and the OPBE/6-311++G(2df,pd)//B3LYP/6-31+G(2d,2p) model chemistry was employed to obtain proton isotropic shieldings that were converted to chemical shifts.

The first aspect of this research work described the behaviour of both the N–H···O and the C_o–H···O interaction in the unsubstituted Ph–NH–NSO. Strong experimental evidence for the participation of the C_o–H···O interaction in Ph–NH–NSO was obtained.

This was achieved through the observation of the concentration dependence of the proton chemical shifts for both the N–H and the C_o–H signals. Thus, the direction for $\Delta\delta$, a characteristic increase in chemical shift, for the two types of nuclei upon an increase in concentration was consistent. This was in contrast to the behaviour of the non-participating protons (the meta- and para-protons), which showed a slight shielding upon dimerization. From the ^{1}H NMR spectra in the N–H region, the equilibrium constant for association (monomer to cyclic, hydrogen-bonded dimer) was obtained to be 1.7 M^{-1}. The computed chemical shifts supported the large deshielding observed experimentally for N–H and C_o–H protons, whereas only very small changes in chemical shift were calculated for protons in meta- and para-position, also in support of the experimental data.

The next section dealt with the investigation of methyl-substituted Ph–NH–NSO at the meta and para position. Proton NMR dilution results, conducted at both room (25 °C) and low (down to –30 °C) temperature, show that the hydrogen-bonding network that was present in the unsubstituted Ph–NH–NSO cyclic dimer also occurred in the dimers of the substituted Ph–NH–NSO's. The chemical shifts over the same concentration range were dependent on substitution at the two different positions, and substituent effects on the hydrogen bond network or on the overall dimer stability were observed, yet all such effects were very small. Thus, the association constants at room temperature were 1.1 M^{-1} for meta- and 1.2 M^{-1} for para-substitution. In the low-temperature studies, the equilibrium constant was larger by a factor of about 4. Interestingly, for the unsymmetrical m-methyl Ph–NH–NSO, the involvement of both ortho-protons could be captured individually from the NMR spectra, and the doublet signal is affected more

strongly. The calculations reveal a somewhat higher stability of the meta-3 monomer (methyl group on the same side as N–H), whereas the homodimer from the rotamer meta-5 was most stable. From the computed, weighted chemical shifts, it was deduced that the experimental equilibria were predicted accurately by the calculations.

Even though all computed chemical shift differences differ from the experimental results in size, all results favour the C_o–H bond as a hydrogen bond donor in Ph–NH–NSO's. The original controversy about the hydrogen-bonding network in the dimer of N-phenyl-N'-sulfinylhydrazine, from diffraction analyses versus a computational study, centered around the involvement of a C–H···O interaction. With the evidence for C_o–H···O interactions provided in this work, through ^{1}H NMR dilution studies, this controversy has finally been resolved.

In the Introduction, both qualitative and quantitative statements about the effect of various substituents on the hydrogen bonding interaction were made. Yet in this work, only the methyl substituent was assessed, and it led to predictably (very) small effects. For a more general treatment, and for possibly much larger effects, further studies should be conducted on strong electron acceptors such as NO_2 or CN and strong electron donors such as OCH_3.

Finally, since the changes in the C–H chemical shifts differences upon dilution were small, it might be desirable to quantify the C_o–H···O interaction through nuclear magnetic coupling, $^1J_{CH}$, as it has been shown to be a valuable tool in hydrogen bonding analyses.

Chapter 6. Experimental

6.1 ^{1}H NMR spectroscopy

^{1}H NMR spectra were run on a Varian VNMR-500 spectrometer at Concordia University. A 5 mm probe was used and the spectra were referenced to tetramethylsilane (TMS), 12 % in deutero-chloroform. For the temperature studies, cold nitrogen gas and dry ice were used for lowering the temperature of the sample. A methanol standard was used to calibrate the temperature probe. Chemical shifts are reported as δ from TMS in ppm.

6.2 ^{1}H NMR sample preparation (dilution studies)

A standard stock solution (1.2 M) was prepared by transferring an accurately weighed amount of the compound (PhNHNSO, m-CH_3-C_6H_4-PhNHNSO, p-CH_3-C_6H_4-PhNHNSO) to a 5 mL volumetric flask and adding deuterochloroform. The flask was covered to prevent evaporation. From the stock solution, aliquots were measured according to the desired concentration (1.0, 0.8, 0.6, 0.4, 0.2, 0.1, 0.05, 0.025, 0.005 M) into a 1 mL volumetric flask. The solutions were diluted as before. With the aid of a clean pasteur pipette, a sample was transferred into the NMR tube, to a height of 5 cm, for analysis.

6.3 Syntheses

6.3.1 N-phenyl-N'-sulfinylhydrazine

A 250 mL three-neck round bottom flask, equipped with two dropping funnels, containing 15 mL of anhydrous diethyl ether and a magnetic stirring bar was fitted with a

calcium chloride drying tube and placed in an ice bath at 0 °C. 3.89 mL (4.82 g, 0.035 mol) of N-thionylaniline was dissolved in 10 mL of anhydrous diethyl ether in one dropping funnel. 3.40 mL (3.74 g, 0.027 mol) of phenylhydrazine was mixed with 10 mL of anhydrous diethyl ether in the second dropping funnel. The reactants were added simultaneously, at a rate of one drop per second, with continuous stirring. After completion of the addition, the mixture was stirred for 1 h at 0 °C. The yellow precipitate was collected by vacuum filtration and was washed with cold diethyl ether. The filtrate was transferred into a round bottom flask, and most of the ether was evaporated under vacuum. The remaining mixture was cooled in an ice bath until further yellow crystals were formed. The second batch of crude product was collected by suction filtration and washed with diethyl ether. The total product obtained was recrystallized from 99 % ethanol. Crude yield: 2.80 g (86% recovered from free base). Yield: 2.10 g (66 % recovered from recrystallization) (lit. 89 %), yellow crystals. Melting point: 102 – 105 °C (lit. 103.5 – 105.5 °C).[7]

6.3.2 p-Methyl N-phenyl-N'-sulfinylhydrazine

6.3.2.1 p-Tolylhydrazine free base

In a 250 mL beaker containing a magnetic stirrer, 8.00 g (0.051 mol) p-tolylhydrazine hydrochloride was dissolved in 90 mL warm (50 °C) distilled water. After dissolution, the solution pH was adjusted to about 11 through addition of 2 M aqueous NaOH (2.0 g of NaOH in 25 mL of distilled water). A colourless precipitate was obtained and collected by vacuum filtration. The precipitate was washed with 40 mL of cold distilled water and the product was allowed to dry through suction. About 40 g of NaCl was added

to the filtrate to precipitate further crude product. These were again collected by vacuum filtration, wash with about 10ml of water and added to the first crop Yield: 5.60 g (90 %), colourless crystals, m.p. 56 – 58 °C (55 – 57 °C).[143]

6.3.2.2 p-Methyl N-phenyl-N'-sulfinylhydrazine

A 100 mL three-neck round bottom flask, equipped with two dropping funnels, containing 50 mL chloroform and a magnetic stirring bar was fitted with a calcium chloride drying tube and placed in an ice bath at 0 °C. The free base p-tolylhydrazine (5.60 g, 0.046 mol) was dissolved in 30 mL of chloroform in one dropping funnel. 8.1mL (10.0 g, 0.072 mol) of N-thionylaniline was measured into the second dropping funnel. The reactants were added simultaneously, at a rate of one drop per second, with continuous stirring for 30 min. After completion of the addition, the mixture was stirred for 1 h at 0 °C, then poured into a 100 mL round bottom flask, and most of the chloroform was evaporated under vacuum. A solid yellow crude was collected by vacuum filtration. The crude was washed with 30 mL of cold ethanol, followed with 25 mL of water. The residue was air dried and was recrystallized from 99 % ethanol. Crude yield: 5.51g (71.4 %), yield: 3.9 g (51 %) yellow needle-like crystals, m.p. 109 – 110.5 °C (lit. 112 °C).[19]

6.3.3 m-Methyl N-phenyl-N'-sulfinylhydrazine

6.3.3.1 m-Tolylhydrazine free base

In a 100 mL beaker containing a magnetic stirrer, 5.0 g (0.032 mol) m-tolylhydrazine hydrochloride was dissolved in 45 mL warm (50 °C) distilled water. After dissolution,

the solution pH was adjusted to about 11 through addition of 2 M aqueous NaOH (2.0 g of NaOH in 25 mL of distilled water). The solution was transferred to a separatory funnel and NaCl was added. The mixture was extracted using diethyl ether. A final brownish red liquid product was obtained by evaporating most of ether. Yield: 2.6 g (52%).

6.3.3.2 m-Methyl N-phenyl-N'-sulfinylhydrazine

A 50 mL three-neck round bottom flask, fitted with a dropping funnel (a drying tube filled with $CaCl_2$ was attached to the three three-neck round bottom flask.), and containing a magnetic stirrer, 5 mL of chloroform and 2.9 g (0.024 mol) m-tolylhydrazine, was placed in an ice bath at 0 °C. 6.0 g (0.043mol) of N-thionylaniline was added dropwise under stirring. After addition, 40 mL of diethyl ether was added, and stirring was continued for 1 hour. Most of the ether was evaporated under vacuum and a yellow solid precipitate was collected by vacuum filtration. The solid was washed with a small amount of ether, followed by 20 mL of distilled water. The crude product was purified by recrystallization from 99 % ethanol. Crude yield: 2.98 g (75 %), yield: 1.92 g (48 %) yellow powder, m.p. 86 – 88 °C (lit. 90 °C).[19]

6.3.4 p-Chloro N-phenyl-N'-sulfinylhydrazine

6.3.4.1 p-Chlorophenylhydrazine free base

In a 100 mL beaker containing a magnetic stirrer, 8.35 g (0.047 mol) p-chlorophenylhydrazine hydrochloride was dissolved in 50 mL warm (50 °C) water. After dissolution, the solution pH was adjusted to about 11 through addition of 2 M aqueous NaOH (2.0 g of NaOH in 25 mL of distilled water). The solution was transferred into a

separatory funnel and NaCl was added. The mixture was extracted using diethyl ether, and the organic layer was dried over Na_2SO_4. The mixture was transferred into a round bottom flask and most of the ether was evaporated under vacuum. After evaporation of the ether, colourless crystals were obtained. Yield: 4.82 g (72 %).

6.3.4.2 p-Chloro N-phenyl-N'-sulfinylhydrazine

A 50 mL three-neck round bottom flask, fitted with a $CaCl_2$ drying tube and a dropping funnel, and containing a magnetic stirrer, 5 mL diethyl ether and 4.8 g (0.034 mol) p-chlorophenylhydrazine, was placed in an ice bath at 0 °C. 8.0 g (0.058mol) of N-thionylaniline was added dropwise under stirring. After addition, 20 mL of diethyl ether was added and stirring was continued for 1 hour. Most of the ether was evaporated under vacuum and a yellow solid precipitate was collected after vacuum filtration. The solid was washed with a small amount of diethyl ether and recrystallized from 99 % ethanol. Crude Yield: 2.4 g (38 %), yield: 2.0 g (31 %) yellow crystals, m.p. 154 – 156 °C (lit. 159 °C).[19]

6.3.5 m-Chloro N-phenyl-N'-sulfinylhydrazine

6.3.5.1 m-Chorophenylhydrazine free base

In a 100 mL beaker containing a magnetic stirrer, 8.35 g (0.047 mol) m-chlorophenylhydrazine hydrochloride was dissolved in 50 mL warm (50 °C) water. After dissolution, the solution pH was adjusted to about 11 through addition of 2 M aqueous NaOH (2.0 g of NaOH in 25 mL of distilled water). The solution was transferred into a separatory funnel and NaCl was added. The mixture was extracted using diethyl ether,

and the organic layer was dried over Na_2SO_4. The mixture was transferred into a round bottom flask and most of the ether was evaporated under vacuum. An oily brown liquid was obtained after evaporation of most of the ether. Yield: 2.8 g (42 %).

6.3.5.2 m-Chloro N-phenyl-N'-sulfinylhydrazine

A 50 mL three-neck round bottom flask, fitted with a $CaCl_2$ drying tube and a dropping funnel, and containing a magnetic stirrer, 5 mL diethyl ether and 4.8 g (0.034 mol) m-chlorophenylhydrazine, was placed in an ice bath at 0 °C. 8.0 g (0.058 mol) of N-thionylaniline was added dropwise under stirring. After addition, 20 mL of diethyl ether was added and stirring was continued for 1 hour. Most of the ether was evaporated under vacuum and a yellow solid precipitate was collected after vacuum filtration. The solid was washed with a small amount of diethyl ether and recrystallized from 99 % ethanol. Crude Yield: 1.8 g (28 %), yield: 1.02 g (16 %) yellow crystals, m.p. 117 – 119 °C.

6.3.6 p-Nitro N-phenyl-N'-sulfinylhydrazine

6.3.6 1 p-Nitro N-phenyl-N'-sulfinylhydrazine free base

In a 100 mL beaker containing a magnetic stirrer, 8.40 g (0.044 mol) p-nitrophenylhydrazine hydrochloride was dissolved in 50 mL warm (50 °C) water. After dissolution, the solution pH was adjusted to about 11 through addition of 2 M aqueous NaOH (2.0 g of NaOH in 25 mL of distilled water). The solution was transferred into a separatory funnel and NaCl was added. The mixture was extracted using diethyl ether, and the organic layer was dried over Na_2SO_4. The mixture was transferred into a round

bottom flask and most of the ether was evaporated under vacuum. Colourless to brown crystals was obtained after evaporation of the ether. Yield: 4.2 g (62 %).

6.3.6 2 p-Nitro N-phenyl-N'-sulfinylhydrazine

A 50 mL three-neck round bottom flask, fitted with a $CaCl_2$ drying tube and a dropping funnel, and containing a magnetic stirrer, 5 mL diethyl ether and 4.2 g (0.027 mol) p-nitrophenylhydrazine, was placed in an ice bath at 0 °C. 8.0 g (0.058 mol) of N-thionylaniline was added dropwise under stirring. After addition, 20 mL of diethyl ether was added and stirring was continued for 1 hour. Most of the ether was evaporated under vacuum and a yellowish to brown powder was obtained which was collected after vacuum filtration. The product was washed with a small amount of diethyl ether and recrystallized from 99 % ethanol. Crude Yield: 2.5 g (47%), yield: 1.86 g (35 %) yellowish to brown needle-like crystals, m.p. 120 – 122 °C (lit. 209 °C).[19]

6.3.7 m-Nitro N-phenyl-N'-sulfinylhydrazine

6.3.7 1 m-Nitro N-phenyl-N'-sulfinylhydrazine free base

In a 100 mL beaker containing a magnetic stirrer, 8.0 g (0.042 mol) m-nitrophenylhydrazine hydrochloride was dissolved in 50 mL warm (50 °C) water. After dissolution, the solution pH was adjusted to about 11 through addition of 2 M aqueous NaOH (2.0 g of NaOH in 25 mL of distilled water). The solution was transferred into a separatory funnel and NaCl was added. The mixture was extracted using diethyl ether, and the organic layer was dried over Na_2SO_4. The mixture was transferred into a round

bottom flask and most of the ether was evaporated under vacuum An oily brown liquid was obtained after evaporation of most of the ether. Yield: 3.2 g (50 %).

6.3.7.2 m-Nitro N-phenyl-N'-sulfinylhydrazine

A 50 mL three-neck round bottom flask, fitted with a $CaCl_2$ drying tube and a dropping funnel, and containing a magnetic stirrer, 5 mL diethyl ether and 3.2 g (0.021 mol) m-nitrophenylhydrazine, was placed in an ice bath at 0 °C. 8.0 g (0.058 mol) of N-thionylaniline was added dropwise under stirring. After addition, 20 mL of diethyl ether was added and stirring was continued for 10 hours. Most of the ether was evaporated under vacuum and a yellow solid precipitate was collected after vacuum filtration. The solid was washed with a small amount of diethyl ether and recrystallized from 99 % ethanol. Crude Yield: 2.2 g (53%), yield: 1.60 g (38 %) light yellow crystals, m.p. 110 – 114 °C (lit. 185°C).[19]

References

(1) Böttinger, C. *Ber.* **1878**, *11*, 1407.

(2) Michaelis, A.; Herz, R. *Chem. Ber.* **1890**, *23*, 3480.

(3) Michaelis, A. *Chem. Ber.* **1891**, *24*, 745.

(4) Michaelis, A. *Ann.* **1893**, 173.

(5) Michaelis, A. *Ann.* **1893**, *274*, 200.

(6) Michaelis, A.; Storbeck, O. *Ann.* **1893**, *274*, 187.

(7) Pearce, L. B.; Feingold, M. H.; Cerny, K. F.; Anselme, J. P. *J. Org. Chem* **1979**, *44*, 1881-1883.

(8) Ivanova, E. V. PhD Thesis, Concordia University, 2010.

(9) Klamann, D.; Kramer, U.; Weyerstahl, P. *Chem. Ber.*, *95*, 2695.

(10) Kresze, G.; Maschke, A.; Albrecht, R.; Bederke, K.; Patzschke, H. P.; Smalla, H.; Trede, A. *Angew. Chem. Int. Ed.* **1962**, *1*, 89.

(11) Garigipati, R. S.; Freyer, A. J.; Whittle, R. R.; Weinreb, S. M. *J. Am. Chem. Soc.* **1984**, *106*, 7861-7867.

(12) Weinreb, S. M. *Acc. Chem. Res.* **1988**, *21*, 313-318.

(13) Butler, R. N.; O'Halloran, G. A.; Burke, L. A. *J. Chem. Soc. Perkin Trans. 2* **1989**, 1855-1860.

(14) Zhang, Y.; Flann, C. J. *J. Org. Chem* **1998**, *63*, 1372-1378.

(15) Park, Y. S.; Kim, W. K.; Kim, Y. B.; Lee, I. *J. Phys. Org. Chem.* **2000**, *65*, 3997-4002.

(16) Hee, L. J.; Lee, I.; Kyung, K. C.; Lee, B.-S.; Whang, L. H. *New J. Chem.* **2002**, *26*, 1693-1697.

(17) Cerioni, G.; Culeddu, N.; Plumitallo, A. *Tetrahedron* **1993**, *49*, 2957-2964.

(18) Muchall, H. M. *J. Phys. Chem. A* **2008**, *112*, 9118-9127.

(19) Baumann, N.; Fachmann, H.-J.; Heibel, B.; Jotter, R.; Kubny, A. *S-N compounds, part 6.* In *Gmelin Handbook of Inorganic Chemistry*; 8 ed.; Springer-Verlag: Berlin, 1990.

(20) Kroner, J.; Strack, W.; Holsboer, F.; Wolfgang, K. *Z. Naturforsch., Teil B* **1973**, *28*, 188.

(21) Leandri, G.; Mangini, A. *Spectrochim. Acta* **1959**, *421*.

(22) Collins, N. C.; Glass, W. K. *Spectrochim. Acta* **1974**, *30A*, 1335.

(23) Smith, W. T.; Trimnell, D.; Grinninger, L. D. *J. Org. Chem* **1959**, *24*, 664-666.

(24) Smith, W. T.; Chen, W. Y. *J. Med. Chem.* **1968**, *11*, 504-505.

(25) Butler, R. N.; Duffy, J. P.; McArdle, P.; Cunningham, D.; O'Halloran, G. A. *J. Chem. Soc., Chem.Commun.* **1989**, 1210-1211.

(26) Romano, R. M.; Della Vedova, C. O. *J. Mol. Struct.* **2000**, *522*, 1-26.

(27) Rao, V. M.; Yardley, J. T.; Curl, R. F. *J. Chem. Phys.* **1965**, *42*, 284-288.

(28) Kirchhoff, W. H. *J. Am. Chem. Soc.* **1969**, *91*, 2437-2442.

(29) Gobbato, K. I.; Della Vedova, C. O.; Oberhammer, H. *J. Mol. Struct.* **1995**, *350*, 227-231.

(30) Faegri Jr, K.; Kosmus, W. *J. Mol. Struct.* **1980**, *66*, 217-220.
(31) Abu-Eittah, R.; Moustafa, H.; Al-Omar, A. M. *Can. J. Chem.* **1997**, *75*, 934-941.
(32) Romano, R. M.; Della Vedova, C. O.; Hildebrandt, P. *J. Mol. Struct.* **1999**, *508*, 5-17.
(33) Muchall, H. M. *ARKIVOC* **2001**, *82*.
(34) Post, B.; Schwartz, R. S.; Fankuchen, I. *Acta Crystallogr.* **1952**, *5*, 372-374.
(35) Verbeek, W.; Sundermeyer, W. *Angew. Chem. Int. Ed. Engl.* **1969**, *8*, 376-376.
(36) Kresze, G.; Wucherpfennig, W. *Angew. Chem. Int. Ed. Engl.* **1967**, *6*, 149.
(37) Wegler, R.; Unterstenhoefer, G.; Kuehler, E.; Enders, E. In *DE Patent 1143667* 1963.
(38) Kuehler, E.; Klauke, E.; Frohberger, P. E. *DE Patent 2244616,* 1974.
(39) Malla, P.; Marion, D.; Ivanova, E. V.; Muchall, H. M. *J. Mol. Struct.*, **2010**, *979*, 101-107.
(40) Malla, P. MSc. Thesis, Concordia University, 2005.
(41) Gieren, A.; Dederer, B. *Angew. Chem. Int. Ed. Engl.* **1977**, *16*, 179.
(42) Schanda, F.; Gieren, A.; Filhol, A. *Acta Crystallogr. Sect. C* **1984**, *40*, 306-308.
(43) Pimental, G. C.; McClellan, A. L. *The Hydrogen Bond*; Reinhold Pub. Corp.: New York, 1960.
(44) Jeffery, G. *An Introduction to Hydrogen Bonding*; Oxford University Press, 1997.
(45) Desiraju, G. R.; Steiner, T. *The Weak Hydrogen Bond in Structural Chemistry and Biology*; Oxford University Press: New York, 1999.
(46) Dias, L. C.; Ferreira, A. B.; Tormena, C. F. *J. Phys. Chem. A* **2008**, *112*, 232-237.
(47) Steiner, T.; R. Desiraju, G. *Chem. Commun.* **1998**, 891-892.
(48) Scheiner, S. *Hydrogen Bonding, A Therortical Perspective*; Oxford University Press: New York, 1997.
(49) Cubero, E.; Orozco, M.; Hobza, P.; Luque, F. J. *J. Phys. Chem. A* **1999**, *103*, 6394-6401.
(50) Lammermann, A.; Szatmari, I.; Fulop, F.; Kleinpeter, E. *J. Phys. Chem. A* **2009**, *113*, 6197-6205.
(51) Cubero, E.; Orozco, M.; Luque, F. J. *Chem. Phys. Lett.* **1999**, *310*, 445-450.
(52) Arnold, J. T.; Packard, M. E. *J. Chem. Phys.* **1951**, *19*, 1608-1609.
(53) Liddel, U.; Ramsey, N. F. *J. Chem. Phy.s* **1951**, *19*, 1608-1608.
(54) Cohen, A. D.; Reid, C. *J. Chem. Phys.* **1956**, *25*, 790-791.
(55) Huggins, C. M.; Pimentel, G. C.; Shoolery, J. N. *J. Chem. Phys.* **1955**, *23*, 1244-1247.
(56) Weinberg, I.; Zimmerman, J. R. *J Phys. Chem.* **1955**, *23*, 748-749.
(57) Li, C.; Sammes, M. P. *J. Chem. Soc., Perkin Trans. 1* **1983**, 2193-2196.
(58) Afonin, A. V.; Sigalov, M. V.; Korostova, S. E.; Aliev, I. A.; Vashchenko, A. V.; Trofimov, B. A. *Magn. Reson. Chem.* **1990**, *28*, 580-586.

(59) Afonin, A. V.; Vashchenko, A. V.; Fujiwara, H. *Bull. Chem. Soc. Jpn.* **1996**, *69*, 933-945.
(60) Afonin, A. V.; Vashchenko, A. V.; Takagi, T.; Kimura, A.; Fujiwara, H. *Can. J. Chem.* **1999**, *77*, 416-424.
(61) Afonin, A. V.; Ushakov, I. A.; Kuznetsova, S. Y.; Petrova, O. V.; Schmidt, E. Y.; Mikhaleva, A. I. *Magn. Reson. Chem.* **2002**, *40*, 114-122.
(62) Lin, C.-H.; Yan, L.-F.; Wang, F.-C.; Sun, Y.-L.; Lin, C.-C. *J. Organomet. Chem.* **1999**, *587*, 151-159.
(63) Mele, A.; Vergani, B.; Viani, F.; Meille, S. V.; Farina, A.; Bravo, P. *Eur. J. Org. Chem.* **1999**, *1999*, 187-196.
(64) Harris, T. K.; Zhao, Q.; Mildvan, A. S. *J. Mol. Struct.* **2000**, *552*, 97-109.
(65) van der Veken, B. J.; Herrebout, W. A.; Szostak, R.; Shchepkin, D. N.; Havlas, Z.; Hobza, P. *J. Am. Chem. Soc.* **2001**, *123*, 12290-12293.
(66) Delanoye, S. N.; Herrebout, W. A.; van der Veken, B. J. *J. Am. Chem. Soc.* **2002**, *124*, 7490-7498.
(67) Mizuno, K.; Ochi, T.; Shindo, Y. *J. Chem. Phys.* **1998**, *109*, 9502-9507.
(68) Chaney, J. D.; Goss, C. R.; Folting, K.; Santarsiero, B. D.; Hollingsworth, M. D. *J. Am. Chem. Soc.* **1996**, *118*, 9432-9433.
(69) Karger, N.; Amorim da Costa, A. M.; Ribeiro-Claro, P. J. A. *J. Phys. Chem. A* **1999**, *103*, 8672-8677.
(70) Marques, M. P. M.; Amorim da Costa, A. M.; Ribeiro-Claro, P. J. A. *J. Phys. Chem. A* **2001**, *105*, 5292-5297.
(71) Ribeiro-Claro, P. J. A.; Marques, M. P. M.; Amado, A. M. *ChemPhysChem* **2002**, *3*, 599-606.
(72) Ribeiro-Claro, P. J. A.; Drew, M. G. B.; Flix, V. *Chem. Phys. Lett.* **2002**, *356*, 318-324.
(73) Gu, Y.; Kar, T.; Scheiner, S. *J. Am. Chem. Soc.* **1999**, *121*, 9411-9422.
(74) Scheiner, S.; Kar, T. *J. Phys. Chem. A* **2002**, *106*, 1784-1789.
(75) Qian, W.; Krimm, S. *J. Phys. Chem. A* **2002**, *106*, 6628-6636.
(76) Hermansson, K. *J. Phys. Chem. A* **2002**, *106*, 4695-4702.
(77) Vaz, P. D.; Ribeiro-Claro, P. J. A. *J. Phys. Chem. A* **2003**, *107*, 6301-6305.
(78) Sutor, D. J. *J. Chem. Soc.(Resumed)* **1963**, 1105-1110.
(79) Allerhand, A.; von Rague Schleyer, P. *J. Am. Chem. Soc.* **1963**, *85*, 1715-1723.
(80) Budesinsky, M.; Fiedler, P.; Arnold, Z. *Synthesis* **1989**, 858-860.
(81) Boldeskul, I. E.; Tsymbal, I. F.; Ryltsev, E. V.; Latajka, Z.; Barnes, A. J. *J. Mol. Struct.* **1997**, *437*, 167-171.
(82) Hobza, P.; Spirko, V.; Selzle, H. L.; Schlag, E. W. *J. Phys. Chem. A* **1998**, *102*, 2501-2504.
(83) Muller-Dethlefs, K.; Hobza, P. *Chem. Rev.* **1999**, *100*, 143-168.
(84) Hobza, P.; Spirko, V.; Havlas, Z.; Buchhold, K.; Reimann, B.; Barth, H.-D.; Brutschy, B. *Chem. Phys. Lett.* **1999**, *299*, 180-186.
(85) Hobza, P.; Havlas, Z. *Chem. Phys. Lett.* **1999**, *303*, 447-452.
(86) Hobza, P.; Havlas, Z. *Chem. Rev.* **2000**, *100*, 4253-4264.

(87) Wojcik, J.; Kamienska-Trela, K.; Pecul, M.; Bartoszak-Adamska, E.; Vdovienko, S. I.; Gerus, I. I. *ChemPhysChem* **2004**, *5*, 209-215.
(88) Koch, U.; Popelier, P. L. A. *J. Phys. Chem.* **1995**, *99*, 9747-9754.
(89) Steed, J. W. *Supramolecular Chemistry,* Wiley: England, 2000.
(90) Carroll, M. T.; Bader, R. F. W. *Mol. Phys.* **1988**, *65*, 695-722.
(91) Scheiner, S.; Gu, Y.; Kar, T. *J. Mol. Struct: THEOCHEM* **2000**, *500*, 441-452.
(92) Peralta, J. E.; Ruiz de Azua, M. C.; Contreras, R. H. *J.Mol. Struct: THEOCHEM* **1999**, *491*, 23-31.
(93) Sigalov, M.; Vashchenko, A.; Khodorkovsky, V. *J. Org. Chem.* **2005**, *70*, 92-100.
(94) Liddel, U.; Wulf, O. R. *J. Am. Chem. Soc.* **1933**, *55*, 3574-3583.
(95) Hilbert, G. E.; Wulf, O. R.; Hendricks, S. B.; Liddel, U. *J. Am. Chem. Soc.* **1936**, *58*, 548-555.
(96) Hendricks, S. B.; Wulf, O. R.; Hilbert, G. E.; Liddel, U. *J. Am. Chem. Soc.* **1936**, *58*, 1991-1996.
(97) Kim, N.-K.; Lee, H.-J.; Choi, K.-H.; Yu, J.-A.; Yoon, C.-J.; Park, J.; Choi, Y.-S. *J. Phys. Chem. A* **2000**, *104*, 5572-5578.
(98) Becke, A. D.; *J. Chem. Phys.* **1993**, *98*, 5648-5652.
(99) Lee, C.; Yang, W.; Parr, R. G. *Phys. Rev. B* **1988**, *37*, 785-789.
(100) Popelier, P. *Atom in Molecules. An Introduction,* Prentice Hall, 2000.
(101) Bader, R. F. W. *Atoms in Molecules. A Quantum Theory*; Clarendon Press, 1994.
(102) Konrat, M.; Tollinger, G.; Kontaxis, B. K. *Monatsh. Chem.* **1999**, *130*, 961-982.
(103) Nudelman, N. S.; Alvaro, C. E. S. *J. Phys. Org. Chem.*, **2011**, *24*, 1067-1071.
(104) Wash, P. L.; Maverick, E.; Chiefari, J.; Lightner, D. A. *J. Am. Chem. Soc.* **1997**, *119*, 3802-3806.
(105) Nogales, D. F.; Ma, J.-S.; Lightner, D. A. *Tetrahedron* **1993**, *49*, 2361-2372.
(106) Baures, P. W.; Beatty, A. M.; Dhanasekaran, M.; Helfrich, B. A.; Prez-Segarra, W.; Desper, J. *J. Am. Chem. Soc.* **2002**, *124*, 11315-11323.
(107) Sonicki, J. G.; Hansen, P. E. *J. Mol. Struct.* **2004**, *700*, 91-103.
(108) Kopple, K. D.; Ohnishi, M.; Go, A. *J. Am. Chem. Soc.* **1969**, *91*, 4264-4272.
(109) Llinas, M.; Klein, M. P. *J. Am. Chem. Soc.* **1975**, *97*, 4731-4737.
(110) Gellman, S. H.; Adams, B. R.; Dado, G. P. *J. Am. Chem. Soc.* **1990**, *112*, 460-461.
(111) Liang, G. B.; Rito, C. J.; Gellman, S. H. *J. Am. Chem. Soc.* **1992**, *114*, 4440-4442.
(112) Andersen, N. H.; Neidigh, J. W.; Harris, S. M.; Lee, G. M.; Liu, Z.; Tong, H. *J. Am. Chem. Soc.* **1997**, *119*, 8547-8561.
(113) Nelson, J. H. *Nuclear Magnetic Resonance Spectroscopy*; Pearson Education Inc: USA, 2003.

(114) Pavia, D. L.; Lampman, G. M.; Kriz, G. S. *Introduction to Spectroscopy*, 3rd edition, Harcourt, 2001.

(115) Klemperer, W.; Cronyn, M. W.; Maki, A. H.; Pimentel, G. C. *J. Am. Chem. Soc.* **1954**, *76*, 5846-5848.

(116) Affsprung, H. E.; Christian, S. D.; Worley, J. D. *Spectrochim. Acta* **1964**, *20*, 1415-1420.

(117) Purcell, J. M.; Susi, H.; Cavanaugh, J. R. *Can. J. Chem.* **1969**, *47*, 3655-3660.

(118) Kudryavtsev, A. B.; Linert, W. *Physico-Chemical Applications of NMR*; World Scientific Publishing Co Pte Ltd: Singapore, 1996.

(119) Huggins, C. M.; Pimentel, G. C.; Shoolery, J. N. *J. Phys. Chem.* **1956**, *60*, 1311-1315.

(120) Krikorian, S. E. *J. Phys. Chem.* **1982**, *86*, 1875-1881.

(121) Blackwell, L. F.; Buckley, P. D.; Jolley, K. W.; Watson, I. D. *Aust. J. Chem.* **1972**, *25*, 67-73.

(122) Hansch, C.; Leo, A.; Taft, R. W. *Chem. Rev.* **1991**, *91*, 165-195.

(123) Swart, M.; Fonseca Guerra, C.; Bickelhaupt, F. M. *J. Am. Chem. Soc.* **2004**, *126*, 16718-16719.

(124) Isaacs, N. S. *Physical Organic Chemistry,*; Harlow Essex, England: Longman Scientific & Technical,: New Wiley, 1987.

(125) Chen, R.; Zhang, K.-C.; Liu, L.; Li, X.-S.; Guo, Q.-X. *Chem. Phys. Lett.* **2001**, *338*, 61-66.

(126) Kawahara, S.; Wada, T.; Kawauchi, S.; Uchimaru, T.; Sekine, M. *J. Phys. Chem. A* **1999**, *103*, 8516-8523.

(127) Frisch, M. J.; Trucks, G. S., H.B.; Scuseria, G.E.; Robb, M.A.; Cheeseman, J.R.; Scalmani, G.; Barone, V.; Mennucci, B.; Petersson, G.A.; Nakatsuji, H.; Caricato, M.; Li, X.; Hratchian, H.P.; Izmaylov, A.F.; Bloino, J.; Zheng, G.; Sonnenberg, J.L.; Hada, M.; Ehara, M.; Toyota, K.; Fukuda, R.; Hasegawa, J.; Ishida, M.; Nakajima, T.; Honda, Y.; Kitao, O.; Nakai, H.; Vreven, T.; Montgomery, J.A., Jr.; Peralta, J.E.; Ogliaro, F.; Bearpark, M.; Heyd, J.J. ; Brothers, E.; Kudin, K.N.; Staroverov, V.N.; Keith, T.; Kobayashi, R.; Normand, J.; Raghavachari, K.; Rendell, A.; Burant, J.C.; Iyengar, S.S.; Tomasi, J.; Cossi, M.; Rega, N.; Millam, J.M.; Klene, M.; Knox, J.E.; Cross, J.B.; Bakken, V.; Adamo, C.; Jaramillo, J.; Gomperts, R.; Stratmann, R.E.; Yazyev, O.; Austin, A.J.; Cammi, R.; Pomelli, C.; Ochterski, J.W.; Martin, R.L.; Morokuma, K.; Zakrzewski, V.G.; Voth, G.A.; Salvador, P.; Dannenberg, J.J.; Dapprich, S.; Daniels, A.D.; Farkas, O.; Foresman, J.B.; Ortiz, J.V.; Cioslowski, J.; Fox, D.J. , Gaussian 09, Revision B.01; Gaussian, Inc.: Wallingford, CT 2010.

(128) Stephens, P. J.; Devlin, F. J.; Chabalowski, C. F.; Frisch, M. J. *J. Phys. Chem.* **1994**, *98*, 11623-11627.

(129) Novoa, J. J.; Sosa, C. *J. Phys. Chem. A* **1995**, 15837-15845.

(130) Latajka, Z.; Bouteiller, Y. *J. Chem. Phys.* **1994**, *101*, 9793-9799.

(131) Bertran, J.; Oliva, A.; Rodriguez-Santiago, L.; Sodupe, M. *J. Am. Chem. Soc.* **1998**, *120*, 8159-8167.

(132) Sim, F.; St-Amant, A.; Papai, I.; Salahub, D. R. *J. Am. Chem. Soc.* **1992**, *114*, 4391-4400.

(133) Perdew, J. P.; Burke, K.; Ernzerhof, M. *Phys. Rev. Lett.* **1996**, *77*, 3865-3868.
(134) Wu, A.; Zhang, Y.; Xu, X.; Yan, Y. *J. Comput. Chem.* **2007**, *28*, 2431-2442
(135) Schreckenbach, G.; Ziegler, T.; *J. Phys. Chem.* **1995**, *99*, 606-611.
(136) Ditchfield, R. *Mol. Phys.* **1974,**, *27*, 789-807.
(137) Wolinski, K.; Hinton, J. F.; Pulay, P. *J. Am. Chem. Soc.* **1990**, *112*, 8251-8260.
(138) Thomas, S.; Gautam, R. D. *Chem. Commun.* **1998**, 891.
(139) Brzezinski, B.; Szafran, M. *Org. Magn. Reson.* **1981**, *15*, 78-82.
(140) Wilcox, C. S.; Kim, E.-i.; Romano, D.; Kuo, L. H.; Burt, A. L.; Curran, D. P. *Tetrahedron* **1995**, *51*, 621-634.
(141) Laing, M.; Nicholson, J. *J. S. Afr. Chem. Inst.* **1971**, *24*, 186.
(142) Boateng, S.; Kariuki, M. N.; Muchall, H. M. *J Phys. Chem. A*, To be submitted.
(143) Zang, D. J. CHEM 450 Project, Concordia University, 2003.

Appendix A. Derivation for the modified equation developed by Schoolery, which was used in the determination of the self-association constant

For the chemical shift δ of an exchange average NMR line in a selfassociation reaction equilibrium mixture:

$$2M \underset{}{\overset{K}{\rightleftharpoons}} (M)_2$$

$\delta = \delta_M\ [M]/c_M + 2\delta_D\ (c_M\text{-}[M])/2c_M = [M]\ (\delta_M\text{-}\delta_D)/c_M + \delta_D$ ...……eq. 1

where [M] is the concentration of the monomer at equilibrium, c_M is the initial concentration of the monomer and δ_M and δ_D are the chemical shifts of the monomer and the dimer, respectively.

The initial concentration of monomers may be found as the root of the quadratic equation:

$c_M = [M] + 2K\ [M]^2$ ……eq. 2

where K is the constant for the self-association equilibrium.

$[M] = 2c_M/(1+\sqrt{1 + 8Kc_M})$……..eq. 3

Using the expression in (1) and differentiating with respect to c_M we get:

$d\delta/dc_M = -8K(\delta_M\text{-}\delta_D)/\ \{(1+\sqrt{1 + 8Kc_M})^2\sqrt{1 + 8Kc_M}\}$……..eq. 4

With c_M approaching zero, the denominator approaches 4. Hence:

$d\delta/(dc_M)_0 = 2K\ (\delta_D - \delta_M)$…….....eq. 5

where $d\delta/dc_M$ is the initial slope and $(\delta_D - \delta_M)$ is the change in chemical shift, $\Delta\delta$, between dimer (δ_D) and momer (δ_M).

Appendix B. Experimental N–H and C–H chemical shifts (ppm) for varying concentrations for unsubstituted and substituted PhNHNSO

Raw data

Table B1 Experimental N–H and C–H chemical shifts (ppm) for varying concentrations (M) of Ph–NH–NSO in $CDCl_3$ (one experiment only), run 1

Table B2 Experimental N–H and C–H chemical shifts (ppm) for varying concentrations (M) of Ph–NH–NSO in $CDCl_3$ (one experiment only), run 2

Table B3 Experimental N–H and C–H chemical shifts (ppm) for varying concentrations (M) of Ph–NH–NSO in $CDCl_3$ (one experiment only), run 3

Table B4 Experimental N–H and C–H chemical shifts (ppm) for varying concentrations (M) of p-Me Ph–NH–NSO in $CDCl_3$ (one experiment only)

Table B5 Experimental N–H and C–H chemical shifts (ppm) for varying concentrations (M) of p-Me Ph–NH–NSO in $CDCl_3$ (one experiment only)

Table B6 Experimental N–H and C–H chemical shifts (ppm) for varying concentrations (M) of p-Me Ph–NH–NSO in $CDCl_3$ (one experiment only)

Table B7 Experimental N–H and C–H chemical shifts (ppm) for varying concentrations (M) of m-Me Ph–NH–NSO in $CDCl_3$ (one experiment only)

Table B8 Experimental N–H and C–H chemical shifts (ppm) for varying concentrations (M) of m-Me Ph–NH–NSO in $CDCl_3$ (one experiment only)

Table B9 Experimental N–H and C–H chemical shifts (ppm) for varying concentrations (M) of m-Me Ph–NH–NSO in $CDCl_3$ (one experiment only)

Table B1 Experimental N–H and C–H chemical shifts (ppm) for varying concentrations (M) of Ph–NH–NSO in $CDCl_3$ (one experiment only), run 1.

c	δ(N–H)	δ(ortho C–H)	δ(meta C–H)	δ(para C–H)
1.200	10.914	7.285	7.326	7.073
1.000	10.892	7.287	7.316	7.077
0.800	10.839	7.285	7.334	7.079
0.600	10.777	7.287	7.343	7.087
0.400	10.668	7.283	7.359	7.102
0.200	10.513	7.275	7.373	7.117
0.100	10.374	7.263	7.379	7.122
0.050	10.288	7.252	7.383	7.125
0.025	10.211	7.244	7.385	7.128
0.005	10.135	7.236	7.387	7.130

Table B2 Experimental N–H and C–H chemical shifts (ppm) for varying concentrations (M) of Ph–NH–NSO in $CDCl_3$ (one experiment only), run 2.

c	δ(N–H)	δ(ortho C–H)	δ(meta C–H)	δ(para C–H)
1.200	10.916	7.288	7.323	7.07
1.000	10.898	7.285	7.328	7.069
0.800	10.868	7.285	7.339	7.075
0.600	10.822	7.285	7.349	7.096
0.400	10.705	7.281	7.362	7.106
0.200	10.53	7.273	7.373	7.116
0.100	10.387	7.263	7.381	7.124
0.050	10.278	7.253	7.382	7.125
0.025	10.193	7.245	7.384	7.127
0.005	10.118	7.238	7.387	7.129

Table B3 Experimental N–H and C–H chemical shifts (ppm) for varying concentrations (M) of Ph–NH–NSO in $CDCl_3$ (one experiment only), run 3.

c	δ(N–H)	δ(ortho C–H)	δ(meta C–H)	δ(para C–H)
1.200	10.915	7.287	7.328	7.073
1.000	10.898	7.285	7.327	7.073
0.800	10.853	7.286	7.336	7.074
0.600	10.765	7.285	7.353	7.087
0.400	10.663	7.283	7.360	7.102
0.200	10.507	7.273	7.372	7.117
0.100	10.36	7.261	7.382	7.122
0.050	10.248	7.249	7.381	7.125
0.025	10.184	7.246	7.385	7.128
0.005	10.127	7.234	7.386	7.130

Table B4 Experimental N–H and C–H chemical shifts (ppm) for varying concentrations (M) of p-Me Ph–NH–NSO in $CDCl_3$ (one experiment only), run 1.

c	δ(N–H)	δ(ortho C–H)	δ(meta C–H)	δ(CH_3)
1.200	10.871	7.181	7.118	2.289
1.000	10.837	7.182	7.124	2.294
0.800	10.787	7.182	7.133	2.302
0.600	10.712	7.182	7.1144	2.311
0.400	10.598	7.172	7.154	2.319
0.200	10.454	7.166	7.166	2.327
0.100	10.311	7.159	7.168	2.331
0.050	10.220	7.142	7.180	2.333
0.025	10.166	7.138	7.181	2.334
0.005	10.098	7.132	7.183	2.327

Table B5 Experimental N–H and C–H chemical shifts (ppm) for varying concentrations (M) of p-Me Ph–NH–NSO in $CDCl_3$ (one experiment only), run 2.

c	δ(N–H)	δ(ortho C–H)	δ(meta C–H)	δ(CH_3)
1.200	10.887	7.120	7.180	2.288
1.000	10.84	7.131	7.181	2.298
0.800	10.787	7.138	7.181	2.304
0.600	10.695	7.156	7.179	2.314
0.400	10.625	7.162	7.175	2.320
0.200	10.415	7.161	7.167	2.330
0.100	10.321	7.156	7.172	2.332
0.050	10.290	7.143	7.179	2.333
0.025	10.143	7.137	7.181	2.335
0.005	10.103	7.132	7.184	2.337

Table B6 Experimental N–H and C–H chemical shifts (ppm) for varying concentrations (M) of p-Me Ph–NH–NSO in $CDCl_3$ (one experiment only), run 3.

c	δ(N–H)	δ(ortho C–H)	δ(meta C–H)	δ(CH_3)
1.200	10.885	7.120	7.180	2.290
1.000	10.848	7.131	7.181	2.296
0.800	10.801	7.138	7.181	2.303
0.600	10.718	7.156	7.179	2.312
0.400	10.608	7.162	7.175	2.320
0.200	10.505	7.161	7.167	2.324
0.100	10.271	7.156	7.172	2.338
0.050	10.238	7.143	7.179	2.333
0.025	10.207	7.137	7.181	2.335
0.005	10.112	7.132	7.184	2.336

Table B7 Experimental N–H and C–H chemical shifts (ppm) for varying concentrations (M) of m-Me Ph–NH–NSO in $CDCl_3$ (one experiment only), run 1.

c	δ(N–H)	δ(C_{o1}–H)	δ(C_{o2}–H)	δ(C_m–H)	δ(C_p–H)	δ(CH_3)
1.2	10.760	7.099	7.071	7.218	6.900	2.342
1.0	10.723	7.102	7.072	7.223	6.906	2.347
0.8	10.679	7.102	7.069	7.225	6.909	2.349
0.6	10.646	7.102	7.068	7.233	6.916	2.355
0.4	10.559	7.101	7.062	7.241	6.924	2.362
0.2	10.387	7.093	7.051	7.251	6.933	2.371
0.1	10.271	7.084	7.04	7.256	6.939	2.375
0.05	10.205	7.080	7.032	7.258	6.942	2.376
0.025	10.149	7.076	7.03	7.259	6.943	2.377
0.005	10.084	7.073	7.022	7.260	6.944	2.377

Table B8 Experimental N–H and C–H chemical shifts (ppm) for varying concentrations (M) of m-Me Ph–NH–NSO in $CDCl_3$ (one experiment only), run 2.

c	δ(N–H)	δ(C_{o1}–H)	δ(C_{o2}–H)	δ(C_m–H)	δ(C_p–H)	δ(CH_3)
1.2	10.758	7.099	7.071	7.212	6.894	2.337
1.0	10.730	7.101	7.070	7.218	6.901	2.342
0.8	10.680	7.102	7.068	7.224	6.908	2.348
0.6	10.616	7.103	7.064	7.236	6.919	2.358
0.4	10.513	7.101	7.062	7.245	6.928	2.366
0.2	10.337	7.095	7.047	7.251	6.934	2.371
0.1	10.217	7.086	7.036	7.256	6.940	2.371
0.05	10.155	7.081	7.031	7.258	6.941	2.376
0.025	10.112	7.08	7.026	7.259	6.943	2.377
0.005	10.081	7.073	7.022	7.259	6.944	2.377

Table B9 Experimental N–H and C–H chemical shifts (ppm) for varying concentrations (M) of m-Me Ph–NH–NSO in $CDCl_3$(one experiment only), run 3.

c	δ(N–H)	δ(C_{o1}–H)	δ(C_{o2}–H)	δ(C_m–H)	δ(C_p–H)	δ(CH_3)
1.2	10.763	7.095	7.071	7.211	6.894	2.336
1.0	10.734	7.095	7.071	7.215	6.898	2.340
0.8	10.690	7.099	7.071	7.222	6.905	2.346
0.6	10.613	7.102	7.072	7.231	6.915	2.354
0.4	10.513	7.102	7.065	7.240	6.923	2.362
0.2	10.366	7.094	7.049	7.250	6.933	2.370
0.1	10.245	7.085	7.037	7.211	6.938	2.370
0.05	10.181	7.080	7.031	7.256	6.940	2.374
0.025	10.136	7.0790	7.026	7.261	6.943	2.378
0.005	10.082	7.073	7.024	7.259	6.943	2.377

Appendix C. ^{1}H NMR spectra for unsubstituted and substituted PhNHNSO's

Full sample spectra

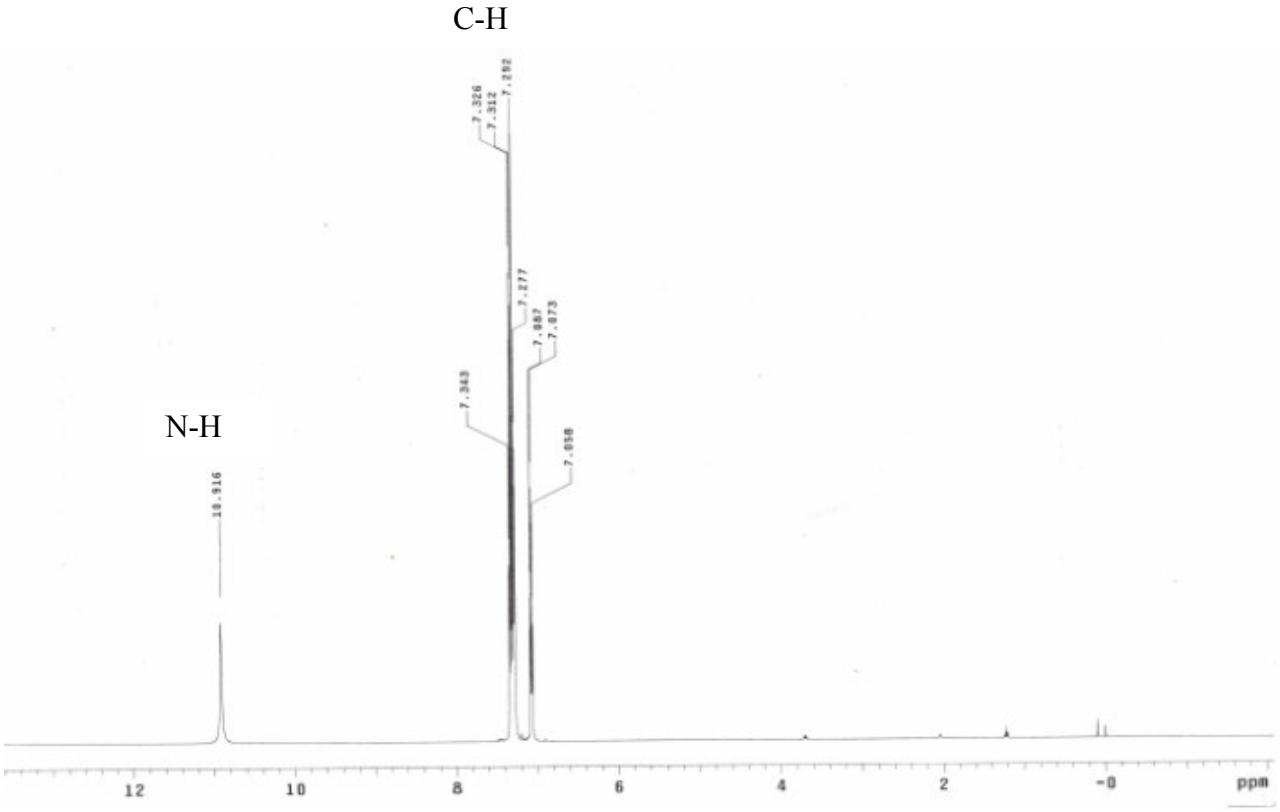

Fig. C1 ^{1}H NMR spectrum of N-phenyl-N'-sulfinylhydrazine for 1.2 M at 25 ºC.

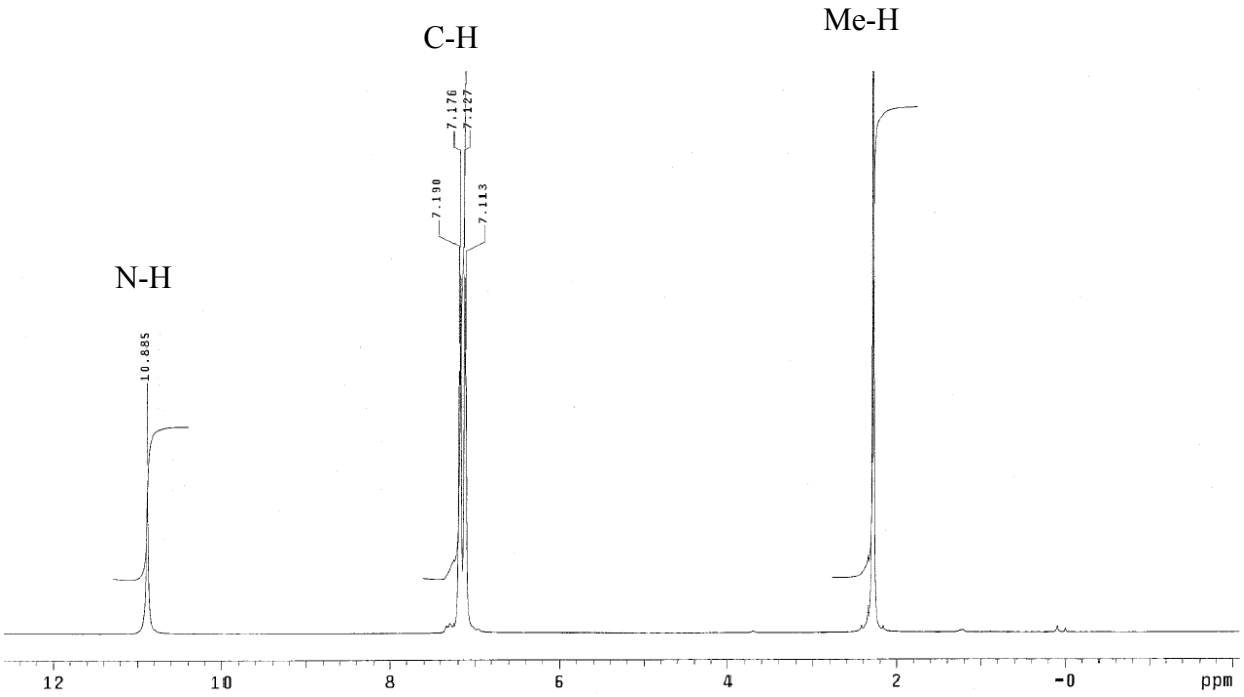

Fig. C2 ^{1}H NMR spectrum of p-Me N-phenyl-N'-sulfinylhydrazine for 1.2 M at 25 ºC.

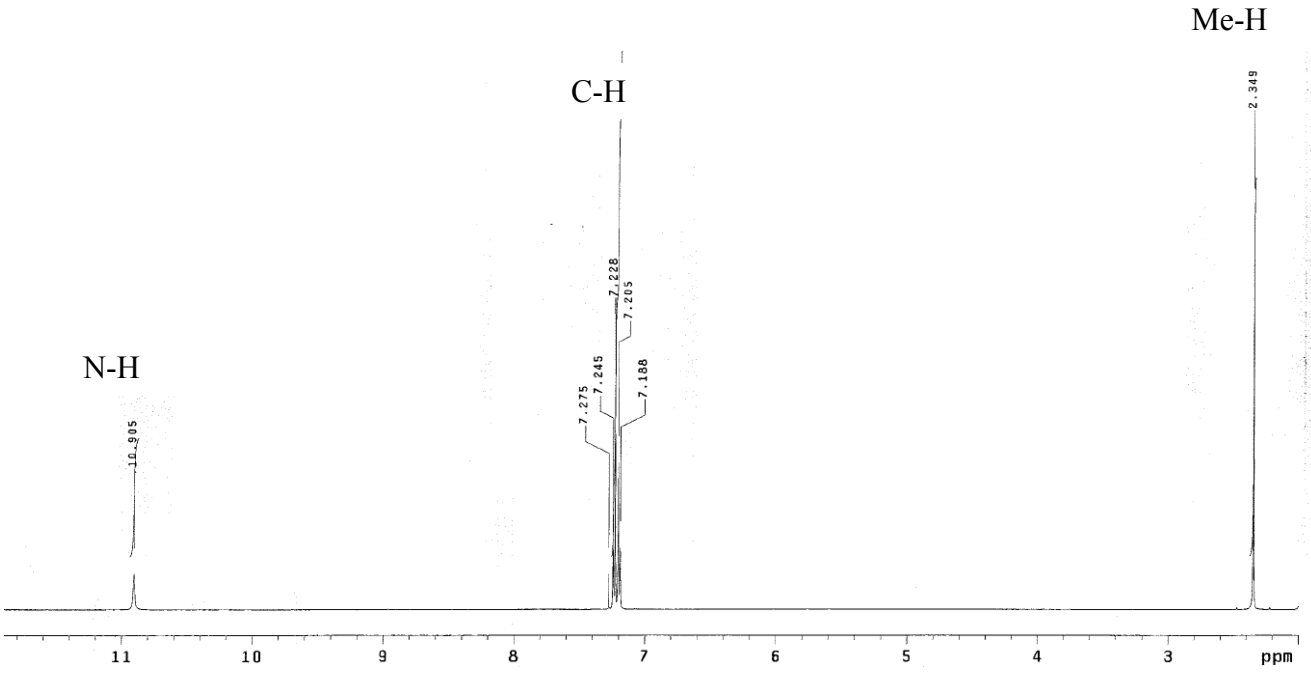

Fig. C3 ^{1}H NMR spectrum of p-Me N-phenyl-N'-sulfinylhydrazine for 1.2 M at –30 ºC.

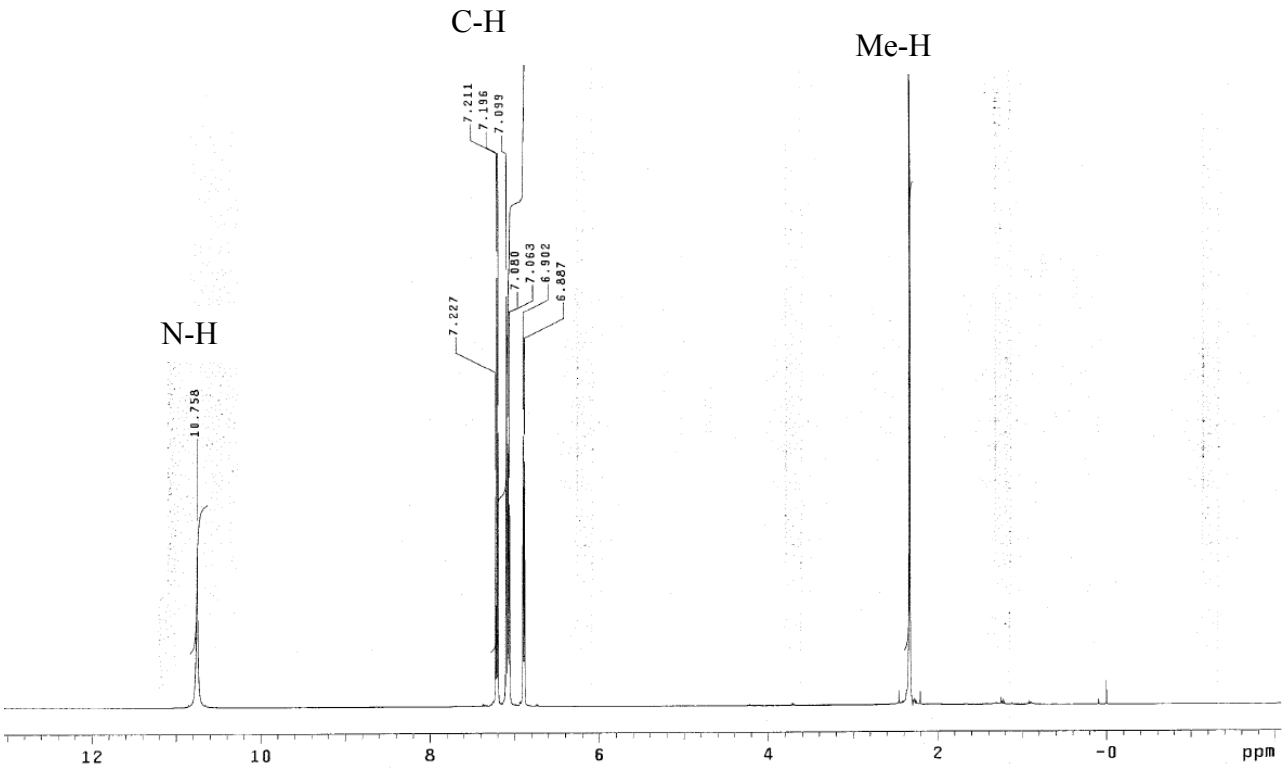

Fig. C4 ^{1}H NMR spectrum of m-Me N-phenyl-N'-sulfinylhydrazine for 1.2 M at 25 ºC.

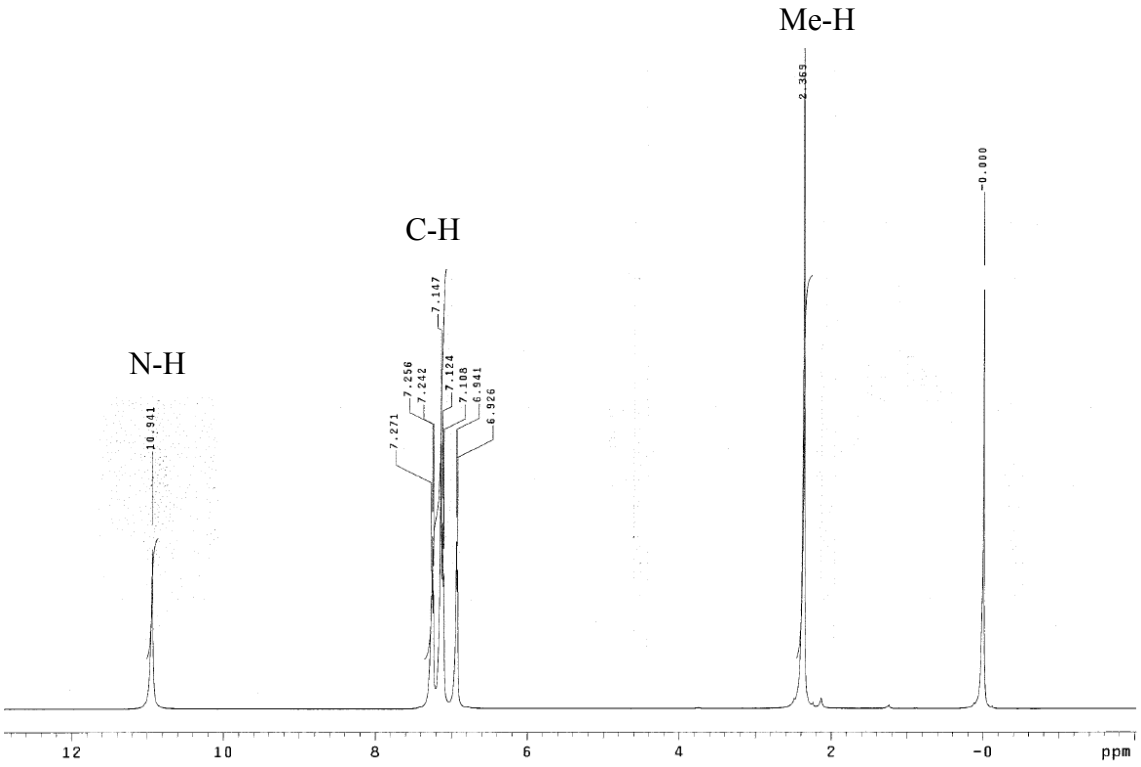

Fig. C5 ^{1}H NMR spectrum of m-Me N-phenyl-N'-sulfinylhydrazine for 1.2 M at –15 ºC.

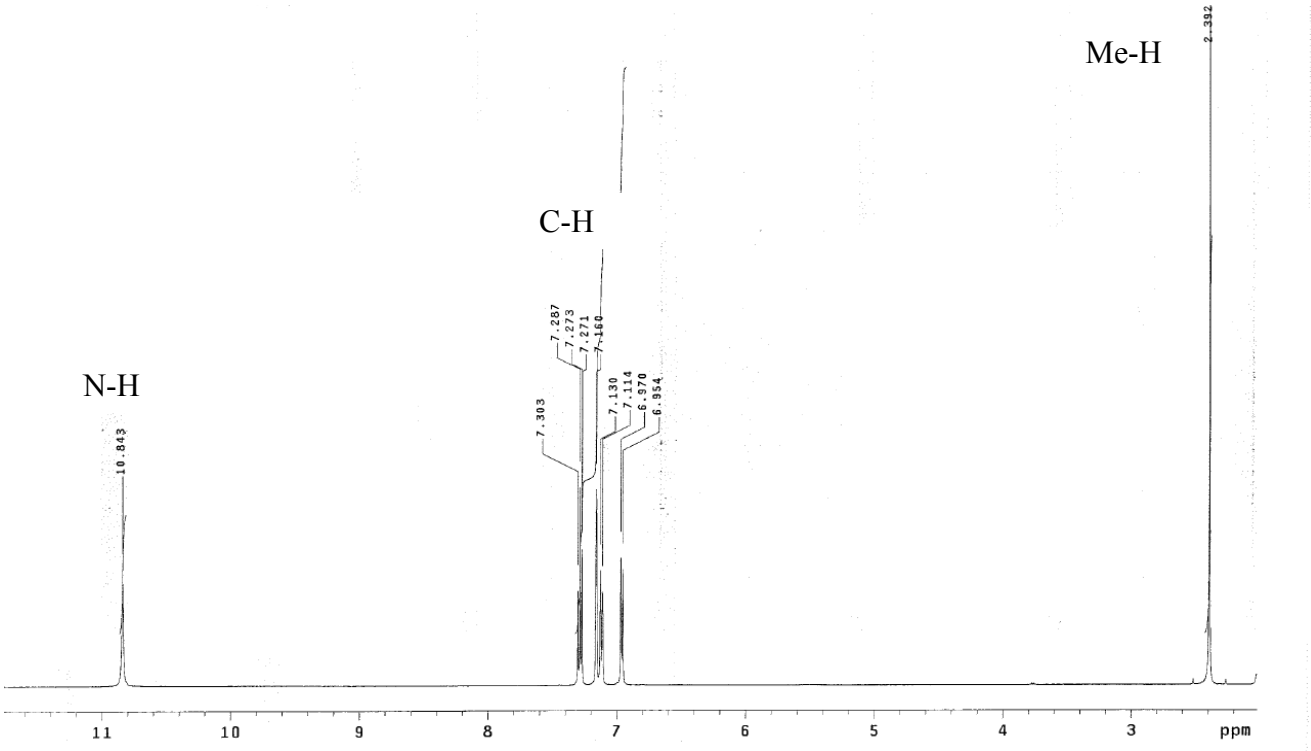

Fig. C6 ^{1}H NMR spectrum of m-Me N-phenyl-N'-sulfinylhydrazine for 1.2 M at –30 ºC.

Appendix D. Computational data provided from OPBE/6311++G(2df,pd)//B3LYP/ 6-31+G(2d,2p)

D1 N-phenyl-N'-sulfinylhydrazine *syn* monomer

D2 N-phenyl-N'-sulfinylhydrazine dimer

D3 p-Me N-phenyl-N'-sulfinylhydrazine *syn* monomer

D4 p-Me N-phenyl-N'-sulfinylhydrazine dimer

D5 m3-Me N-phenyl-N'-sulfinylhydrazine *syn* monomer

D6 m5-Me N-phenyl-N'-sulfinylhydrazine *syn* monomer

D7 m3-Me N-phenyl-N'-sulfinylhydrazine homo-dimer

D8 m5-Me N-phenyl-N'-sulfinylhydrazine homo-dimer

D9 m3- and m5-Me N-phenyl-N'-sulfinylhydrazine hetero-dimer

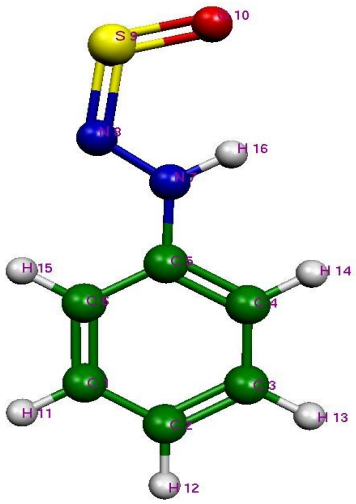

Fig. D1 *syn* Monomer PhNHNSO.

Electronic energy (Hartree): -815.153185
Free energy (Hartree): -815.071579

Table D1 Calculated isotropic shielding σ and derived chemical shift δ (ppm) for N-phenyl-N'-sulfinylhydrazine *syn* monomer (for TMS σ_{iso} (H) 31.5056).

Ar-H			N-H		
atom#	σ	δ	atom#	σ	δ
14	24.4789	7.03	**16**	21.2081	10.30
13	23.9034	7.60			
12	24.1644	7.34			
11	23.8204	7.69			
15	23.6743	7.83			

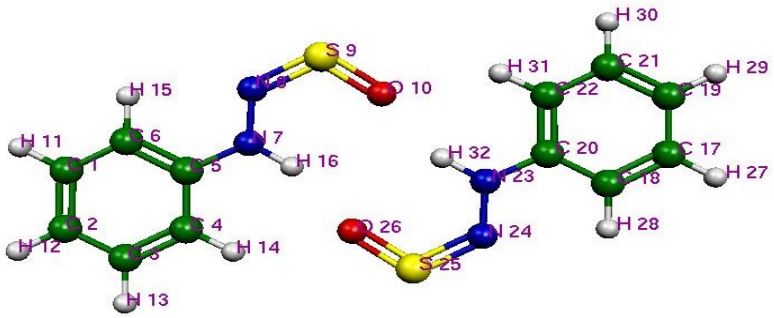

Fig. D2 Dimer PhNHNSO.

Electronic energy (Hartree): -1630.322259
Free energy (Hartree): -1630.140767

Table D2 Calculated isotropic shielding σ and derived chemical shift δ (ppm) for N-phenyl-N'-sulfinylhydrazine dimer (for TMS σ_{iso}(H) 31.5056).

Ar-H			Ar-H			N-H		
atom#	σ	δ	atom#	σ	δ	atom#	σ	δ
14	23.4833	8.02	**31**	23.4835	8.02	**16**	19.1650	12.34
13	23.8619	7.64	**30**	23.8619	7.64	**32**	19.1653	12.34
12	24.1227	7.38	**29**	24.1227	7.38			
11	23.7940	7.71	**27**	23.7940	7.71			
15	23.6712	7.83	**28**	23.6711	7.83			

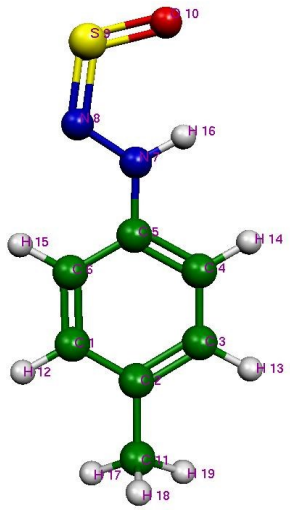

Fig. D3 *syn* Monomer p-Me PhNHNSO.

Electronic energy (Hartree): -854.474774
Free energy (Hartree): -854.370138

Table D3 Calculated isotropic shielding σ and derived chemical shift δ (ppm) for p-Me N-phenyl-N'-sulfinylhydrazine *syn* monomer (for TMS σ_{iso}(H) 31.5056).

Ar-H			N-H		
atom#	σ	δ	atom#	σ	δ
14	24.5767	6.93	**16**	21.2420	10.26
13	24.1045	7.40			
12	24.0069	7.50			
15	23.7766	7.73			

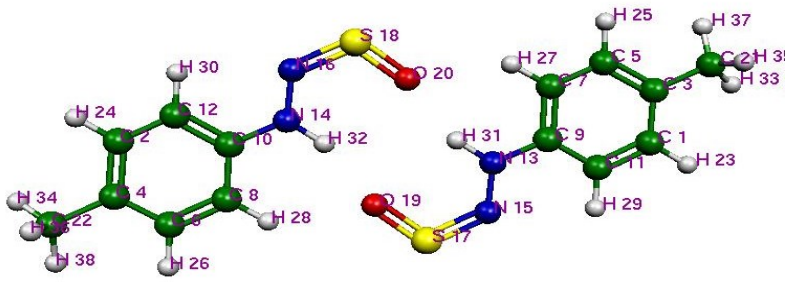

Fig. D4 Dimer p-Me PhNHNSO.

Electronic energy (Hartree): -1708.965469
Free energy (Hartree): -1708.735844

Table D4 Calculated isotropic shielding σ and derived chemical shift δ (ppm) for p-Me N-phenyl-N'-sulfinylhydrazine dimer (for TMS σ_{iso} (H) 31.5056).

Ar-H			Ar-H			N-H		
atom#	σ	δ	atom#	σ	δ	atom#	σ	δ
28	23.5619	7.94	**27**	23.5686	7.94	**31**	19.2045	12.30
26	24.0665	7.44	**25**	24.0701	7.44	**32**	19.2137	12.29
24	24.0039	7.50	**23**	24.0001	7.51			
30	23.7571	7.75	**29**	23.7536	7.75			

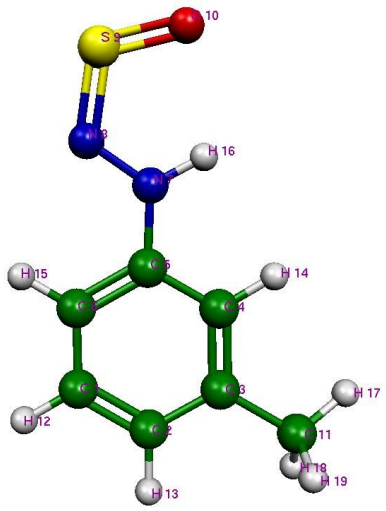

Fig. D5 *syn* Monomer m3-Me PhNHNSO.

Electronic energy (Hartree): -854.475211
Free energy (Hartree): -854.370861

Table D5 Calculated isotropic shielding σ and derived chemical shift δ (ppm) for m3-Me N-phenyl-N'-sulfinylhydrazine *syn* monomer (for TMS σ_{iso} (H) 31.5056).

Ar-H			N-H		
atom#	σ	δ	atom#	σ	δ
14	24.6866	6.82	**16**	21.2519	10.25
13	24.2894	7.22			
12	23.9268	7.58			
15	23.8975	7.61			

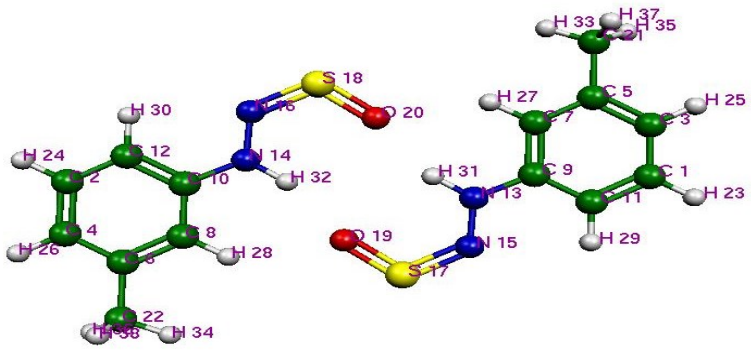

Fig. D6 Homo-dimer m3-Me PhNHNSO.

Electronic energy (Hartree): -1708.965999
Free energy (Hartree): -1708.736341

Table D6 Calculated isotropic shielding σ and derived chemical shift δ (ppm) for m3-Me N-phenyl-N'-sulfinylhydrazine homo-dimer (for TMS σ_{iso}(H) 31.5056).

Ar-H			Ar-H			N-H		
atom#	σ	δ	atom#	σ	δ	atom#	σ	δ
28	23.6477	7.86	**27**	23.6362	7.87	**32**	19.2262	12.28
26	24.2648	7.24	**25**	24.2687	7.24	**31**	19.2354	12.27
24	23.9285	7.58	**23**	23.9333	7.57			
30	23.8633	7.64	**29**	23.8572	7.65			

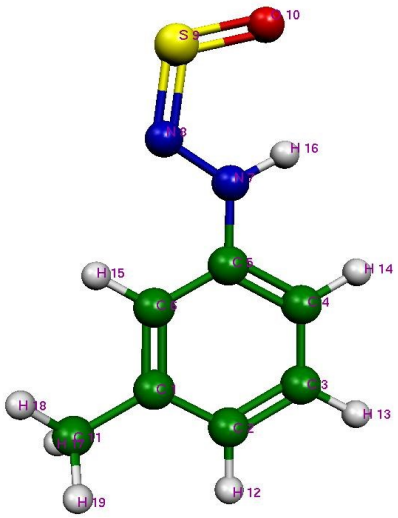

Fig. D7 *syn* Monomer m5-Me PhNHNSO.

Electronic energy (Hartree): -854.475273
Free energy (Hartree): -854.370019

Table D7 Calculated isotropic shielding σ and derived chemical shift δ (ppm) for m5-Me N-phenyl-N'-sulfinylhydrazine *syn* monomer (for TMS σ_{iso} (H) 31.5056).

Ar-H			N-H		
atom#	σ	δ	atom#	σ	δ
14	24.6713	6.83	**16**	21.2417	10.26
13	24.0350	7.47			
12	24.3111	7.19			
15	23.8391	7.67			

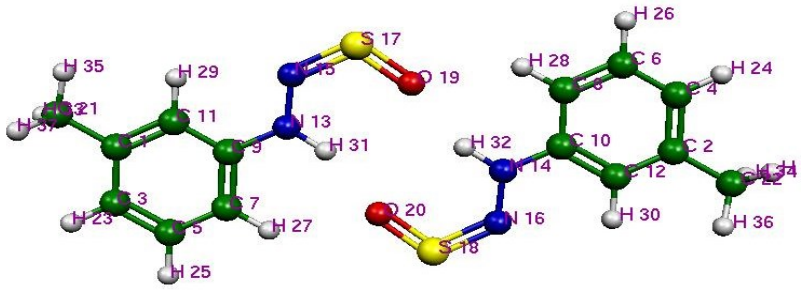

Fig. D8 Homo-dimer m5-Me PhNHNSO.

Electronic energy (Hartree): -1708.966007
Free energy (Hartree): -1708.737018

Table D8 Calculated isotropic shielding σ and derived chemical shift δ (ppm) for m5-Me N-phenyl-N'-sulfinylhydrazine homo-dimer (for TMS σ_{iso}(H) 31.5056).

Ar-H			Ar-H			N-H		
atom#	σ	δ	atom#	σ	δ	atom#	σ	δ
27	23.6762	7.83	**28**	23.6710	7.83	**31**	19.2134	12.29
25	23.9793	7.53	**26**	23.9798	7.53	**32**	19.2113	12.29
23	24.2466	7.26	**24**	24.2479	7.26			
29	23.8271	7.68	**30**	23.8273	7.68			

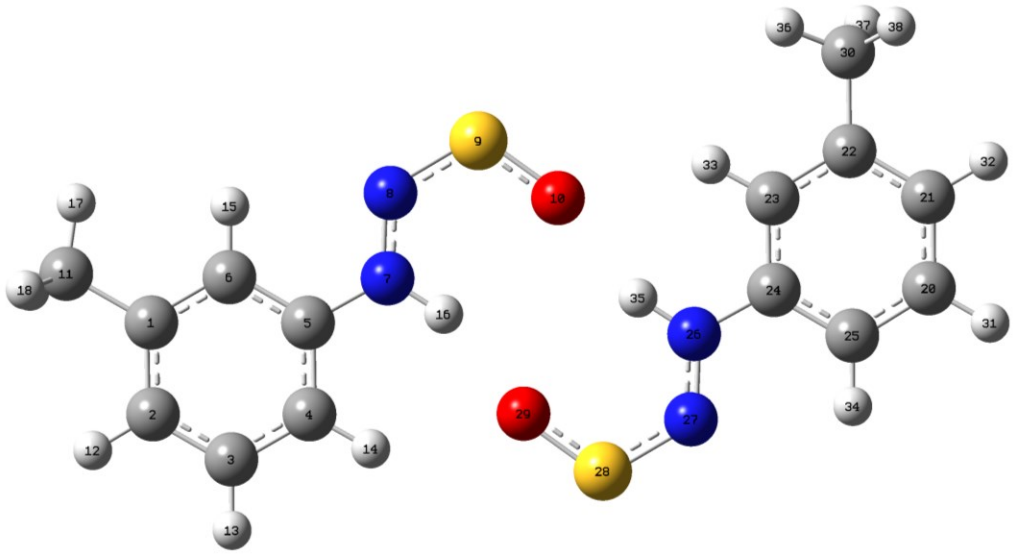

Fig. D9 Hetero-dimer m3- and m5-Me PhNHNSO.

Electronic energy (Hartree): -1708.966037
Free energy (Hartree): -1708.736725

Table D9 Calculated isotropic shielding σ and derived chemical shift δ (ppm) for m3- and m5-Me N-phenyl-N'-sulfinylhydrazine hetero-dimer (for TMS σ_{iso}(H) 31.5056).

Ar-H			Ar-H			N-H		
atom#	σ	δ	atom#	σ	δ	atom#	σ	δ
14	23.6751	7.83	**33**	23.6456	7.86	**16**	19.1722	12.33
13	23.9591	7.55	**32**	24.2780	7.23	**35**	19.2544	12.25
12	24.2554	7.25	**31**	23.9191	7.59			
15	23.8411	7.66	**34**	23.8827	7.62			